

Susceptibility of Enterovirus B strains to disinfectants and heat

Thèse N° 9343

Présentée le 28 juin 2019

à la Faculté de l'environnement naturel, architectural et construit
Laboratoire de chimie environnementale
Programme doctoral en génie civil et environnement

pour l'obtention du grade de Docteur ès Sciences

par

Simon MEISTER

Acceptée sur proposition du jury

Prof. C. Holliger, président du jury
Prof. T. Kohn, directrice de thèse
Prof. B. Mayer, rapporteuse
Prof. C. Gantzer, rapporteur
Prof. M. Dal Peraro, rapporteur

2019

Remerciements

Je tiens tout d'abord à remercier ma directrice de thèse, Tamar Kohn, pour son suivi, son engagement, et sa motivation inébranlable durant ces 4 années et demi. Je la remercie aussi de m'avoir accordé une liberté d'action, tant scientifiques que géographiques, me permettant ainsi de participer à de nombreuses conférences et collaborations.

Je souhaite aussi remercier les membres du jury : Christof Holliger, Matteo Dal Peraro, Brooke Mayer, et Christophe Gantzer pour leur implication dans ma thèse, par d'intéressantes discussions durant la défense privée et de commentaires constructifs sur le document écrit, ainsi que Tim Julian, ayant participé activement à mon examen de candidature trois ans plus tôt.

Mes remerciements s'adressent ensuite à mon étudiant en master, Marius Klinger, qui a grandement participé à la genèse du deuxième chapitre de cette thèse, ainsi que Matthew Verbyla pour sa précieuse aide dans la génération et analyse des données de statistiques bayésiennes de ce même chapitre. Un grand merci également à Alessio Prunotto, pour avoir apporté une dimension d'analyse structurale au troisième et quatrième chapitre, ainsi que pour les nombreuses discussions sur le sujet et échanges de connaissances.

Merci également à Adam Luring et son équipe pour l'accueil durant ce mois de travail à Ann Arbor, et particulièrement Will Fitzsimmons pour sa précieuse aide en laboratoire. Merci aussi à Guillermo Grunauer, ainsi qu'aux employés de la STEP de Vidy, François Murdter et Patrick Chezeaux pour leur accueil et l'aide à l'échantillonnage

Un grand merci aux membres actuels et passés du LCE et LTQE pour ces quelques années/mois passés à vos côtés. Un remerciement spécial à Qingxia, ma voisine de bureau de longue date, pour son humour et sa présence conviviale durant ces années, également Camille, ma camarade de bataille, pour les innombrables pauses cafés et discussions tant scientifiques que personnelles, Loïc, pour les discussions constructives et ses dispositions musicales et sportives, et notre secrétaire Karine, pour sa patience à toute épreuve.

Un grand remerciement à mes anciens mentors, Jérôme Gouttenoire et Angela Ciuffi, qui m'ont permis d'arriver là où je suis actuellement, ainsi qu'aux membres actuels et passés de l'IMUL.

Merci également à mes parents et ma famille, qui m'ont soutenus et encouragés durant ces années, ainsi qu'à mes amis, qui m'ont permis de m'évader occasionnellement du domaine académique. Et un immense remerciement à Nikta, ma compagne, d'avoir supporté mon stress durant ces années, et d'avoir soutenu toutes mes idées et projets d'avenir.

Résumé

La sensibilité à différents traitements d'inactivation est connue pour varier entre les virus, et même entre les des souches de virus apparentés. Cependant, l'étendue de cette variation, ainsi que les mécanismes responsables celle-ci n'est pas connus. Dans cette étude, différents entérovirus (six souches the coxsackievirus B5 (CVB5), deux de coxsackievirus B4 (CVB4), et une souche de coxsackievirus B1 (CVB1)) ont été isolées d'eau usée, et soumises à plusieurs traitements de désinfection (UV₂₅₄, le chlore libre, et le dioxyde de chlore) et autres facteurs de stress rencontrés dans l'environnement (soleil, température). Les cinétiques d'inactivation des souches environnementales ont été comparées avec celles de souche de laboratoire (CVB5 Faulkner et échovirus 11 Gregory) ainsi qu'avec le bactériophage MS2. La plus grande variabilité entre les souche a pu être observée avec le traitement au chlore libre, contrairement au traitement à l'UV₂₅₄, qui ne présentait seulement qu'une variabilité subtile. La cinétique d'inactivation entre les différents sérotypes apparaissait plus grande que celle observée au sein du sérotype CVB5. Quant à MS2, il apparaît comme un substitut conservatif pour l'inactivation des enterovirus à l'UV₂₅₄, au soleil, ainsi qu'à la température, mais sous-estime la désinfection chlore libre et au dioxyde de chlore.

Curieusement, les différences observées entre les virus avec l'inactivation par température apparaissent liés au sérotype, mais aussi à la source (souche environnementale ou de laboratoire). Pour cette raison, nous avons décidé d'orienter le travail sur l'inactivation thermique, afin d'évaluer les mécanismes responsables de ces différences. Plus précisément, nous avons analysé l'inactivation de ces virus à deux températures, 30 et 55°C, ainsi qu'à deux différentes conditions de pH et concentration de sel (NaCl). A 30°C, une lente inactivation a pu être constatée à pH neutre, et plus rapide à pH acide ou alcalin. De plus, l'ajout de 1M de NaCl a provoqué une forte augmentation de l'inactivation observée à ces pH extrêmes, de façon synergétique. Ces résultats apparaissent cohérents avec un clivage de l'ARN, confirmé expérimentalement par une dégradation de l'ARN viral. À 55°C, un effet protecteur du sel a pu être constaté sur tous les virus étudiés, ce qui a pu être justifié par une augmentation des forces d'attraction à l'interface des structures pentamériques constituant la capsid virale. À cette température, des différences importantes entre les souches virales ont été constatées, les souches CVB4 et échovirus 11 étant les plus thermosensibles que toutes les autres, et la souche de laboratoire CVB5 étant plus thermosensible que ses isolats environnementaux correspondants. Ces variations n'ont pas pu être expliquées par un changement dans les forces d'interaction des pentamères, mais possiblement provoquée par des mutations localisées dans la poche hydrophobe de VP1.

L'importance de cette poche a pu être confirmée en adaptant CVB5 à deux températures, 50 et 55°C. Les souches adaptées sont apparues moins compétitives que les souches contrôles, mais étaient plus résistantes à la température. Cette résistance coïncide avec l'apparition de mutations dans cette même poche hydrophobe, mais n'impliquant aucun changement dans les forces d'interaction des pentamères. Ces résultats confirment l'importance de cette poche hydrophobe dans la résistance des virus à la température.

Globalement, ces données nous révèlent que la thermo-résistance des virus peut être renforcée par des facteurs externes, comme la salinité, ou par des modifications structurales de la poche hydrophobe de VP1.

Mots-clés: virus, eau, désinfection, résistance, température

Summary

The susceptibility of waterborne viruses to different inactivating treatments is acknowledged to vary between viruses and even between closely related strains, yet the extent of this variation, or the underlying mechanisms, are not known. Here, different enteroviruses (six strains of coxsackievirus B5 (CVB5), two strains of coxsackievirus B4 (CVB4) and one strain of coxsackievirus B1 (CVB1)) were isolated from wastewater. The different viruses were then exposed to disinfectants used in water and wastewater treatment (UV₂₅₄, free chlorine (FC), chlorine dioxide (ClO₂)) and to stressors encountered in the environment (sunlight, temperature). Inactivation kinetics of the environmental isolates were compared with those of laboratory enterovirus strains (CVB5 Faulkner and echovirus 11 Gregory) and MS2 bacteriophage. FC exhibited the greatest variability in inactivation kinetics between different strains, whereas inactivation by UV₂₅₄ differed only subtly. The variability in inactivation kinetics was greater between serotypes than it was among the seven strains of the CVB5 serotype. MS2 was a conservative surrogate of enterovirus inactivation by UV₂₅₄, sunlight or heat, but frequently underestimated the disinfection requirements for FC and ClO₂.

Interestingly, the differences between the viruses in heat resistance appeared linked to the serotype and the source of isolation (environmental versus laboratory). For this reason, we decided to focus on thermal inactivation and investigate the mechanisms underlying these differences. Specifically, we extensively analyzed the inactivation of these viruses at 30 and 55°C, and under different conditions of pH and NaCl concentrations. At 30°C, inactivation at neutral pH was slow, but both acidic and alkaline pH enhanced inactivation, and the addition of 1 M NaCl exerted a synergistic inactivating effect. These findings are consistent with RNA cleavage being the main mechanism of inactivation, and genome degradation was experimentally confirmed. At 55°C, salt had a protective effect on all viruses. This was rationalized by calculations of the different protein interaction forces, which demonstrated that increasing concentrations of salt resulted in increasing attractive forces at the capsid pentamer interfaces. At this temperature, major differences in thermoresistance between the viruses were observed, with CVB4 and E11 displaying the lowest thermoresistance, and the CVB5 laboratory strain being less thermoresistant than the CVB5 isolates. These differences could not be explained by a shift in capsid pentamer interaction forces, but likely resulted from mutations located in VP1 pocket region.

The importance of the VP1 pocket region was further confirmed by adapting CVB5 to two different temperatures (50 and 55 °C). The thermo-adapted strains exhibited a competitive fitness trade-off compared to control strains, but were significantly more resistant to thermal inactivation. This resistance coincided with the appearance of one or several of four mutations in the VP1 region of the structural proteins. These mutations did not affect the interaction forces at the pentamer interface. Instead, they were located in the VP1 pocket region, confirming the importance of this region in the acquisition of thermotolerance. Overall, these data indicate that the thermostability of a virus can be enhanced by external (matrix) factors, in particular salinity, or by intrinsic (structural) modifications in the VP1 pocket region.

Keywords: virus, water, disinfection, resistance, temperature

Table of content

Remerciements.....	I
Résumé	II
Summary	IV
Table of content.....	VI
List of figures	IX
List of tables	XI
<u>CHAPTER 1 INTRODUCTION.....</u>	<u>1</u>
CONTEXT	1
VIRUSES AND PICORNAVIRUSES	1
BACKGROUND	1
DISINFECTION METHODS AND GUIDELINES	5
DISINFECTION.....	5
CT VALUE DATABASE.....	7
MATRIX- AND VIRUS-RELATED RESISTANCE MECHANISMS.....	10
MISSING INFORMATION AND UNANSWERED QUESTIONS	11
RESEARCH OBJECTIVES AND APPROACH.....	11
CHAPTER 2. VARIABILITY IN DISINFECTION RESISTANCE BETWEEN CURRENTLY CIRCULATING ENTEROVIRUS B SEROTYPES AND STRAINS.	11
CHAPTER 3. EFFECT OF SALT AND PH ON VIRUS THERMOSTABILITY.	11
CHAPTER 4. STRUCTURAL MECHANISMS CAUSING HEAT RESISTANCE MEDIATED BY THERMAL ADAPTATION OR SALT.....	12
<u>CHAPTER 2 VARIABILITY IN DISINFECTION RESISTANCE BETWEEN CURRENTLY CIRCULATING ENTEROVIRUS B SEROTYPES AND STRAINS.....</u>	<u>13</u>
INTRODUCTION	13
EXPERIMENTAL SECTION	15
ISOLATION OF CIRCULATING VIRUSES	15
VIRUS IDENTIFICATION, WHOLE GENOME SEQUENCING AND ALIGNMENT	15
VIRUS PURIFICATION AND ENUMERATION	16
INACTIVATION EXPERIMENTS	17
INACTIVATION RATE MODELLING	18
BAYESIAN ANALYSIS OF RATE CONSTANTS	19

DATA ANALYSIS.....	19
RESULTS AND DISCUSSION	20
VIRUS ISOLATION	20
INACTIVATION KINETICS.....	21
INTER-SEROTYPE COMPARISON OF INACTIVATION KINETICS.....	24
ASSESSMENT OF ENTEROVIRUS LAB STRAINS OR MS2 AS SURROGATES FOR THE DISINFECTION OF ENVIRONMENTAL ISOLATES	26
<u>CHAPTER 3 EFFECT OF SALT AND PH ON VIRUS THERMOSTABILITY.....</u>	30
INTRODUCTION	30
ROLE OF TEMPERATURE IN VIRUS PERSISTENCE OUTSIDE THE HOST	30
THERMOSTABILITY OF ENTEROVIRUSES.....	30
EXPERIMENTAL SECTION	31
CELLS AND VIRUSES	31
INFECTIVITY ASSAY.....	32
ANTIGENIC DIVERGENCE ASSAY	32
THERMAL INACTIVATION EXPERIMENTS.....	32
DETERMINATION OF THE CAPSID MELTING TEMPERATURE (BREAKPOINT).....	33
ASSAY TO MEASURE GENOME INTEGRITY	33
STRUCTURAL MODELLING	34
DATA ANALYSIS.....	35
RESULTS	35
EFFECT OF TEMPERATURE AND SOLUTION COMPOSITION ON INACTIVATION	35
STRUCTURAL ANALYSIS.....	40
DISCUSSION	42
PROPOSED MECHANISMS OF INACTIVATION	42
STRUCTURAL FEATURES LEADING TO ENHANCED THERMOSTABILITY	43
CONCLUSION	45
<u>CHAPTER 4 STRUCTURAL MECHANISMS CAUSING HEAT RESISTANCE MEDIATED BY THERMAL ADAPTATION OR SALT.....</u>	46
INTRODUCTION	46
MATERIAL AND METHODS.....	48
CELLS AND VIRUSES	48

THERMAL INACTIVATION AND DETERMINATION OF BREAKPOINT TEMPERATURES.....	48
THERMAL ADAPTATION	48
GENOME SEQUENCING.....	50
COMPETITION ASSAY TO DETERMINE VIRAL FITNESS.....	50
STRUCTURAL MODELLING.	50
DATA ANALYSIS.....	52
RESULTS AND DISCUSSION	52
THERMAL ADAPTATION AND ITS EFFECTS ON VIRUS INACTIVATION, COMPOSITION AND FITNESS.....	52
INFLUENCE OF PROTEIN INTERACTION FORCES ON THE THERMOSTABILITY OF CVB5.....	56
CONCLUSION	61
<u>CHAPTER 5 CONCLUSION AND PERSPECTIVES</u>	<u>62</u>
<u>REFERENCES</u>	<u>81</u>

List of figures

Figure 1.1. Viruses shape, size and genome diversity	2
Figure 1.2. Waterborne virus transmission routes.....	4
Figure 1.3. Database quality.....	8
Figure 1.4. <i>Ct value</i> database output for UV ₂₅₄	9
Figure 1.5 <i>Ct value</i> database output for chlorine.....	10
Figure 2.1. Unrooted neighbour joining tree.	20
Figure 2.2. Violin plot of inactivation rate constant distribution.	21
Figure 2.3. Intra-serotype probability comparison of inactivation rate constants.	24
Figure 2.4. <i>Ct</i> values to achieve 4- \log_{10} inactivation by FC.....	28
Figure 3.1 Scheme of the pentamer interface.	35
Figure 3.2 Thermostability of different enterovirus strains and serotypes at 30°C.....	36
Figure 3.3 Effect of salt and pH on virus infectivity and genome integrity of CVB5-Faulkner at 30°C	37
Figure 3.4 Effect of salt and pH on virus infectivity of the CVB5-Faulkner strain	38
Figure 3.5 Breakpoint temperature for the viruses.	39
Figure 3.6 Effect of salt and pH on virus breakpoints temperature.....	39
Figure 3.7 Correlation of breaking points with the rate constants <i>k</i> at 55°C.....	39
Figure 3.8 Antigenic divergence from CVB5-Faulkner strain.	40
Figure 3.9. Number of H bonds and salt bridges at the pentamer interface.	41
Figure 3.10 Interaction forces at the pentamer interface.....	41
Figure 3.11 Pocket factor	42
Figure 4.1 Scheme of the thermal adaptation assay.....	49
Figure 4.2 Schematic representation of the competition assay.	50
Figure 4.3 Schematic representation of the pentamer and protomer interfaces.	51
Figure 4.4 Temperature breakpoints after thermal adaptation.	52
Figure 4.5 Correlation of the capsid breakpoint temperatures and inactivation rate constants at 55°C.	53
Figure 4.6 Location of the mutations linked to thermo-resistance.....	54
Figure 4.7 Effect of salt on the thermal stability on the founder virus.	56
Figure 4.8 Effect of salt on the pentamer and protomer interaction forces.....	58
Figure 4.9 Effect of salt concentration on the interaction forces at the pentamer interface of the founder population.	59
Figure 4.10 Effect of salt on the number of H bonds.	60
Figure 4.11 Effect of mutation on pentamer and protomer components.....	61
Figure A.1. UV ₂₅₄ inactivation curves for all viruses.	69

Figure A.2. Sunlight inactivation curves for all viruses.....	70
Figure A.3. Free chlorine (FC) inactivation curves for all viruses.	71
Figure A.4. Chlorine dioxide (ClO ₂) inactivation curves for all viruses.	72
Figure A.5. Heat inactivation curves for all viruses.	73
Figure A.6. Genome length normalization of k_{UV} and k_{SUN}	74
Figure A.7. Correlation of k_{FC} and k_{ClO_2} with exposed oxidizable amino acids.....	74
Figure A.8. Correlation of k_{FC} and k_{ClO_2} with guanosine content.	75
Figure A.9. Bayesian comparison of enteroviruses and MS2.	76
Figure A.10. Dynamic light scattering analysis on virus particles.....	77

List of tables

Table 1.1. Waterborne virus families.	3
Table 2.1. Viruses used in this study.	16
Table 4.1 Mutation after thermal-adaptation.....	54
Table 4.2 Structural parameters of thermo-adapted and founder strains.	57
Table A.1. Primer list.	66
Table A.2. Percentage of nucleotide identity.	67
Table A.3. Percentage of protein identity.	67
Table A.4. Kinetic inactivation parameters for individual virus strains.....	68
Table B.1. Primers couples for genome damage assay.....	78
Table B.2. Inactivation rate constants at 55°C.....	78
Table B.3. Inactivation rate constants at 30°C.....	79
Table B.4. Breakpoint temperature.....	79
Table C.1. Breakpoint temperature.....	80
Table C.2 Inactivation rate constant at 55°C.....	80

CHAPTER 1 INTRODUCTION

CONTEXT

A constant battle has always been waged between animals and viruses. Each time animals developed a natural immunity to avoid or interrupt an ongoing infection, viruses either found a hidden door or evolved to be unrecognizable to the host. Humans then developed vaccinations as an artificial immunity to prepare against potential future infections. Nevertheless, viral infections cannot be completely avoided by vaccines, so synthetic antiviral tools were developed that target specific steps of the viral replication cycle to assist in host recovery. Unfortunately, because certain types of virus remain relatively insensitive to those tools, humans resort to avoiding crossing paths with a virus through sanitation and prevention campaigns. Conscious efforts and investigations into minimizing viral transmission have been accomplished, but viruses still remain a major concern to human health, as they likely always will.

This study tackles viruses through sanitation studies, highlighting several issues caused by current disinfection methods as well as the implications of the content of the viral matrix. In addition, this study describes how the virus source can impact the efficiency of several disinfection methods and the virus's ability to adapt to thermal stress.

VIRUSES AND PICORNAVIRUSES

Background

What is a virus ?

Viruses are one of the smallest infectious agents and possess one of the widest ranges of potential hosts, including plants, bacteria, invertebrates, mammals and even other viruses. Their existence has been traced back at least 19 million years¹, and several studies highlight their significant contributions to human evolution^{2,3}. Viruses can be composed of an incredible number of different shapes, sizes, envelopes and genome types (Figure 1.1), and host invasions can lead to both symptomatic or asymptomatic infections^{4,5}. As an obligate parasite, the life cycle of the virus is entirely dependent on the host machinery, and its infection cycle can be divided into three main steps: viral entry, replication and shedding, which produces new progeny able to infect a host⁶. Even with vaccinations and the advent of antiviral medications, advanced mechanisms for hiding from the host immune system and their rapid adaptation rates mean that viruses are still a major public health concern⁶.

The question of whether a virus is a living organism is still hotly debated and relies mainly on the definition of life. Viruses can be seen as an inert, complex bag of proteins containing genetic information, as they have no metabolic activity and passively infect their host. Regardless, though, of if it is considered a living organism, the strength of a virus lies in the fact that as long as its components remain intact, it can remain infectious *ad (vitam) aeternam*. A notorious example is the discovery and isolation of an infectious virus from a 30,000 year-old permafrost in Siberia⁷. Therefore, the longer a virus persists, the higher the chances are of finding a new host.

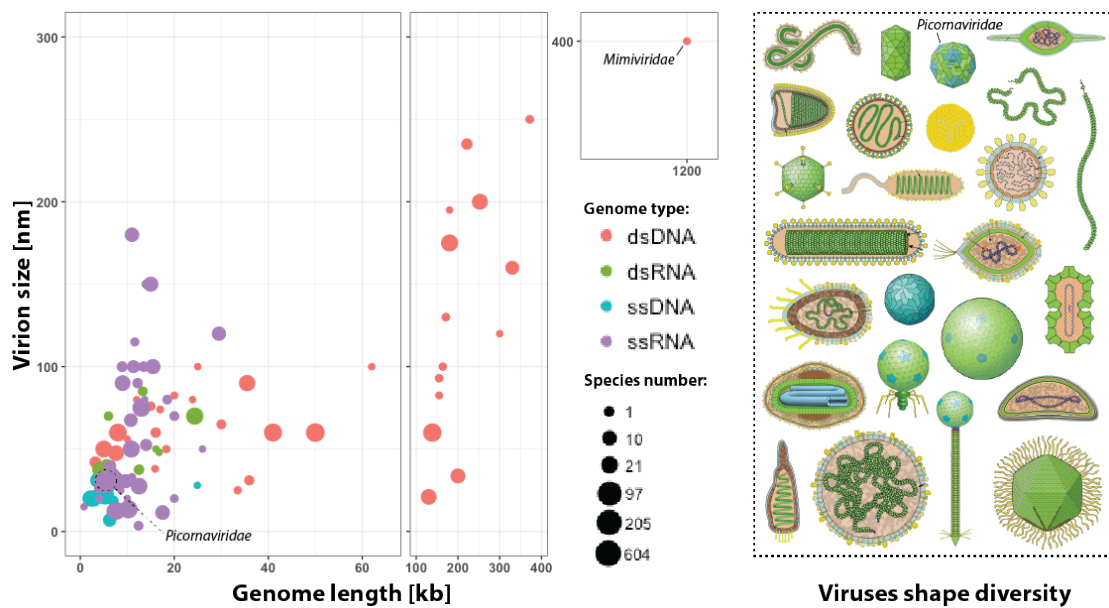


Figure 1.1. Viruses shape, size and genome diversity

This figure highlights the virus diversity. Left side: distribution of the virion size according to the genome length in kilobases (kb), the number of species (dot size) and genome type (dot color). Right side: images showing the virus's shapes diversity. The data and images were extracted from ViralZone⁸.

Waterborne viruses

The waterborne transmission of viruses is a major concern in public health due to the contact of potentially contaminated water by many ways (see "Transmission" section). Six families of waterborne viruses are generally considered, including the *Picornaviridae* family (Table 1.1), which is often implicated in disease outbreaks⁹ mainly due to the high prevalence of disease-causing species from the enterovirus genus of this family¹⁰. In seafood, it was found that even in low-level fecal contamination areas, 8% of oysters sampled were positive for enteroviruses¹¹, and these viruses also appeared to be responsible for 23% of the outbreaks involving recreational water (Sinclair et al. 2009 and

references therein¹²). The cause of this prevalence may be directly linked to the ability of enteroviruses to survive for longer periods in various environmental matrices, such as groundwater, marine water, or estuarine sediments^{13–15}.

Table 1.1. Waterborne virus families.

Table adapted from Rusinol et al. 2017.¹⁶

Family	Genus	Capsid size [nm]	Genome type	Genome size [kb]	Related diseases
Adenoviridae	Mastadenovirus	~ 90	dsDNA	35 - 36	Gastroenteritis, respiratory disease, conjunctivitis, cystitis
Astroviridae	Mastrovirus	~ 35	ssRNA (+)	6.8 - 7	Gastroenteritis, related to respiratory infections
Calciviridae	Norovirus	27 - 40	ssRNA (+)	7.3 - 8.3	Gastroenteritis
	Sapovirus				
Hepeviridae	Orthohepevirus	32 - 34	ssRNA (+)	7.2	Acute hepatitis
Picornaviridae	Enterovirus	~ 30	ssRNA (+)	7.1 - 8.9	Paralysis, meningitis, hand-foot-and-mouth disease, heart anomalies, skin rash
	Hepatovirus				Acute hepatitis
	Kobuvirus				Gastroenteritis
	Parechovirus				Gastroenteritis, respiratory infections, encephalitis, meningitis, hepatitis
Reoviridae	Rotavirus	60 - 80	dsRNA (+)	18.2 - 30.5	Gastroenteritis

Genetic and structural characteristics of picornaviruses

This study focuses on the *Picornaviridae* family, and more precisely, the genus *Enterovirus*. This genus is composed of small-sized non-enveloped viruses (~30 nm diameter) containing a positive single-stranded RNA genome coding for a single, open reading frame. The genome is composed of 5'- and 3'-end noncoding regions, a structural region coding for the capsid proteins, and a non-structural region containing the coding sequence of the viral polymerase and other functional proteins¹⁷. The icosahedral capsid is composed of 60 repeating protomers, which are each made up of four structural proteins (VP1 to VP4). The viral RNA-dependent RNA polymerase (RdRP) in these viruses is known for its lack of proofreading activity, which leads to a higher mutation rate per nucleotide compared to other DNA-genome viruses¹⁸. This low-fidelity replication combined with mutation robustness leads to an improved capacity for adaptation under specific selective events (i.e. tissue specificity or antiviral drug)¹⁹.

Serotypes, genotypes and non-polio enteroviruses

The current classification system based on genetic typing correlates well with the older serotyping technique²⁰ and divides the *Enterovirus* genus into 13 species consisting of 10 enteroviruses and 3 rhinoviruses²¹. Hence, the serotype names used herein were chosen as the ones most commonly appearing in the literature.

Since its discovery in the early 20th century and because it was the first enterovirus to be fully sequenced²², the poliovirus is one of the most studied of the genus *Enterovirus*. Since

then, a considerable number of non-polio enteroviruses (NPEVs) were discovered and became increasingly important pathogens with various serious symptoms and host tissue tropisms (Baggen et al. 2018 and references therein²³). Coxsackieviruses, enteroviruses, and echoviruses have become a growing issue while poliovirus cases gradually decreased^{24–26}.

Human infection, symptoms and shedding

With the exception of rhinoviruses, the primary infection site for enteroviruses is the gastrointestinal tract^{23,27}. This primary infection can be asymptomatic or lead to a systemic infection that invades various organs, even reaching the central nervous system²⁸. In consequence, various symptoms can develop, such as aseptic meningitis, acute flaccid paralysis, hand-foot-and-mouth disease or pericarditis (Table 1.1), all affecting mainly young infants and the immunosuppressed²⁹. Throughout an infection, a high titer of the virus is excreted to the environment through feces or vomit, with up to 10^6 median tissue culture infective dose (TCID50) per gram of stool (Rusinol et al 2017, and references therein¹⁶), which is then free to infect a new host.

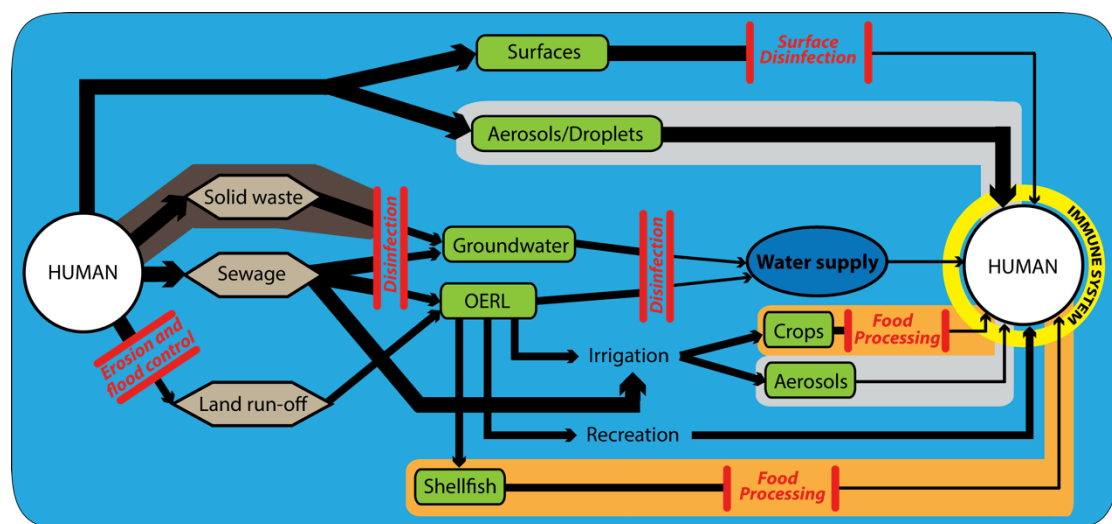


Figure 1.2. Waterborne virus transmission routes

Schematic representation of waterborne virus transmission routes (black lines) and the anthropogenic barriers implemented to avoid or diminish this transmission (red lines), and immunity barrier (yellow). The green boxes are the different existing matrices, and the color background represents the implication of the different means of virus transportation: brown for the solid transportation, blue for water-related transportation, orange for food related transportation, and grey for air-transmission. OERL: Ocean, Estuaries, Rivers and Lakes.

Transmission

After shedding from its current host, the usual enterovirus transmission route is fecal-oral but can also occur through various modes, such as aerosol, droplet, direct and indirect

contact transmission or by a combination thereof^{f30}. When the virus is released, it usually follows environmental indirect transmission that depends on the presence or absence of an urban sewage system, the quality of the treatment applied and on water reuse. As this route for viral transmission implies water as transport vehicle, we consequently call it “waterborne transmission”, which can occur via several waterborne transmission routes, as described in Figure 1.2. From human excretion, various aqueous environments can be contaminated, such as estuarine water, groundwater, rivers or lakes, and can consequently contaminate humans through water-related recreational activities, vegetables due to crop irrigation, seafood consumption, or simply through an insufficiently treated water supply³¹. It is at this point in the viral life cycle that a first efficient barrier in transmission can be implemented using a combination of different treatment methods, which are described in the next section.

DISINFECTION METHODS AND GUIDELINES

Disinfection

Common disinfection treatments and how they target a virus

Different oxidative and non-oxidative disinfection methods can inactivate viruses in the water by inducing damage that can block essential steps in the viral replication cycle. For example, damage to the capsid proteins can eliminate viral binding to its specific host cell receptor, even though the viral genome remains intact and the virus is infectious. Damage to genome will still allow the virus to enter the cell, but the RNA replication step could be inhibited. The most common methods for damage-inducing disinfection are photochemical inactivation (sunlight and UV-C), chlorine, chlorine dioxide, ozone and chloramine. Although these methods all have the same common outcome (inactivating the virus), they have different primary mechanisms for damaging the viral particle and are used in various different ways, meaning that a combination of them can optimize the overall effect on water disinfection.

Briefly, UV has been described as primarily inducing genome damage, whereas sunlight moderately targets the genome but affects the proteins to a larger extent, by direct inactivation, but can also be improved through an exogenous indirect inactivation by the addition of external sensitizers³². Chlorine targets both the genome and proteins, but the type of virus seems to significantly influence the balance between the two effects³³. Chlorine dioxide appears to exclusively target viral proteins, but here again, the rate constants are greatly affected by the type of virus³³. Ozone primarily targets the genome and only

secondarily affects the proteins, as indicated by a greater replication loss than binding loss after treatment³⁴.

Common uses of the disinfection methods

Viral inactivation via sunlight is mainly used in engineered treatment systems, such as waste stabilization ponds³⁵, constructed wetlands³⁶ and SODIS containers³⁷. UV-C treatment is widely used for drinking water disinfection, though, requires meticulous turbidity control to be efficient for wastewater treatment³⁸. Chlorine, chloramine, chlorine dioxide and ozone are commonly used in tertiary wastewater treatment as well as drinking water treatment³⁹. Sometimes, chloramine is preferred over chlorine as it has a longer persistence in the distribution system⁴⁰. Chlorine dioxide is also preferred over chlorine due to a lower amount of toxic by-product formation, even though it has a much lower persistence⁴¹. Ozone is a strong oxidant that reacts with all waterborne pathogens in a short contact time with no residual agents, though the cost of using this method is high, and it must be generated on-site for safety issues. Furthermore, its high reactivity creates a challenging problem for measuring viral exposure to low ozone concentrations⁴².

Downsides of disinfection

The application of these different methods should not be taken lightly, as they all contain certain downsides. For example, beyond a certain concentration, these disinfectants can cause eye, skin, and respiratory problems⁴³, with the persistence of chlorine and chloramine in water used for dialysis patients potentially causing hemolytic anemia⁴⁴. This means medical facilities must control their incoming water, as a strong discrepancy exists in the standards for drinking water and dialysis water⁴⁵. A high chlorine concentration also appears to negatively impact marine biodiversity at the discharge sites of disinfected urban wastewaters⁴⁶. Additionally, disinfection can lead to the formation of disinfection by-products that can be toxic for human health⁴⁷.

For these reasons, the Environmental Protection Agency (EPA) implemented upper concentration limits to constrain the direct effects of these disinfection methods on the environment and human health, and substantial research efforts are currently being conducted on the issue of disinfection by-products (Richardson et al. 2007, and references therein⁴⁸). An equilibrium between efficient viral inactivation and limiting the drawbacks is required and can be improved by experimentally measuring the disinfection sensitivity of the different pathogens (*Ct values*, described in the next section)⁴⁹.

Ct value guidelines, advantages and disadvantages

The *Ct value* is the disinfectant concentration (C) multiplied by the pathogen contact time (t) that results in a certain \log_{10} reduction of the pathogen. This allows for a comparison of viral disinfection sensitivities from one study to another and provides dose threshold guidelines for water treatment plants. As an example, enteroviruses can be found at concentrations of up to 10^3 genome-copies/liter of tertiary wastewater effluent¹⁶. Hence, a disinfectant dose corresponding to at least 3- \log_{10} of virus removal could be applied, which would consequently improve treatment accuracy and limit useless disinfectant overloads.

Unfortunately, the real-life application of these *Ct value* guidelines can be complex. In addition to the type of virus, the temperature, and the pH, many other factors can greatly affect the interactions between the pathogen and the disinfectant, such as the organic and inorganic content of the water⁵⁰. Furthermore, rainfall, time of day and other special events (i.e. wine harvest period) can drastically change the treatment efficiency^{51,52}.

Ct value database

Implementation and benefits of a Ct value database

To have a global overview of viral disinfection in the literature, we built a database containing the *Ct values* for different waterborne viruses from 1 to 4- \log_{10} inactivation and recounted all the factors capable of influencing this value. To do this, the temperature, pH and matrix type were recorded, as well as other factors, such as the genome type and length, the taxonomy of each virus and their source (laboratory strain, environmental isolate or clinical isolate). This database was built by completing and correcting the existing *Ct value* list from the Guillot & Loret book⁵³. However, it has to be noted that this database is still unfinished, and the results found in this thesis were not included. At the moment, it records 571 *Ct values* from 51 studies.

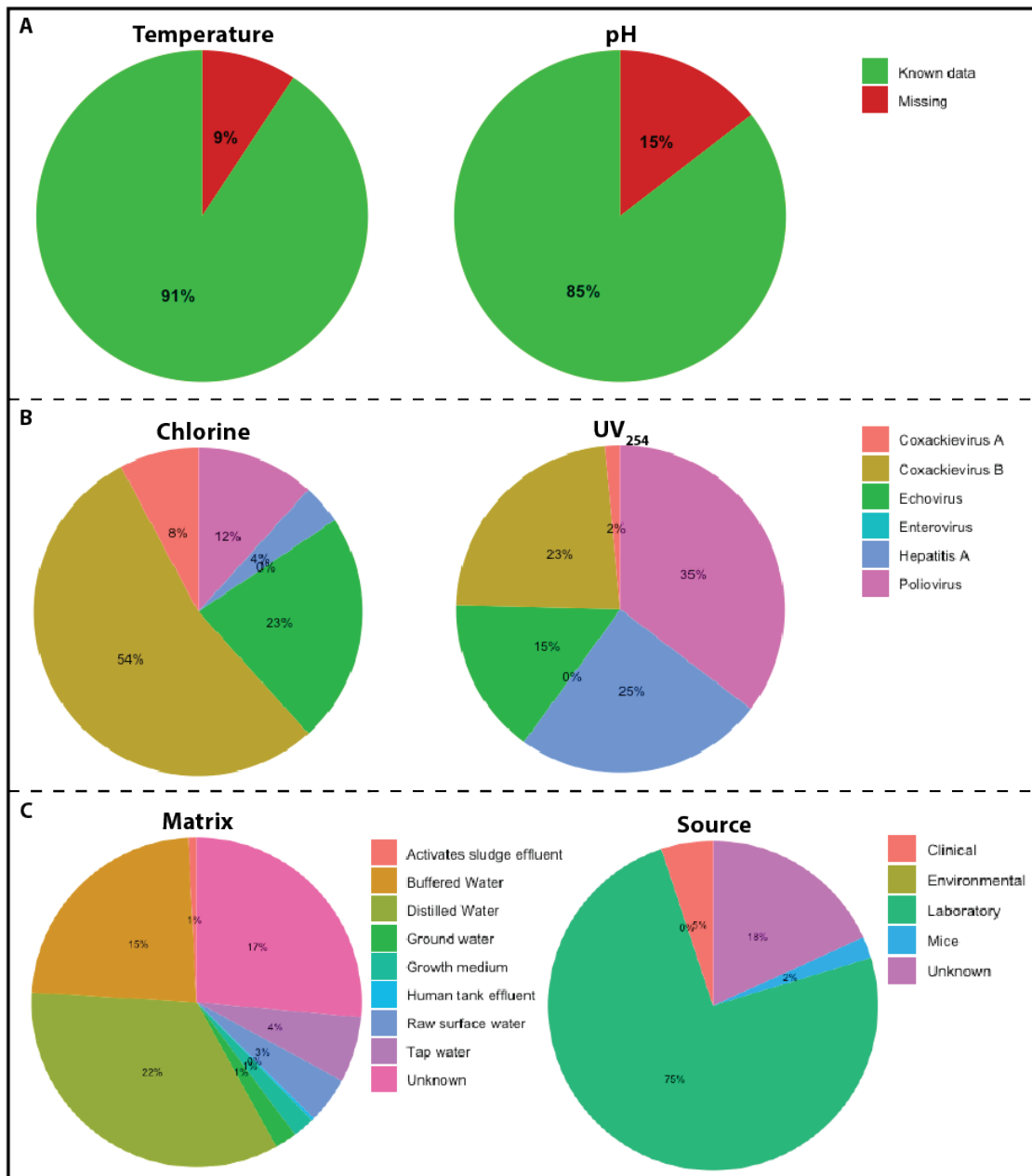


Figure 1.3. Database quality

This figure represents the current quality state of the database, and the problematic discrepancies within specific factors. (A) Percentage of missing information for the temperature and pH. (B) Over- and under-representation of various viruses within the *Picornaviridae* family for chlorine and UV₂₅₄ disinfection treatments. (C) Over- and under-representation of different matrices as well as the virus sources used for the studies included in this database.

Database quality: missing data and under- and over-representations

The first problem encountered when building the database was the amount of missing data among the major factors, such as the matrix type, pH, temperature and viral strain. The

percentages of missing values ranged from 9 to 15% of the total number of records (Figure 1.3A) and occurred mainly due to simple omissions of the research scientists and publishers. The second problem observed in database construction was the under- or over-representation of certain types of data among the different factors. A clear discrepancy within *Picornavirus* serotypes and genus representations between UV and chlorine could be observed (Figure 1.3B), with significantly more coxsackievirus B and echovirus serotypes with data on chlorine than UV disinfection, and more poliovirus and hepatitis A with data on UV than chlorine disinfection. In terms of the matrix factor, buffered water and distilled water were also over-represented in the whole database (Figure 1.3C), making it difficult to always apply these values to real-world scenarios. Finally, a major discrepancy in the source of the viruses exists, with at least 82% of the data coming from laboratory strains, clinical isolates and mice, and no records of environmental isolates were found (Figure 1.3C). This last point may be the most problematic, as the variability in disinfection resistance between laboratory strains and environmental strains is unknown.

Database results: Notes on UV and chlorine

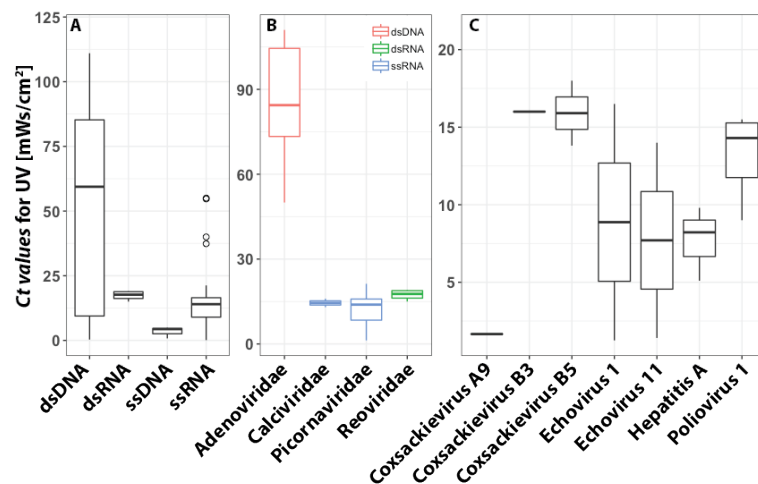


Figure 1.4. Ct value database output for UV₂₅₄.

Discrepancy of the Ct values depending (A) on the genome type, (B) on the virus family, and (C) within the *Picornaviridae* family. The data displayed here are for 2- \log_{10} inactivation.

According to the literature, the amount of UV damage to nucleic acids depends on their type and structure, with the photolysis rate constants exhibiting the following trend, from most to least sensitive: ssDNA > ssRNA \approx dsDNA > dsRNA⁵⁴. Interestingly, the trend observed through the database was similar except for dsDNA viruses, which appeared the least sensitive to UV and had a high variability in the Ct values (Figure 1.4A). Here, the viral genome type is responsible for the differences in UV sensitivity, which can explain the differences observed between the different waterborne virus families (Figure 1.4B). Within the *Picornaviridae* family, the Ct values were highly variable depending on the serotype, with coxsackievirus B5 and B3 displaying the highest resistance (Figure 1.4C).

For chlorine, the effect of temperature and pH could be observed in the *Ct values*. A higher temperature increased the inactivation efficiency, while a higher pH decreased it (Figure 1.5A). Between the different waterborne viruses, *Picornaviridae* displayed the highest resistance to chlorine, and a great variability was observed (Figure 1.5B). Within this family, coxsackievirus A2 was the most resistant serotype followed by coxsackievirus B5 (Figure 1.5C).

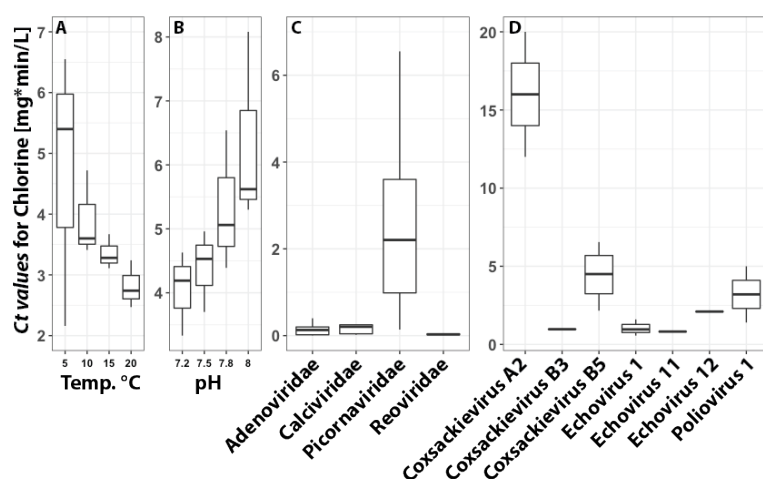


Figure 1.5 *Ct value* database output for chlorine.

Effect of the temperature (A) and pH (B) on the fluctuation of the *Ct values* for coxsackievirus B5. Discrepancy of the *Ct values* depending on the virus family (C) and within the *Picornaviridae* family (D). The data displayed here are for 2- \log_{10} inactivation.

Matrix- and virus-related resistance mechanisms

Matrix-related resistance

Different matrices can greatly influence the sensitivity of the virus to disinfection, as previously seen with pH and chlorine (see section Database results: Notes on UV and chlorine). Environmental matrices significantly increased the survival rate of enteroviruses¹³⁻¹⁵. The adsorption to different particles present in the various matrices, such as wastewater sludge, aquatic sediment or soil, significantly increased the required dose of UV and chlorine (Templeton et al. 2008, and references therein⁵⁵). Furthermore, a higher protein and fat content enhanced viral resistance in food processing⁵⁶.

Virus-related resistance

As previously described with the genome type, factors exclusive to the virus can change their sensitivity to a disinfectant (i.e. ssDNA versus ssRNA). (1) The adsorption, although also linked to the matrix type, can vary from one virus to another⁵⁷. The authors described distinctive viral capsid isoelectric points that should impact the adsorption efficiency, thus impacting the disinfection. (2) Also linked to the type of matrix, viral aggregation increases viral resistance to chemical disinfection by keeping viruses alive due to being protected at

the center of the aggregate⁵⁸. (3) Viral recombination was also described as a possible resistance mechanism to UV-induced genome damage by genetic strand exchange occurring after host entry⁵⁹. However, this resistance mechanism requires a high multiplicity of infection during the host infection process, which is rarely the case upon environmental exposure. (4) Viral adaptation through mutation enhances its resistance to disinfection⁶⁰, occurring through events such as an amino acid changing to one less reactive to chlorine. Finally, (5) a virus with mutation robustness may also be more resistant to genome damage by preserving its phenotype despite a high rate mutagenesis⁶¹.

Missing information and unanswered questions

The main concern herein is the lack of information on currently circulating environmental strains and their resistance to disinfection. This issue, as raised previously (see section Database quality: missing data and under- and over-representations), can lead to inaccurate guidelines for water treatment plants and must be resolved. Also, a high variability in disinfection sensitivity can be observed between different enteroviruses strains, but the reasons for this are unknown.

Second, the mechanisms behind viral viability and the relationship with the matrix are not completely understood. The effect of specific factors, such as pH, ionic strength and temperature, are not well understood, and their exact mechanism of action and subsequent effects on the different viral components are unknown.

Finally, the long-term persistence of a virus in various matrices may depend on its capsid stability. Therefore, a selection of the most stable capsid variant may occur in the environment, but this has not been tested.

RESEARCH OBJECTIVES AND APPROACH

Chapter 2. Variability in disinfection resistance between currently circulating enterovirus B serotypes and strains.

The main objectives of this chapter are to evaluate the accuracy of laboratory strains in modeling the disinfection of currently circulating enteroviruses isolated from untreated domestic sewage and to quantify the extent of variability among those isolates.

Chapter 3. Effect of salt and pH on virus thermostability.

The main objective of this chapter is to determine which simple matrix factors affect viral thermoresistance and which virus components are targeted according to the specific

conditions. Acid to alkaline pH, high and low temperatures (55 and 30°C) and low to high ionic strengths will be tested on both laboratory strains and environmental isolates.

Chapter 4. Structural mechanisms causing heat resistance mediated by thermal adaptation or salt.

In this chapter, we determine whether a virus can increase its capsid stability through heat adaptation and seek to understand the effects of the selected mutation on the structural features of the capsid. The effect of ionic strength on the capsid features will be tested by structural modeling. Several specific capsid changes will be investigated, such as the number of hydrogen or disulfide bonds or changes in the electrostatics.

CHAPTER 2 VARIABILITY IN DISINFECTION RESISTANCE BETWEEN CURRENTLY CIRCULATING ENTEROVIRUS B SEROTYPES AND STRAINS

A modified version was published as:

Meister, S., Verbyla, M. E., Klinger, M., & Kohn, T. (2018). Variability in Disinfection Resistance between Currently Circulating Enterovirus B Serotypes and Strains. *Environmental Science and Technology*, 52(6), 3696–3705. <http://doi.org/10.1021/acs.est.8b00851>

Copyright [2018] American Chemical Society

To view the published open abstract, go to <http://dx.doi.org> and enter the DOI

Experimental design and data analysis were performed by Meister S.; Inactivation experiments were performed by M. Klinger and Meister S.; Bayesian modeling was implemented by Verbyla M. E.

INTRODUCTION

Human enteric viruses are a leading cause of waterborne disease worldwide⁹. Their control remains problematic; compared to bacterial pathogens and fecal indicators, viruses are highly persistent in the environment⁶² and have high resistance to disinfectants such as chlorine⁶³. The Enterovirus genus of the Picornaviridae family in particular is a major source of the waterborne disease burden⁶⁴ and hence was included on the EPA contaminant candidate list (EPA, CCL4⁶⁵). Within this genus, species of concern include Enterovirus A, which contains coxsackievirus A serotypes, Enterovirus B, which includes serotypes of echovirus and coxsackievirus B, and Enterovirus C, which includes poliovirus and other coxsackievirus A serotypes^{20,66}.

Serotypes of the Enterovirus genus are generally more resistant than other enteric viruses to chlorine^{67,68}. The different species and serotypes of this genus, however, have a wide range of susceptibilities to disinfection. For example, differences in chlorine resistance were observed between the serotypes coxsackievirus B4 (CVB4) and B5 (CVB5), as well as poliovirus serotypes (PV) 1, 2 and 3⁶⁹, with CVB5 displaying the highest resistance. Similarly, disinfection by monochloramine exhibited up to three-fold greater inactivation rates of serotypes coxsackievirus B3 (CVB3) compared to CVB5, and more than 100-fold greater rates for serotypes echovirus 1 (E1) compared to 11 (E11)⁶⁸. Finally, disinfection of wastewater effluent by chlorine dioxide (ClO₂) revealed that CVB5 was more resistant than echovirus 1 and PV 1 serotypes⁷⁰. More surprisingly, differences were also observed among strains of the same poliovirus serotype^{71,72}, revealing variability even among closely related viruses. Combined, these studies indicate that differences in resistance to oxidizing disinfectants exists between the different Enterovirus species, between serotypes and even within

serotypes. In contrast, similar susceptibility was found among different enteroviruses to UV light and sunlight^{73,74}.

The reason for variability in Enterovirus susceptibility to oxidants is not well understood, yet it may be driven through selection by the disinfectant for the most resistant variants. For example Bates et al.⁷⁵ demonstrated that the repeated exposure of PV to chlorine led to increased resistance. Similarly, Shaffer et al.⁷⁶ reported that PV isolated from chlorinated drinking water were more resistant to chlorine than unexposed lab strains. More recently, our group has repeatedly exposed echovirus 11 to UV₂₅₄ which resulted selection of UV₂₅₄ resistant strain. Similarly, repeated exposure of echovirus 11 to UV light at 254 nm (UV₂₅₄) led to the selection of UV₂₅₄-resistant strains⁷⁷. Selection of disinfection-resistant viruses may also arise from exposure to environmental stressors. Specifically, Payment et al.⁶⁹ demonstrated that sewage isolates of CVB5 were more resistant to chlorine compared to the corresponding lab strains. Tree et al.⁷⁸ furthermore demonstrated that sewage-borne PV were more resistant to chlorination compared to lab strains.

While it has been previously been reported that disinfection resistance can vary between environmental isolates and laboratory strains, as well as between and within different virus serotypes, the extent of this variability is poorly understood, in particular for environmental isolates. However, to establish adequate disinfection practices, it is important that the diversity in disinfection kinetics of circulating viruses is taken into account. To this end, we isolated nine strains of Enterovirus B from untreated domestic sewage from three geographic locations (Lausanne, Switzerland, Minneapolis, MN and Tampa, FL), and compared their disinfection kinetics with those of two laboratory strains (echovirus 11 Gregory strain and coxsackievirus B5 Faulkner strain). Additionally, inactivation kinetic parameters were compared to those of MS2 bacteriophage, which has been proposed as a surrogate for enteric viruses for the assessment of household water treatment interventions (including chlorination, UV, solar disinfection, and heat treatment)⁷⁹. All viruses were subjected to inactivation by five different treatments of which two mainly act by inducing genome damage (UV₂₅₄ and simulated sunlight), two target both the viral genome and proteins (FC and ClO₂), and one (heat) induces non-oxidative protein denaturation⁶⁰. The ultimate objective of this study was to quantify the extent of variability in disinfection resistance for different Enterovirus B serotypes and strains, as well as for different inactivation methods, and to assess if surrogate viruses can be used to represent the inactivation of circulating viruses.

EXPERIMENTAL SECTION

Isolation of circulating viruses

Viruses were isolated from one liter of untreated domestic sewage from three wastewater treatment plants (Lausanne, Switzerland, Minneapolis, MS, and Tampa, FL), as described previously⁸⁰⁻⁸³. Insoluble contaminants were removed by adding 110 mL of glycine buffer (1M glycine, 3M NaCl, miliQ H₂O, pH9.5), stirring on ice for 20 min, and then centrifuging for 30 min at 6700×g at 4°C. The supernatant was transferred to a clean bottle, the pH was adjusted to 7.2 with HCl, 200 mL of polyethylene glycol (PEG) 8000 (40%) were added and samples were stirred overnight at 4°C. Samples were then centrifuged for 40 min at 4°C, then the supernatant discarded and the pellet was resuspended in 15 mL of phosphate-buffered saline (PBS; 5 mM NaH₂PO₄, 10 mM NaCl, pH7.4). To remove PEG and macromolecular inhibitors, the solution was vigorously mixed with 15 mL chloroform and centrifuged for 15 min at room temperature. The upper phase was harvested, filtered through a 0.45 µm filter (hydrophilic polyethersulfone filter; Millipore), and concentrated to 1.7 mL using an Amicon 100 kDa molecular weight cutoff column (Sigma-Aldrich, Germany). Buffalo Green Monkey Kidney (BGMK) cells were grown to confluence in T25 flasks (TPP Techno Plastic Products, Trasadingen, Switzerland) as described previously⁸⁴, were infected with the concentrated viruses diluted in cell culture media (see SI) at a 1:10 ratio, and the cytopathic effect (CPE) was checked daily. After full CPE was observed (around four days post-infection), the cell lysate was harvested and viruses were clarified by centrifugation. Finally, two successive plaque assays were performed to isolate individual virus strains (see SI for details).

Virus identification, whole genome sequencing and alignment

To identify the virus serotypes isolated, general enterovirus Inosine-degenerated primers targeting the viral protein 1 (VP1) were used⁸⁵. The PCR amplicon size was first controlled by agarose gel, then sequenced by Sanger technique using the same primers. The resulting sequences were identified by the NCBI basic local alignment search tool (BLAST). Whole genome sequencing of the CVB5 isolates was accomplished first by aligning 86 CVB5 complete genomes listed in the ViPR⁸⁶ database. Several primer couples were designed along the consensus sequence and used to sequence the whole genome of each isolate (Table 1). CVB4 isolates were sequenced with primers designed according to a single CVB4 sequence (accession number: S76772⁸⁷), and CVB1 was sequenced with CVB5-derived and

strain-specific CVB1 primers. Virus genome sequences were controlled, aligned, assembled, and annotated using the Geneious software version 8.1.8⁸⁸.

The whole sequence of VP1 was used to align the different viruses and calculate their pairwise identity using multiple sequence comparison by log-expectation (MUSCLE)⁸⁹ with an iteration of 8, a gap open penalty of 400, and a gap extension penalty of 0. An unrooted tree was built using the neighbor-joining estimation method⁹⁰. The protein pairwise identity was determined using the translated region of the structural proteins (VP1 to VP4).

Table 2.1. Viruses used in this study.

Serotype, genus, strain, and isolation location of viruses used in this work. The environmental isolates are named according to first letter of the city (Minneapolis, Tampa, or Lausanne) and the isolation date (month/day/year).

Name	Serotype	Genus	Location	Strain	Access.No
MS2		Levivirus	Lab strain	ATCC 15597-B1	NC001417
Echovirus 11	Echovirus 11	Enterovirus	Lab strain	ATCC-Gregory	X80059
CVB1-L071615	Coxsackievirus B1	Enterovirus	Lausanne	Env. isolate	MG845887
CVB4-M063015	Coxsackievirus B4	Enterovirus	Minneapolis	Env. isolate	MG845888
CVB4-T051217	Coxsackievirus B4	Enterovirus	Tampa	Env. isolate	MG845889
CVB5-Faulkner	Coxsackievirus B5	Enterovirus	Lab strain	ATCC-Faulkner	AF114383
CVB5-L030315	Coxsackievirus B5	Enterovirus	Lausanne	Env. isolate	MG845890
CVB5-L060815	Coxsackievirus B5	Enterovirus	Lausanne	Env. isolate	MG845891
CVB5-L061815	Coxsackievirus B5	Enterovirus	Lausanne	Env. isolate	MG845892
CVB5-L070215	Coxsackievirus B5	Enterovirus	Lausanne	Env. isolate	MG845893
CVB5-L070915	Coxsackievirus B5	Enterovirus	Lausanne	Env. isolate	MG845894
CVB5-M063015	Coxsackievirus B5	Enterovirus	Minneapolis	Env. isolate	MG845895

Virus purification and enumeration

To prepare viral stock solutions, each strain was individually amplified in BGMK cells, purified by PEG precipitation and chloroform treatment⁹¹, concentrated, and divided into aliquots of 100 µL. At least two separate amplifications stocks were preformed per virus. Viruses in all stock solutions were analyzed by dynamic light scattering as described previously⁵⁹ and were found to be generally monodispersed at pH 7.4 and aggregated at pH 3 (Figure A.10). Unfortunately, the viruses stock concentrations used for the DLS measurements did not allowed a proper identification of monodispersed viruses at neutral pH (Figure A.10). Infective virus concentrations were determined by endpoint dilutions with Most Probable Number (MPN) statistics⁹², and are reported as most probable number of cytopathic units per mL (MPNCU·mL⁻¹). Endpoint dilutions were performed on BGMK cells in 96-well plates, with five replicates and eight dilutions per experimental sample. After inoculation, plates were incubated at 37°C with 5% CO₂, and the presence or absence of CPE in each well was determined five days post-infection through microscopy. MS2

bacteriophage was propagated, purified by PEG and chloroform, and enumerated using the double agar layer plaque assay method as described previously⁹¹, and its infectivity was measured in plaque forming units per mL (PFU·mL⁻¹).

Inactivation experiments

Inactivation experiments were performed two to four times per virus and disinfectant, and eight samples were taken to construct each inactivation curve. All experiments were performed in PBS at an initial virus concentrations of 10⁷ to 10⁸ MPNCU·mL⁻¹ or PFU·mL⁻¹.

UV₂₅₄.

A low-pressure monochromatic UVC lamp was used to test the virus inactivation at a wavelength of 254 nm (UV₂₅₄). A bench scale device containing a 17 W mercury UV lamp (Philips, TUV F17T8) with a manual shutter was used. Two mL of PBS were added to a darkened glass beaker, were spiked with viruses, and were exposed to UV₂₅₄ for up to four minutes under constant stirring. Aliquots of 100 µL were harvested every thirty seconds. The UV₂₅₄ fluence rate was measured by iodide/iodate actinometry^{93,94}, and corresponded to 1.398 W·m⁻².

Simulated sunlight.

Sunlight was simulated using Sun 2000 (Abet Technologies) equipped with a 1000W Xenon lamp, an AirMass 1.5 filter, and a 2 mm atmospheric edge filter. The irradiance spectrum was determined using a radiometer (ILT 900-R; International Light Technologies, Peabody, MA). The average UVB fluence rate was calculated by integrating the irradiance from 280 to 320 nm corresponding to 0.563 W·m⁻². For typical 12-hour exposure, this corresponds to four times the equatorial UVB fluence determined elsewhere⁹⁵. 100 µL of virus concentrate were added to 10 mL of PBS in a glass beaker immersed in a 22°C temperature-controlled water bath, and were exposed to simulated sunlight under constant stirring. Samples of 100 µL were taken each 2-3 hours over the course of up to 24 hours.

Free chlorine.

Prior to experiments, 10 mL glass beakers were incubated overnight in a concentrated FC solution to quench any chlorine demand. The FC working solution was prepared by diluting bleach solution (15% HOCl) in PBS to a final concentration between 0.8 and 3.1 mg·L⁻¹. The FC concentration was measured by the N,N-diethyl-p-phenylenediamine colorimetric method⁹⁶ at the beginning and end of each experiment, and typically varied by less than 20% throughout the experiment. Therefore the average of the initial and final FC concentration in each experiment was considered as the working concentration. Prior to each experiment,

beakers were rinsed twice with the working solution. Then 50 μL of virus stock solution were spiked into a 2 mL working solution under constant stirring. 10 μL aliquots were harvested every 10-30 seconds over the course of 3 minutes, and were directly mixed with 90 μL PBS containing 1.4 M sodium thiosulfate to quench the residual FC. The initial virus concentration was sampled from a 2 mL PBS solution without FC spiked with 50 μL virus stock.

Chlorine dioxide.

A concentrated ClO_2 solution was obtained by mixing 100 mL 4% $\text{K}_2\text{S}_2\text{O}_8$ with 100 mL 2% NaClO_2 as described elsewhere³³, and was kept at 4 °C. ClO_2 concentrations were measured by spectrophotometer (UV-2550; Shimadzu) at 358 nm. The concentrated solution was mixed with PBS in order to obtain a supply solution (4-7 $\text{mg}\cdot\text{L}^{-1}$) and a working solution (0.25-1 $\text{mg}\cdot\text{L}^{-1}$). All beakers were rinsed three times with the working solution. Then 2 mL of working solution were amended with 50 μL of virus stock solution under constant stirring. Throughout the experiment, the ClO_2 concentration was maintained approximately constant ($\pm 7\%$) by continuously adding the supply solution with a syringe pump at a flow rate of 5-20 $\mu\text{L}\cdot\text{min}^{-1}$. The sampling procedure, ClO_2 quenching, and measurement of the initial virus concentration were performed as described for FC.

Heat.

Inactivation experiments by heat were performed in a PCR thermocycler (Applied Biosystems, GeneAmp PCR system 9700). PCR tubes containing 90 μL of PBS were heated to 55°C, then 10 μL of virus stock solution was spiked into each tube. At each time point, a sample was removed and quickly placed in an aluminium PCR cooling block on ice. The initial virus concentration was measured by spiking 10 μL of viruses in 90 μL of PBS at room temperature.

Inactivation Rate Modelling

The rates of infectivity loss for all viruses and disinfectants (except heat) were modeled by first-order kinetics according to the Chick-Watson model^{97,98}, where k is the decay rate constant, C is the concentration (or fluence rate) of the disinfectant, N is the concentration of viruses at time t , and η is the coefficient of dilution, assumed to be equal to one:

$$(1) \quad \frac{\partial N}{\partial t} = -kC^\eta N$$

Given that C was approximately constant in our experimental systems, the integration of Equation 1 gives the following,

$$(2) \quad N = N_0 e^{-kCt}$$

where Ct is the dose, and the decay rate constants (k) have the units $\text{mJ}^{-1} \cdot \text{cm}^2$ (for UV₂₅₄ and sunlight), and $\text{mg}^{-1} \cdot \text{min}^{-1} \cdot \text{L}$ (for FC and ClO₂).

Exponential rates of infectivity loss by ClO₂ and heat were modeled by segmental regression, according to the following equation,

$$(3) \quad N = N_0 e^{-k_1 Ct} + N_1 e^{-k_2 Ct}$$

where N₁ is the breakpoint (the virus concentration at which kinetics deviate from the initial exponential decay), and k₁ (hereafter denoted as k_{ClO₂} or k_{heat}) and k₂ are the rate constants associated with inactivation before and after the breakpoint. Here, Ct is the dose in $\text{mg}^{-1} \cdot \text{min}^{-1} \cdot \text{L}$ for ClO₂ and sec^{-1} for heat.

Bayesian analysis of rate constants

The probabilities associated with the values of k were estimated using Bayesian inference (Figure 2.3 and Figure A.9). The probability of one virus strain or serotype being more or less resistant than another was calculated as the difference between the posterior distributions of the two inactivation rate constants. Bayesian inference was used instead of conventional hypothesis testing (e.g., with p-values and confidence intervals) to provide a more intuitive assessment of the probabilities that a given virus has an inactivation rate constant, and hence a disinfection resistance, that differs from a reference virus considered (e.g., CVB5 Faulkner strain). Furthermore, the use of Bayesian inference allows for the reduction of uncertainty in the rate constant by utilizing raw endpoint dilution data (number of positive wells in a given dilution sample) directly in the model a likelihood model⁹⁹, instead of using MPN values from different dose levels as “data” to fit a log-linear inactivation curve using the least squares method. For the analysis of combined serotypes, k distribution of each virus from each serotype were pooled and 30'000 values were randomly sampled from this pool for the proper calculation of posterior distribution difference.

Data analysis

All computations of kinetic parameters and pairwise identities were performed using the statistic software R¹⁰⁰, supplemented with JAGS for Bayesian analysis¹⁰¹. The following CRAN packages were used: ggplot2¹⁰², gridExtra¹⁰³, rjags¹⁰⁴, segmented¹⁰⁵, seqinr¹⁰⁶, sjPlot¹⁰⁷, bbmle¹⁰⁸, coda¹⁰⁹, msa¹¹⁰, ape¹¹¹, ggtree¹¹².

RESULTS AND DISCUSSION

Virus Isolation

A total of nine virus strains were isolated from untreated domestic sewage. By sequencing their whole genomes, five isolates were identified as serotype coxsackievirus B5, two as serotype coxsackievirus B4 and one as serotype coxsackievirus B1. All CVB5 isolates belong to genotype IV, which mostly contains viruses isolated after 1984, whereas the Faulkner strain, which was isolated in 1952, belongs to genotype I¹¹³. The different isolates were named according to the isolation date and the first letter of the city they were isolated from (Table 2.1).

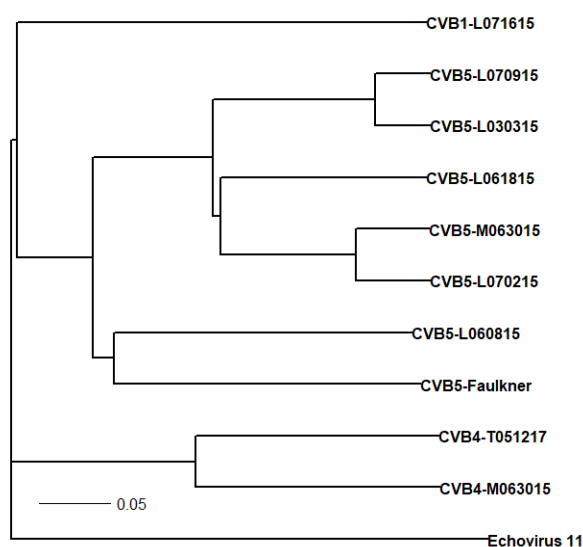


Figure 2.1. Unrooted neighbour joining tree.

This tree is built based on the virus VP1 coding region of the virus studied. The horizontal line lengths are proportional to the genetic distance (see Table A.3). The four serotypes represented can be clearly differentiated by their genetic distance.

The genetic distance between isolates, determined by comparison of their VP1 genes, is illustrated in a neighbor-joining tree (Figure 2.1). All CVB5 isolates exhibited 79.1-99.4% pairwise identity, whereas they shared 76.8-81.7% with the CVB5 Faulkner strain (Table A.3). This discrepancy can be explained by the different year of isolation of the CVB5 isolates and the Faulkner strain (2015 versus 1952 respectively), and their different genotypes (IV versus I, respectively). The CVB4 isolates had 88.1% identity among each other, and shared 63.4-66.1% with CVB5 isolates. The single CVB1 isolate (CVB1-L071615) shared 61.3-67.6% identity with all other viruses. Finally, E11 exhibited the greatest genetic distance, sharing only 59.3-62.2% of its VP1 gene with the other viruses considered. At the protein level, the pairwise identity among CVB5 environmental isolates corresponded to 99%, but was only 92 and 90% when compared to CVB4 isolates and E11, respectively (Table A.4). The distribution of isolated serotypes is consistent with literature reporting that CVB5 is the most recurrent enterovirus, with high isolation frequencies¹¹⁴ and high annual prevalence^{115,116}.

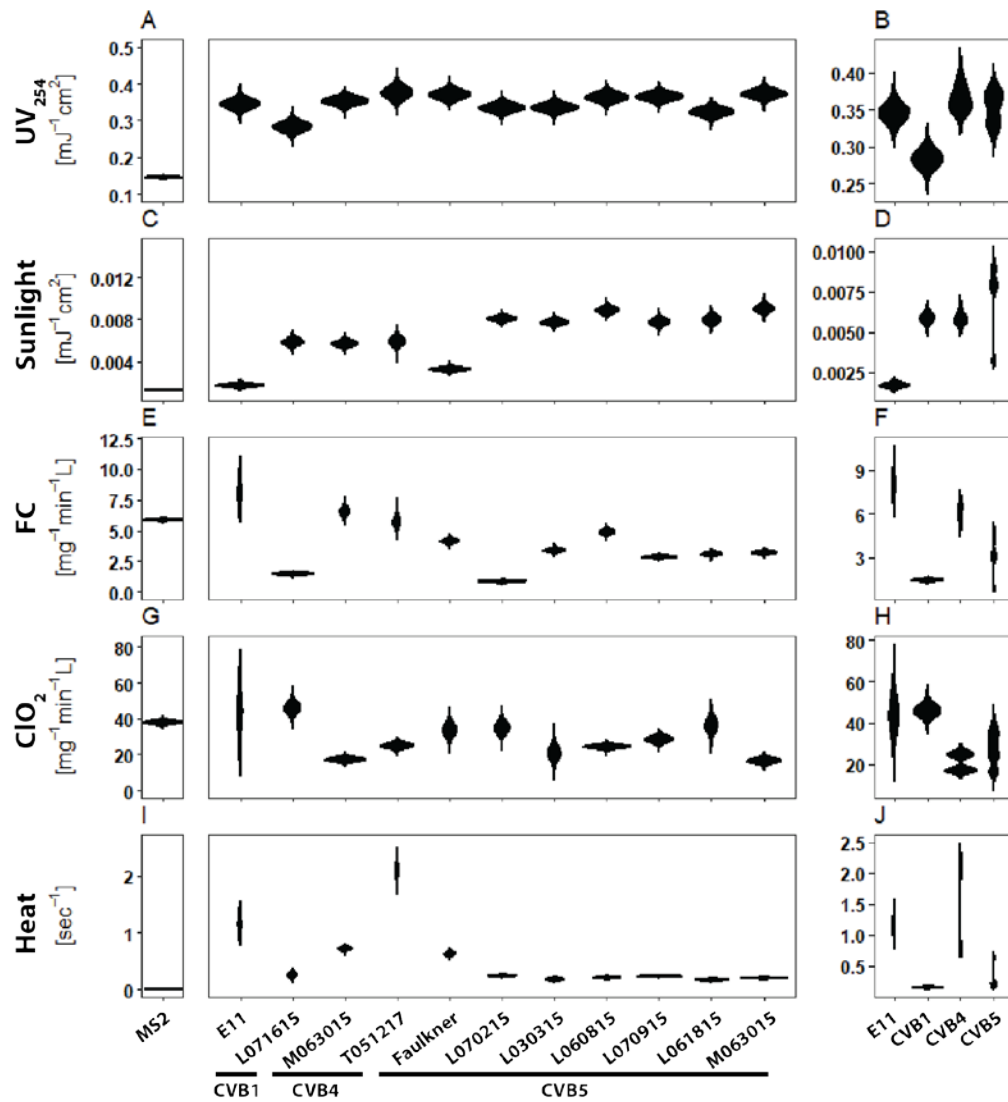


Figure 2.2. Violin plot of inactivation rate constant distribution.

Violin plots of showing the distribution and probability density of rate constants k associated with inactivation by UV_{254} (panels A and B), sunlight (C and D), FC (E and F), ClO_2 (G and H) and heat (I and J). The values of k for individual viruses (MS2 and all enteroviruses) are shown in the left panels. The right panels show the probability distribution of grouped serotypes (E11, CVB1, CVB4, and CVB5). The exact values of k are given in **Table A4.**

Inactivation kinetics

The distributions of the inactivation rate constants for all viruses and treatment methods studied is shown in Figure 2.2. The values of the inactivation rate constants, along with the inactivation curves and associated statistics, are shown in the annexes (Table A.4. and Figure A.1 to Figure A.5). From these data it is evident that variability exists among different viruses in their susceptibility to disinfectant, and that the extent of this variability differs between the inactivation methods tested. An ANCOVA analysis furthermore confirmed that the

observed rate constant were consistent between experimental replicates, even if stock solutions produced by different amplification were used (see A).

UV and Sunlight inactivation.

Inactivation by UV₂₅₄ and sunlight were first-order with respect to fluence (Figure A.1. and Figure A.2). The mean UV₂₅₄ inactivation rate constants (k_{UV}) for all enteroviruses tested ranged from 0.28 to 0.38 $\text{mJ}^{-1}\cdot\text{cm}^2$ (Figure 2.2A). These rate constants are consistent with those previously reported for different enteroviruses (Hijnen et al. 2006, and references therein¹¹⁷). If only strains of the CVB5 serotype are considered, the variability is smaller, with mean values of k_{UV} ranging from 0.32 to 0.37 $\text{mJ}^{-1}\cdot\text{cm}^2$. MS2 was more resistant to UV₂₅₄ (0.15 $\text{mJ}^{-1}\cdot\text{cm}^2$) than all enteroviruses.

Inactivation by sunlight led to a wider distribution of inactivation rate constants. Specifically, the mean k_{SUN} values for the different enteroviruses spanned a range from $1.3\cdot 10^{-3}$ to $9.0\cdot 10^{-3}$ $\text{mJ}^{-1}\cdot\text{cm}^2$ (Figure 2.2C). These values correspond well to those previously reported for the inactivation of PV3 by simulated sunlight in PBS¹¹⁸. The variability of inactivation by sunlight was slightly reduced if only CVB5 strains were considered, with the most resistant strain (Faulkner) exhibiting a mean rate constant of $3.2\cdot 10^{-3}$ $\text{mJ}^{-1}\cdot\text{cm}^2$. As for UV₂₅₄, MS2 was more resistant than any of the enteroviruses tested.

The differences in susceptibility of the different viruses to UV₂₅₄ and sunlight can be partly explained by the difference in the genome length. Given that all viruses tested have the same genome type (ssRNA), and assuming a constant rate of genome lesion formation during exposure to radiation, a longer genome will result in a higher number of lesions per genome¹¹⁹. Correspondingly, if k of each virus is normalized by its respective genome length, the variability in k decreases, though does not disappear (Figure A.6).

Free chlorine and chlorine dioxide.

Inactivation by FC was first-order with respect to dose (Figure A.3.), and yielded enterovirus inactivation rate constants (k_{FC}) ranging from 0.8 to 8.0 $\text{mg}^{-1}\cdot\text{min}^{-1}\cdot\text{L}$ (Figure 2.2E). As such, inactivation by FC exhibited the greatest variability among the disinfectants tested. Considerable variability was also observed within the different CVB5 strains, for which the k_{FC} ranged from 0.8 to 4.9 $\text{mg}^{-1}\cdot\text{min}^{-1}\cdot\text{L}$. This range also includes FC inactivation rates constants of CVB5 Faulkner determined by others under similar experimental conditions¹²⁰. The k_{FC} of MS2, which corresponded to 5.9 $\text{mg}^{-1}\cdot\text{min}^{-1}\cdot\text{L}$, fell within the upper range of enteroviruses.

In contrast to FC, inactivation by ClO₂ deviated from first-order and exhibited a tail at higher ClO₂ doses (Figure A.4.). This tail could not be attributed to ClO₂ depletion, as the ClO₂ concentration was approximately constant throughout the experiment (see Experimental Section). Tailing during ClO₂ disinfection has frequently been reported and has been attributed to various causes including virus aggregation⁵⁹, heterogeneity of the virus population¹²¹, or the accumulation of oxidation products that form a protective layer around the residual infective viruses¹²². Aggregation at neutral pH was not observed among the viruses studied herein (see Experimental Section), which rules out this feature as a cause of tailing (Figure A.10). Among enteroviruses, the earliest onset of the tail was observed at a dose of approximately 0.5 mg·min·L⁻¹. Therefore only doses up to 0.5 mg·min·L⁻¹ were included in the first-order kinetic model (equation 2) to determine k_{ClO₂}. Values of k_{ClO₂} for all viruses tested ranged from 9.6 to 26.1 mg⁻¹·min⁻¹·L (Figure 2.2G). A similar range in mean k_{ClO₂} values was observed among strains of CVB5, which ranged from 9.6 to 24.3 mg⁻¹·min⁻¹·L. The k_{ClO₂} for MS2 (14.8 mg⁻¹·min⁻¹·L) fell within the lower range of the enteroviruses.

For E11, it was previously found that FC and ClO₂ act on both the viral proteins and genome⁶⁰. Differences in the chemical reactivity of the viral proteins or genome toward FC and ClO₂ may thus explain some of the variability in the observed inactivation rate constants of the viruses considered in the present study. The abundance of readily oxidizable, solvent-exposed amino acids on the structural proteins was correlated with k_{FC} (Pearson's r=0.79), but not with k_{ClO₂} (Pearson's r=-0.22; Figure A.7). At the genome level, guanosine is the most reactive nucleotide toward both FC and ClO₂^{123,124}, and the degradation of the 5' non-coding region was previously found to correlate with inactivation by ClO₂¹²⁵. Here, we therefore explored if the guanosine content of the 5' non-coding region could be used as an indicator of a virus susceptibility to FC or ClO₂. A weak correlation with the respective inactivation rate constants was observed for FC (Pearson's r=0.51), but weakly with ClO₂ (Pearson's r=0.31; Figure A.8.). To improve these correlations, further information on the RNA and protein secondary and tertiary structure may be needed. This analysis indicates that kinetics of inactivation by FC may be influenced by the chemical virus composition, whereas inactivation by ClO₂ is mainly linked to biological factors, such as the use of different host cell receptor sites or different recombination efficiencies.

Heat.

Similar to inactivation by ClO₂, exposing the different enteroviruses to a temperature of 55 °C resulted in tailing inactivation curves (Figure A.5). The onset of the tail varied greatly between the different viruses, ranging from 15 seconds of heat exposure (CVB5-Faulkner,

CVB5-L030315, CVB5-L061815, CVB4-M063015, and E11, Figure A.5) to no observable tail throughout the experimental time considered. For the early tailing viruses, only the linear part of the inactivation curve was considered to determine the inactivation rate constant k_{heat} (equation 3). The mean values of k_{heat} for the enteroviruses considered ranged from 0.15 to 2.11 sec^{-1} . The corresponding range for only CVB5 strains was slightly narrower, reaching from mean values of 0.16 to 0.63 sec^{-1} , whereas MS2 displayed a much lower mean value of k_{heat} of 0.006 sec^{-1} (Figure 2.2I).

Changes in capsid amino acid residues have been previously linked to increases in the thermal stability of foot-and-mouth disease virus, another virus in the Picornaviridae family¹²⁶. A similar effect may be caused by small differences in the amino acid content of the structural virus proteins (Table A.4), which may cause the observed differences in k_{heat} among the different enteroviruses considered. Furthermore, at the treatment temperature used (55°C), capsid disruption followed by RNA escape is a probable reason for the inactivation of enteroviruses^{127,128}. Heat resistance is thus likely linked to the strength of the interaction between the virus capsid subunits¹²⁸, which may differ among the different serotypes and strains. A corresponding analysis is the subject of an ongoing study in our laboratory.

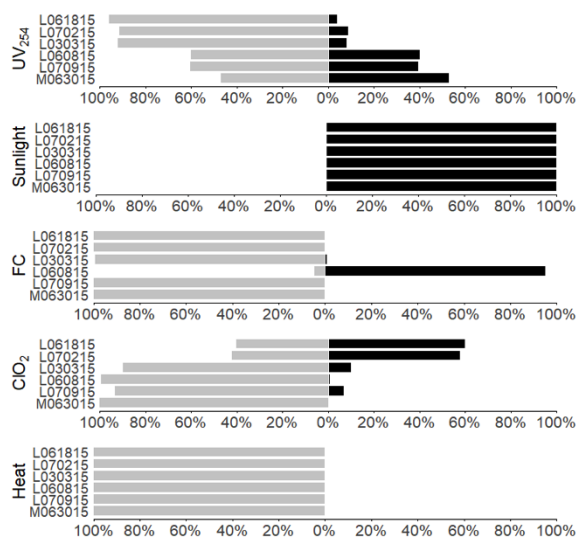


Figure 2.3. Intra-serotype probability comparison of inactivation rate constants.

Bar plots showing a comparison of the probabilities of inactivation rate constants (k values) for all environmental isolates of CVB5 with the CVB5-Faulkner laboratory strain. Grey bars indicate the probability that the environmental isolate is more resistant than the Faulkner strain; black bars indicate the probability that the environmental isolate is less resistant than the Faulkner strain.

Inter-serotype comparison of inactivation kinetics

The different enterovirus strains considered herein exhibit similar genomic and protein features (Table A.3 and Table A.4), yet the different serotypes are still genetically distant from one another (Figure 2.1). To determine how this genetic diversity is reflected in disinfection susceptibility, we grouped the tested viruses by serotype (Figure 2.2B, D, F, H,

and J) and compared the corresponding overall mixture distribution of the observed rate constants. We then determined the probability that a given serotype is more or less resistant than any of the other serotypes tested. Because the different disinfectants inactivate viruses via different mechanisms¹²⁹, these analyses were carried out for each disinfectant individually, to capture mechanism- or disinfectant-specific variability in virus resistance.

UV254 and Sunlight inactivation.

Comparisons between the four different serotypes revealed that despite their similarity in genome length and composition, their sensitivities to UV₂₅₄ nevertheless differed (Figure 2.2B). Specifically, CVB1 exhibited a >99% probability of being more resistant than the other serotypes tested, whereas the rate constants for the other serotypes grouped more closely. However, while the observed differences in k_{UV} between CVB1 and the other enterovirus serotypes were quantifiable, they are of little practical significance: to achieve a 4- \log_{10} inactivation, CVB1 required a UV₂₅₄ dose of 32.5 $\text{mJ}\cdot\text{cm}^{-2}$, whereas the most susceptible serotype (CVB4) required a similar dose of 25.3 $\text{mJ}\cdot\text{cm}^{-2}$ (Table A.2).

A very different resistance pattern was observed for inactivation by sunlight (Figure 2.2D). CVB5 was the least resistant virus, with a >85% probability of being less resistant than any other serotype, whereas E11 had a >99% probability of being the most resistant. In contrast to UV₂₅₄ inactivation, this variability translates into a substantial difference in the environmental persistence in sunlit waters, or the inactivation performance by devices relying on disinfection by solar UVB: to achieve a 4- \log_{10} inactivation, CVB5 required a UVB dose of 1369 $\text{mJ}\cdot\text{cm}^{-2}$, which is the equivalent of 2.3 days of solar UVB exposure at the equator. To achieve the same \log_{10} reduction, E11 required a dose of 5430 $\text{mJ}\cdot\text{cm}^{-2}$, which corresponds to approximately 9.1 days of solar UVB exposure at the equator.

The discrepant resistance patterns of viruses toward UV₂₅₄ and sunlight indicates that the mechanism of action of these two inactivating treatments differ. This can be rationalized by a number of causes. First, the wavelength spectrum and fluence rates of these two methods are different, and thus the type and yield of lesions to the viral genome likely differs¹³⁰. Second, differences in thermal stability of the viruses may influence the observed inactivation rates, in particular if thermal inactivation during the lengthy sunlight inactivation experiments synergistically promoted inactivation by sunlight. And finally, inactivation by sunlight may involve a greater portion of protein damage compared to UV₂₅₄, which may contribute to inactivation¹³¹.

Free chlorine and chlorine dioxide.

FC and ClO₂ treatment varied in their effect on the different enterovirus serotypes (Figure 2.2F and H). For inactivation by FC, E11 had a >98% probability of being less resistant than the other serotypes, whereas CVB1 was the most resistant serotype (>85% probability). The susceptibility of the different serotypes result in considerable differences in the FC dose to achieve a 4-log₁₀ inactivation: E11 required a dose of 1.15 mg·min·L⁻¹ while CVB1 required a dose of 6.41 mg·min·L⁻¹.

For disinfection by ClO₂, CVB4 and CVB5 had high probabilities (>99% and >92%, respectively) of being more resistant than CVB1 or E11. The latter two serotypes exhibited comparable susceptibility to ClO₂ as E11. This latter finding is surprising, as CVB1 was the most resistant serotype toward FC. The observed extent of variability in disinfection kinetics among serotypes did not lead to significant differences in the ClO₂ disinfection requirements. Specifically, the most resistant serotype (CVB4) required a dose of 0.23 mg·min·L⁻¹ for a 3-log₁₀ inactivation, and the most susceptible serotype (CVB1) a dose of 0.1 mg·min·L⁻¹. These dose requirements, however, differ more dramatically if the individual strains within the serotypes are considered, as for some environmental isolates a 4-log₁₀ inactivation could not be achieved due to extensive tailing of the disinfection curve (Figure A.4. and Table A.2).

Heat.

Inactivation by heat was the least effective against CVB1 and CVB5, which were more thermally stable than the other two serotype tested with >99% probability (Figure 2.2J). The most heat sensitive serotype was CVB4, though the two strains contained in this serotype exhibited vastly different susceptibilities to heat.

In summary, the results of this study demonstrate pronounced variability in disinfection susceptibility among four different enterovirus serotypes. While disinfection requirements were fairly homogeneous across serotypes and strains for UV and ClO₂, the sunlight, FC and heat requirements for a given enterovirus serotype were not predictive of other serotypes.

Assessment of enterovirus lab strains or MS2 as surrogates for the disinfection of environmental isolates

Many virus disinfection studies to date rely on laboratory strains^{68,120,132-136}, which are easy to obtain because they are commercially available. Results from such studies should be interpreted with caution, since we showed here that a single laboratory strain of a single serotype may not accurately reflect the inactivation kinetics of other serotypes (Figure 2.2).

Additionally, as illustrated below, environmental isolates of CVB5 may not even be suitable representatives for other strains from the same serotype.

Specifically, inactivation kinetics of different isolates of CVB5 by sunlight and heat were only poorly represented by the corresponding laboratory strain (Figure 2.2 and Figure 2.3). While the Faulkner strain was more resistant to solar disinfection compared to the environmental isolates, it had a lower thermal tolerance. This indicates that the lab strain is not a good surrogate to assess the environmental stability of isolates. Similarly, the Faulkner strain was also not a good surrogate for inactivation of environmental isolates by FC. All but one of the CVB5 isolates (CVB5-L060815) had a high (>99%) probability of being more resistant to FC than the Faulkner strain, and exhibited inactivation rate constants that were up to five times lower than the Faulkner strain (Figure 2.2 and Table A.2).

The Faulkner strain appeared to be more suitable as a surrogate for the inactivation of environmental CVB5 strains by UV_{254} and ClO_2 . While several of the environmental isolates (CVB5-L061815, CVB5-L070215 and CVB5-L030315) were more resistant to UV_{254} than the Faulkner strain, others (CVB5-L060815, CVB5-L070915 and CVB5-M063015) had similar probabilities of being more or less resistant than the Faulkner strain. For ClO_2 , half of the isolates was more resistant and the other half was less resistant than the Faulkner strain. The Faulkner strain thus fell well within the range of UV_{254} and ClO_2 inactivation kinetics of the environmental CVB5 isolates tested.

Our data thus imply that disinfection studies based on lab strains may not be representative of many viruses circulating in the environment. Reliance on laboratory strains may therefore lead to the underestimation of actual treatment requirements. This latter point is emphasized in Figure 2.4, which compares our data with the US EPA's recommended Ct value for a 4 \log_{10} inactivation of viruses by FC at 20°C⁴⁹. While both laboratory strains (E11 Gregory and CVB5 Faulkner) tested fall well below the EPA Ct requirement, several of the environmental isolates exceed it, such that the EPA recommendation would not guarantee a 4- \log_{10} reduction for these viruses.

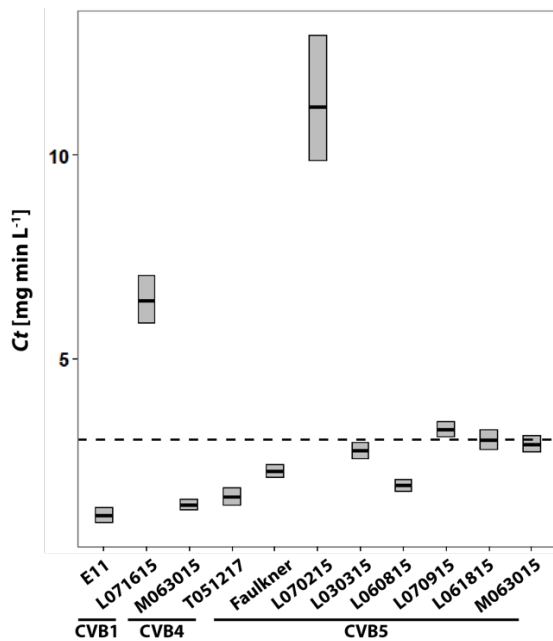


Figure 2.4. Ct values to achieve 4- \log_{10} inactivation by FC.

The dashed line corresponds to the US EPA's recommendation for Ct value at 20°C⁴⁹ (3 mg·min·L⁻¹). The bar plots indicate the mean Ct (black line) calculated based on the k_{FC} measured herein, along with the upper and lower 95% confidence intervals (top and bottom of box).

Bacteriophages such as MS2 have also been proposed as surrogates for the disinfection of enteric viruses⁷⁹, since they have similar properties as enteric viruses¹³⁷. This approach is popular because phages are easier and cheaper to handle than actual human viruses. However, as is evident from Figure 2.2 and confirmed by Bayesian analysis (Figure A.9.), MS2 is not always a good indicator for the inactivation kinetics of enteroviruses species present in the treatment systems. Specifically, MS2 was significantly more resistant to heat than any enterovirus studied, making it a poor surrogate for thermal inactivation. In contrast, MS2 underestimated the inactivation of enteroviruses by UV₂₅₄ and sunlight; as such, it can be considered a good conservative indicator for enterovirus inactivation by these two disinfection methods. As discussed above, this can be partly explained by the difference in the genome length of MS2 (3569 bases) and enteroviruses (ca. 7400 bases). However, even if corrected for genome length (Figure A.6.), MS2 still mostly underestimated enterovirus inactivation by UV₂₅₄ and sunlight.

For disinfection by FC, MS2 was conservative surrogate for E11, and representative of the inactivation of the two CVB4 strains considered. However, the other coxsackievirus strains were more resistant. For ClO₂, MS2 was conservative for CVB1-L071615, representative for E11 and CVB5-L061815, but all the other coxsackievirus B strains were more resistant (Figure A.9.).

Overall, this analysis reveals that neither the lab strains nor MS2 bacteriophage can satisfactorily model inactivation behavior of all enteroviruses. Given the significant variability of inactivation kinetics among commonly occurring enteroviruses, we therefore

recommend that future disinfection studies be conducted based on a range of viruses that include environmental isolates, as well as different serotypes.

CHAPTER 3 Effect of salt and pH on virus thermostability.

Experimental design, inactivation experiments, and data analysis were performed by Meister S.; structural modeling was performed by Prunotto A. (Laboratory for Biomolecular Modeling, EPFL).

INTRODUCTION

Role of temperature in virus persistence outside the host

Temperature is an important factor controlling virus stability outside the host (Bertrand et al. 2012 and references therein¹³⁸). Several studies highlight its importance in different topics, such as food preservation and consumption, vaccine storage, as well as virus persistence in the aqueous environment. Few examples are exposed below.

In food preservation, the freezing temperature has little to no effect on enteric virus stability¹³⁹, and only high temperature processing, such as pasteurization or sterilization are efficient treatments for foodborne viruses (Hirneisen et al. 2010 and references therein⁵⁶). Nevertheless, the risks of virus contamination were described to be relevant, especially for raw or lightly cooked foods such as shellfish^{140–142}.

Temperature was also described as significant factor in the stability of attenuated vaccines. Cold chain problems during storage can lead to an undetected vaccine potency loss due to thermal inactivation^{143,144}. Despite the implementation of heat-sensitive vaccine vial monitors, the cold chain is difficult to maintain in rural areas of developing countries¹⁴⁵. Several studies demonstrate that a targeted engineering of recombinant virus capsid can efficiently increase the vaccine stability against heat^{126,128,146}.

Finally, temperature was found to be a major determinant of environmental virus persistence, regardless the type of matrix. For example, heat was found to decrease virus persistence in groundwater¹⁴⁷, soil¹⁴⁸, or on non-porous surfaces¹⁴⁹. However, a higher environmental persistence was observed in specific viruses and strains, potentially allowing them to increase their chances to find a new host¹⁵⁰. This indicates that the thermostability of a virus is an important trait for the virus. Yet, the exact mechanism responsible of an enhanced thermostability in environmental viruses is unknown, and requires an inquiry.

Thermostability of enteroviruses

Waterborne viruses are known to survive over long periods of time in environmental matrices, making them important contributors to water and foodborne disease outbreaks

(Sinclair et al. 2009 and references therein¹²). Among them, the *Picornaviridae* family is known to significantly contribute to these outbreaks¹⁰.

In chapter 2, we described a high variability in the thermostability of different environmental strains of coxsackievirus B (CVB) species¹⁵¹, both among strains and serotypes. Specifically, coxsackievirus B4, as well as echovirus 11 (E11) were more heat sensitive than coxsackievirus B5 and B1 serotypes. In addition, the CVB5 laboratory strain was generally more heat sensitive than CVB5 environmental isolates, indicating that the environmental exposure may lead to the selection of the most thermostable viruses.

Enteroviruses have been shown to readily adapt to high temperatures. Specifically, Shiomi et al. (2004)¹⁵² subjected poliovirus to successive passages of thermal inactivation, which resulted in the emergence of a thermostable strain. Furthermore, enterovirus thermostability appears to be determined by two structural components: first, the interface of the different capsid pentamers has been identified as a critical features¹²⁸. A single introduction of a disulfide bond at this interface can increase the thermostability of the viral capsid¹⁴⁶. Similarly, decreasing the electrostatic repulsion forces between the capsid pentamers also resulted in a higher thermostability¹²⁶. Second, the VP1 pocket region was also described to influence thermostability, and few mutations in this region resulted in a thermostabilizing effect in foot-and-mouth-disease virus¹⁵³.

In this study, we combined structural modelling and *in vitro* experiments to identify the virus characteristics determining the thermostability of enteroviruses. Specifically, we tested the tolerance of various environmental coxsackievirus B strains and serotypes to different temperatures and in different simple aqueous matrices, and evaluated the results against modelled capsid parameters typically associated with thermostability, including salt bridges, disulfide bonds, electrostatic forces at the capsid subunits interfaces, or structural differences located in the VP1 pocket region. Finally, our findings were invoked to explain the observed differences in thermostability among different serotypes of coxsackievirus B.

EXPERIMENTAL SECTION

Cells and viruses

Environmental strains of Coxsackievirus B serotypes were purified from untreated domestic sewage as described elsewhere¹⁵¹. Five coxsackievirus B5, two coxsackievirus B4 and one coxsackievirus B1 were isolated and their whole genome sequenced (GenBank accession numbers: MG845887 to MG845895). CVB5 Faulkner strain (ATCC VR-185) and echovirus 11

Gregory strain (ATCC VR-41) were obtained from LGC Standards (Molsheim, France). Buffalo Green Monkey Kidney cells were obtained from the Spiez Laboratory (Switzerland) and were cultured in Minimum Essential Medium (MEM) completed with 1% penicillin-streptomycin together with 10% (growth medium) or 2% (maintenance medium) of heat-inactivated fetal bovine serum (all purchased from Gibco (Molsheim, France). Stocks of viral strains from 10^7 to 10^8 MPNCU mL⁻¹ were produced by propagating the viruses on n BGMK cells, followed by purification by polyethylene glycol precipitation and chloroform treatment, as described elsewhere¹⁵¹.

Infectivity assay

The concentration of infectious viruses was determined by endpoint dilution with Most Probable Number (MPN) statistics⁹², using confluent BGMK cells on 96-well plates, with five replicates and eight dilutions for each experimental sample. The cytopathic effect was determined through microscopy after five days of incubation at 37°C with 5% CO₂. The infectious concentration is reported as most probable number of cytopathic units per mL (MPNCU mL⁻¹).

Antigenic divergence assay

To quantify the possible virus antigenic divergence, we used two horse sera: a CVB5 Faulkner specific antiserum (ATCC: VR-1036AS), and a pre-immunization serum (ATCC: VR-1036PI) as negative control. The viruses were separately incubated with and without the two sera diluted at a final dilution of 1:200 and incubated for 1h at room-temperature. Then, the infectivity was measured by MPNCU ml⁻¹.

Thermal inactivation experiments

Thermal inactivation experiments were performed at two different temperatures (30 and 55°C) in aqueous buffers with different pH and ionic strengths. Experiments were conducted in 25 mM glycine-HCl (pH3), neutral pH experiments in 5 mM Na₂HPO₄ (pH7.4), and high pH experiments in 25 mM glycine-NaOH (pH9). The ionic strength was varied by addition of 10 mM to 1 M of NaCl. The information on the chemicals and providers are detailed in the annexes (see Annexes – Chapter 3).

Kinetic experiments at 55°C and were performed in a PCR thermocycler (Applied Biosystems, GeneAmp PCR system 9700). 10 µl of virus stock were spiked into PCR tubes containing 90 µl of pre-heated buffer to reach an initial concentration around 10^7 MPNCU mL⁻¹. Samples

were maintained at 55°C for varying amounts of time ranging from 0 to 2 minutes, and were then quickly cooled down by placing them on an aluminium PCR cooling block on ice. The residual infectious virus concentration in each sample was enumerated the same day. Kinetic experiments at 30°C were performed in an incubator (Mettler Modell 300, Schwabach, Germany). 100 µl of virus stock was spiked into a 900 µl of buffer to an initial concentration of 10⁶ MPNCU mL⁻¹. Over the course of 9 days, 100 µl aliquots were sampled daily. Each sample was directly mixed with 900 µl of cell culture medium and stored at -20°C prior to enumeration by the infectivity assay described above. Each experiment was conducted at least in replicate.

The inactivation curves were fitted to a first-order model, where N and N_0 are the infective virus concentration at time 0 and time t , and k is the inactivation rate constant in day⁻¹ (at 30 °C) or sec⁻¹ (at 55 °C). C is the concentration of disinfectant, which in the case of heat inactivation is constant and equals to 1.

$$(1) \quad \ln\left(\frac{N}{N_0}\right) = -kCt$$

At 55°C, several isolates displayed a rapid, initial decay, followed by a tailing curve. For these viruses, only the initial decay was taken in account to determine rate constants.

Determination of the capsid melting temperature (breakpoint).

The melting temperature, or breakpoint, of the viral capsids was determined by a thermal-shift assay. The assay was performed in an PCR thermocycler as described above, but each PCR tube was held at a different temperature ranging from 25 to 60°C at 2 degree intervals, and was incubated for one minute at each temperature. The capsid melting temperature was determined by modelling a segmental linear regression and extracting the breakpoints values together with their respective standard errors. The modelling was applied to at least on two pooled experimental replicates.

Assay to measure genome integrity

The extent of genome damage upon thermal inactivation was quantified by real-time quantitative polymerase chain reaction (RT-qPCR) as described elsewhere¹⁵⁴. Briefly, seven primer couples were designed (Table B.1. Primers couples for genome damage assay), which targeted amplicons that jointly covered approximately 45 % of the total CVB5 genome. Prior to and after thermal inactivation, the integrity of each amplicon was quantified separately by RT-qPCR. The integrity of the total genome was then determined by extrapolation as

follows, where (N_t/N_0) is the extent of genome damage at time t , ΔCq_t is the measured difference in qPCR signal at time t in the amplicon i , and i is one of each seven amplicons tested:

$$(2) \quad \frac{N_t}{N_0} = \left[\prod_i 2^{-\Delta Cq_t} \right]^{\frac{\text{genome length}}{\text{total amplicon length}}}$$

RNA was extracted using PureLink viral RNA/DNA kit from Invitrogen (Carlsbad, USA), and the qPCR was performed using One Step SYBR PrimeScript RT-PCR kit from Takara (Dalian, China), and using a MIC qPCR cycler from Thermofisher (Waltham, USA). Cycling conditions were the following: 20 minutes at 42°C for reverse transcription, then (repeated 40 times) 15 seconds at 95°C, 30 seconds at 60°C, 20 seconds at 72°C, and a final incubation for 45 seconds at 72°C.

Structural modelling

Details concerning the modeling protocol and conditions are explained in depth in chapter 4. Briefly, 3D capsid models were built using the known crystal structure of coxsackievirus B3 as a scaffold (PDB accession code: 1cov)¹⁵⁵. As the main structural investigations are focused on the pentamer interface, one single pentamer together with a portion the neighboring pentamer was generated (Figure 3.1), and different parameters were calculated in this region, specifically the number of hydrogen bonds and salt bridges, as well as the electrostatic interactions and Van der Waals forces interactions (in kcal/mol*Å). The overall pentamer interaction forces were calculated as the sum of the electrostatic interactions and Van der Waals forces. The modelling of the interaction forces was performed seven times, and outlier values were excluded ($< \pm 1000$ kcal/mol*Å).

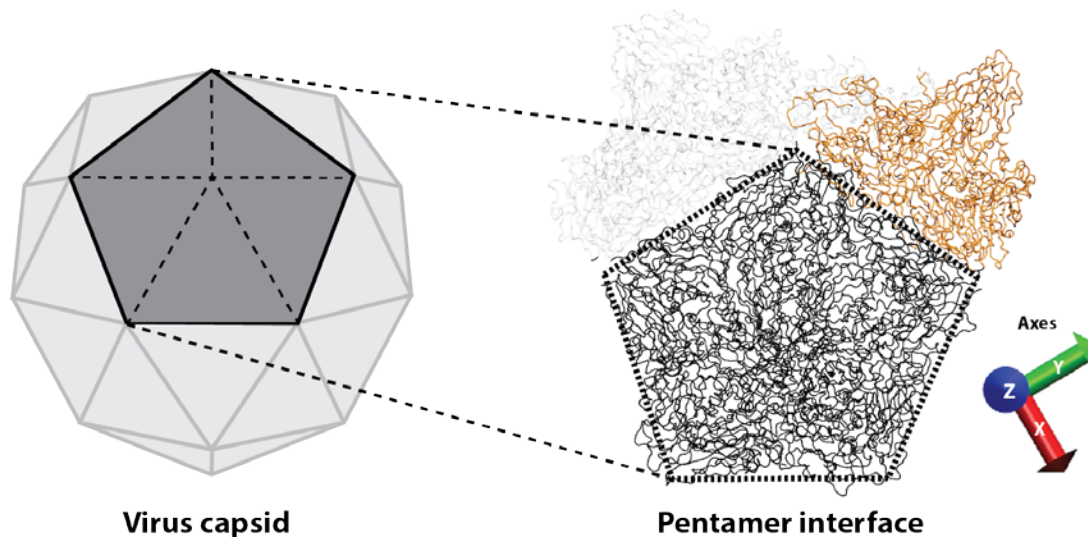


Figure 3.1 Scheme of the pentamer interface.

Right: schematic representation of the icosahedral structure of the virus capsid. In dark grey are represented a single pentamer. Left: single pentamer with its neighbor. The axes are represented by 3 vector forces, x, y and z. X and z represent the interface shearing forces, and y the opposing forces of interest.

Data analysis

Data handling, MPN calculation and statistical analyses were performed in R (R development core team). The following CRAN packages were used: ggplot2¹⁰², gridExtra¹⁰³, segmented¹⁰⁵ and peptides¹⁵⁶. The virus breakpoint was determined using the segmented function from the segmented package using the linear model function (lm) as object, with 40 as the starting value estimate.

RESULTS

Effect of temperature and solution composition on inactivation

Inactivation at 30°C

At pH7.4 and 10 mM NaCl the inactivation of all viruses was slow, with rate constants k ranging from 0.13 (± 0.09 95% CI) to 0.54 (± 0.11 95% CI) day⁻¹. No effect on inactivation was observed when increasing the pH from 7.4 to 9. (Figure 3.2C). At pH3, all viruses displayed faster inactivation kinetics with k ranging from 0.71 (± 0.16 95% CI) to 1.36 (± 0.38 95% CI) day⁻¹. This rapid inactivation may be an artefact caused by viral aggregation, known to occur at low pH in low ionic strength solutions⁵⁸. The observed loss in infective virus at pH3 and 10 mM NaCl is thus likely a combination of true inactivation and aggregation (see also Figure 5.10). At pH 3 with 1M NaCl, the inactivation was too fast to determine an inactivation rate

constant. Salt did not affect inactivation kinetics at pH7.4 (Figure 3.2D). Interestingly, however, 1 M NaCl and pH 9 synergistically led to very rapid virus inactivation. (Figure 3.2E). As virus aggregation is unlikely under these conditions of pH and salt, the decrease in infective virus titer must stem from virus inactivation.

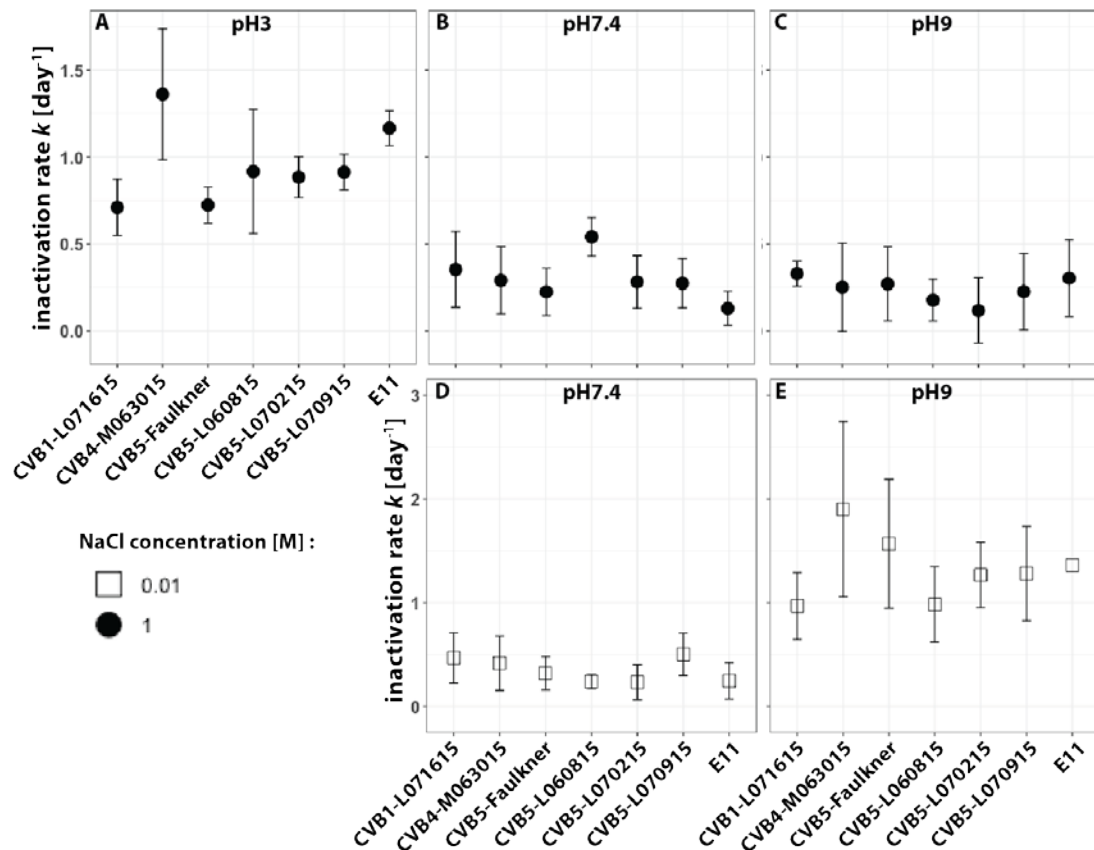


Figure 3.2 Thermostability of different enterovirus strains and serotypes at 30°C.

Overview over all measured inactivation rate constant k of the different viruses included in this study. The results for pH3 and 0.01 M NaCl are not shown, as the inactivation kinetics were too fast to determine a k -value. The error bars correspond to the 95% confidence intervals.

No major differences in the inactivation rate constants of the different viruses were observed at pH7.4 (both low and high salt concentration; Figure 3.2B and D), or at pH9 for low salt concentration (Figure 3.2C). At pH9 and 1M NaCl, CVB4 displayed a higher inactivation rate constant, but the difference was only significant compared to the CVB1 strain. (Figure 3.2E). Finally, at pH3 and low salt, CVB4 and E11 were significantly less thermostable than the other viruses (Figure 3.2A). Still, viral aggregation should be taken in account for this condition.

Genome degradation at 30°C

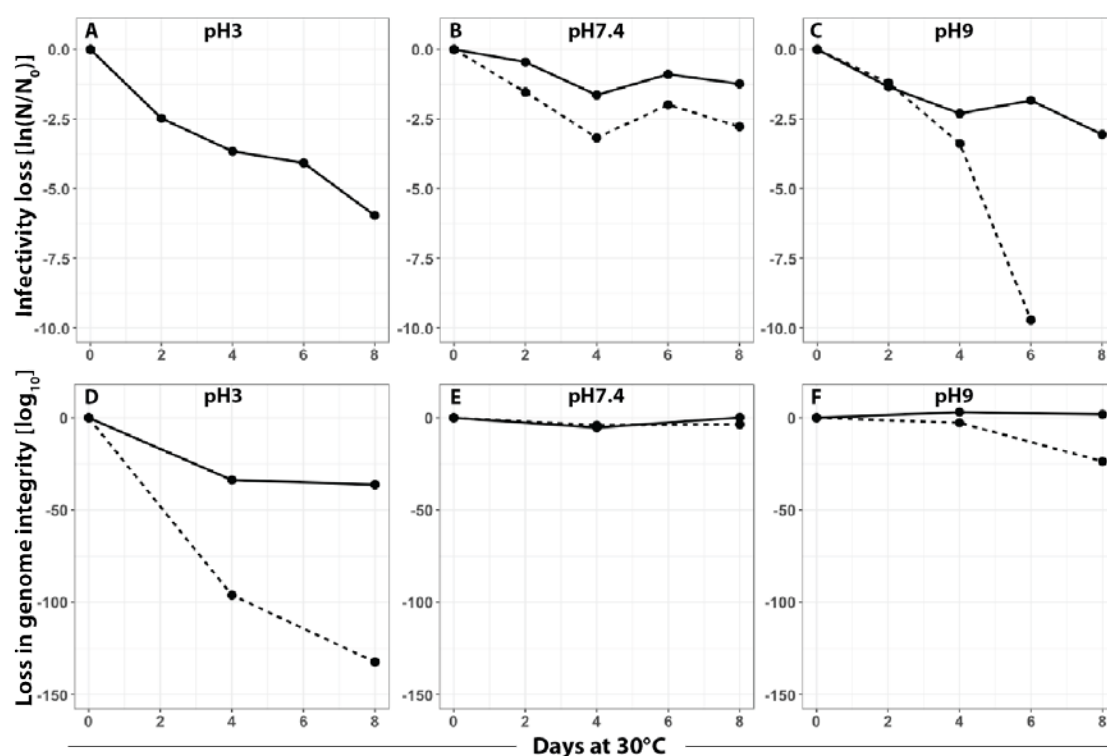


Figure 3.3 Effect of salt and pH on virus infectivity and genome integrity of CVB5-Faulkner at 30°C

A to C: inactivation. D to E: genome degradation, as determined by RT-qPCR. Black line: low salt condition (10 mM NaCl); dotted line: high salt condition (1M NaCl). Differences in inactivation can only be observed at extreme pH in the presence of 1 M NaCl. Virus inactivation at pH 3 (panel A) reflects both true inactivation and aggregation. For clarity, only the data for the CVB5-Faulkner strain are displayed. The remaining inactivation rate constants and breakpoints values are shown in the appendix B (Table B2 to B3). The error bars correspond to the 95% confidence intervals

No genome degradation was observed at pH7.4 for low and high salt conditions (Figure 3.3E), which is consistent with the lack of inactivation observe at this pH. Genome degradation did occur at pH3, in both salt conditions, but to a larger extent at the high salt concentration (Figure 3.3D). At pH9, genome degradation was observed only at the high salt concentration (Figure 3.3F), indicating a potential synergistic effect of pH and salt.

Inactivation at 55°C

Inactivation at 55 °C was much more rapid compared to 30 °C for all viruses studied, with rate constants k ranging from 0.16 (\pm 0.05 95% CI) sec^{-1} for CVB5-L061815 to 1.48 (\pm 0.69 95% CI) sec^{-1} for CVB4-T051217 (Table B.). At low salt, CVB4 strains as well as E11 appeared to be the less thermoresistant compared to CVB5 isolates, with CVB1-L071615 being the most thermoresistant (Table 1.1). In addition, CVB5 Faulkner laboratory strain was always

found less thermostable than the CVB5 isolates. For CVB5-Faulkner, the pH was found to have no obvious effect on inactivation at 10 mM NaCl, a notable tail in the inactivation curve was observed after around 20 seconds of treatment. However, the level of this tail appeared to be lower at pH9 (Figure 3.4C). On the other hand, the addition of 1M NaCl alone dramatically increased the thermostability, shifting the rate constant k of the Faulkner strain from $0.62 (\pm 0.06 \text{ 95\% CI}) \text{ sec}^{-1}$ for low salt to undetected inactivation ($k \cong 0$) for high salt at pH7.4 (Figure 3.4B).

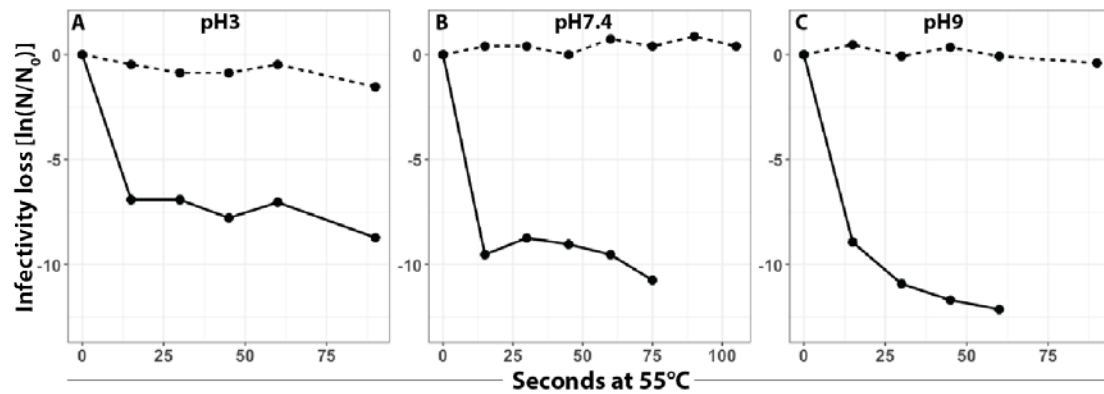


Figure 3.4 Effect of salt and pH on virus infectivity of the CVB5-Faulkner strain

Black line: low salt condition (10 mM NaCl); dotted line: high salt condition (1M NaCl). (A to C) inactivation.

Breakpoint temperatures

The breakpoint temperatures ranged from 38.8 to 51.2 °C (Figure 3.5). Interestingly, and consistent with the 55°C inactivation kinetics, serotypes CVB4 and E11 were the least thermoresistant, with breakpoint temperatures of 38.8, 44.4 and 43.3 °C for CVB4-T051217, CVB4-M063015 and E11, respectively. A protective effect of salt was also observed for the capsid breakpoint, shifting the CVB5-Faulkner breakpoint temperature around 15 °C upward (Figure 3.6). A destabilizing effect of increasing pH on the capsid breakpoints could be observed at low salt conditions, with breakpoint temperatures of $47.0 (\pm 1.9 \text{ 95\% CI})$ °C, $44.9 (\pm 1.4 \text{ 95\% CI})$ °C and $40.7 (\pm 1.6 \text{ 95\% CI})$ °C for pH3, 7.4 and 9, respectively. A strong negative correlation of the breakpoint temperatures and the inactivation rate constants at 55 °C (Pearson's $r = -0.97$) was found (Figure 3.7).

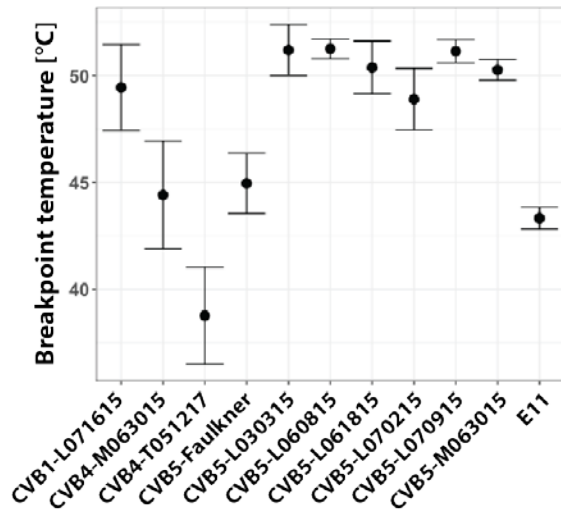


Figure 3.5 Breakpoint temperature for the viruses.

Both CVB4 strains, as well as E11 have the lowest breakpoint temperatures. The laboratory strain CVB5-Faulkner appeared more thermosensitive than the corresponding CVB5 isolates. The error bars correspond to the 95% confidence intervals.

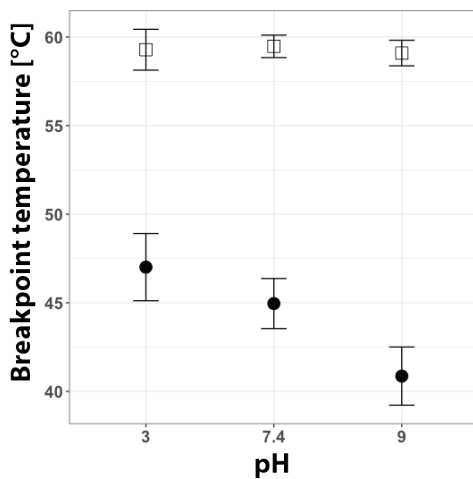


Figure 3.6 Effect of salt and pH on virus breakpoints temperature.

Effect of salt and pH on the breakpoints temperatures of CVB5-Faulkner strain. In the presence of 10 mM NaCl (black circles), an increase in pH lowered the breakpoint. In 1 M NaCl (open squares) the breakpoint increase close to 60 C for all pH conditions considered. The error bars correspond to the 95% confidence intervals.

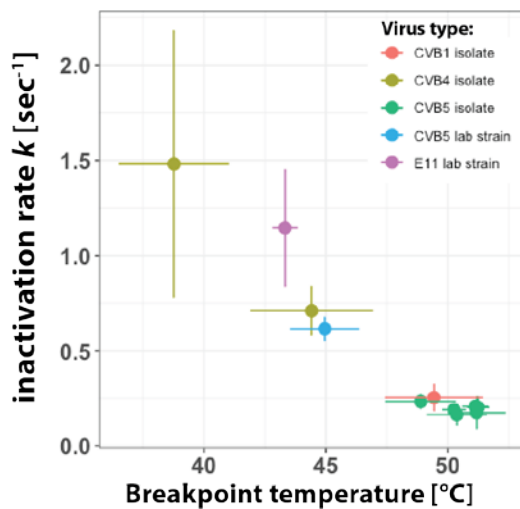


Figure 3.7 Correlation of breaking points with the rate constants k at 55°C.

Inactivation rate constants at 55 C exhibit a strong negative correlation with breakpoints (Pearson's $r = -0.97$), whereby the CVB5 isolates are clustered in the lower right quadrant. The error bars correspond to the 95% confidence intervals

Antigenic divergence

An antigenic divergence assay was conducted in order to assess if the CVB5 laboratory strain differed in structure from the CVB5 environmental isolates. Interestingly, a divergence was observed where the isolates were only partially inactivated by the CVB5 Faulkner specific antiserum, whereas the Faulkner strain was fully inactivated (Figure 3.8), indicating a structural change from the lab strain to the environmental isolates. No effect of the serum was observed on CVB4 and CVB1 serotypes, indicating that they are structurally sufficiently different from the CVB5-Faulkner strain to not being targeted by the polyclonal CVB5 Faulkner antibodies present in the serum.

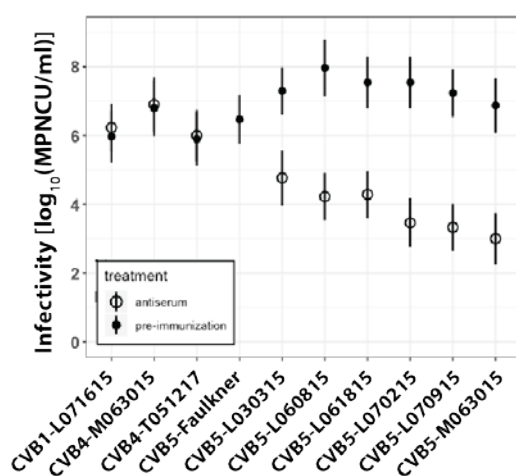


Figure 3.8 Antigenic divergence from CVB5-Faulkner strain.

Viruses were exposed to an antiserum specific to the CVB5-Faulkner strain. The smaller the infectivity loss caused by the antiserum, the greater is the antigenicity shift of the capsid compared to the Faulkner strain. As expected, non-CVB5 serotypes exhibit no infectivity loss. CVB5 isolates only display a partial infectivity loss, indicating a partial antigenicity shift from the Faulkner strain. The error bars correspond to the 95% confidence intervals.

Structural analysis

Hydrophobic core pocket, disulfide bonds, H bonds and salt bridges

No differences in the total hydrophobic core pocket volume was found except for E11, which appeared as a strong outlier. Similarly, no differences in the number of disulfide bonds could be found between any of the viruses studied (data not shown). At the pentamer interface, CVB1 and E11 displayed a higher number of H bonds compared to all CVB4 and CVB5 serotypes (Figure 3.9A). In addition, discrepancies in the number of salt bridges could be noted. Both CVB4 isolates displayed six salt bridges, compared to for the CVB1 and CVB5 serotypes, and two for E11 (Figure 3.9B).

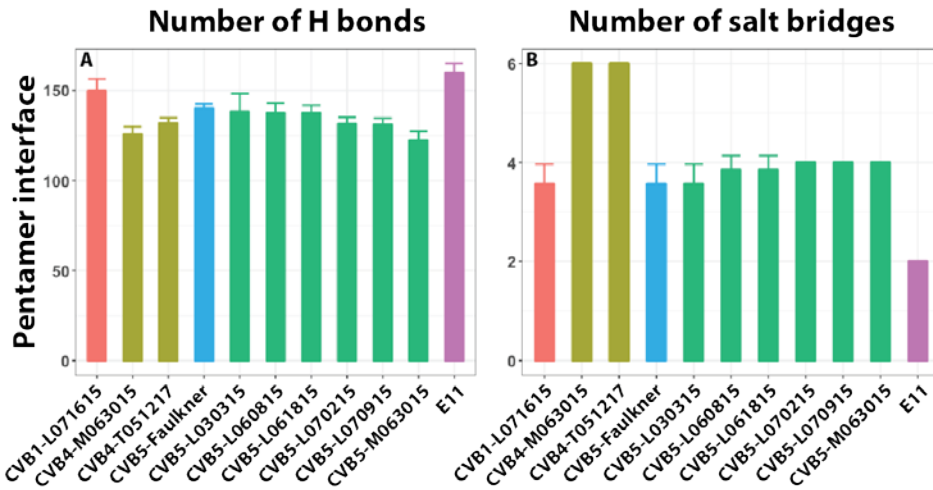


Figure 3.9. Number of H bonds and salt bridges at the pentamer interface.

Pentamer interaction forces

The resulting directions (attractive or repulsive) of interaction forces at the pentamer interface were variable from one virus to another. Van de Waal forces were always attractive (negative values) and electrostatic forces always repulsive (positive values) (Figure 3.10A and B). The overall force was negative (Figure 3.10C), indicating that the Van der Waal forces provide enough attraction to overcome the repulsive forces from the electrostatics, and prevent the natural disruption of the virus capsid, without any external stressor.

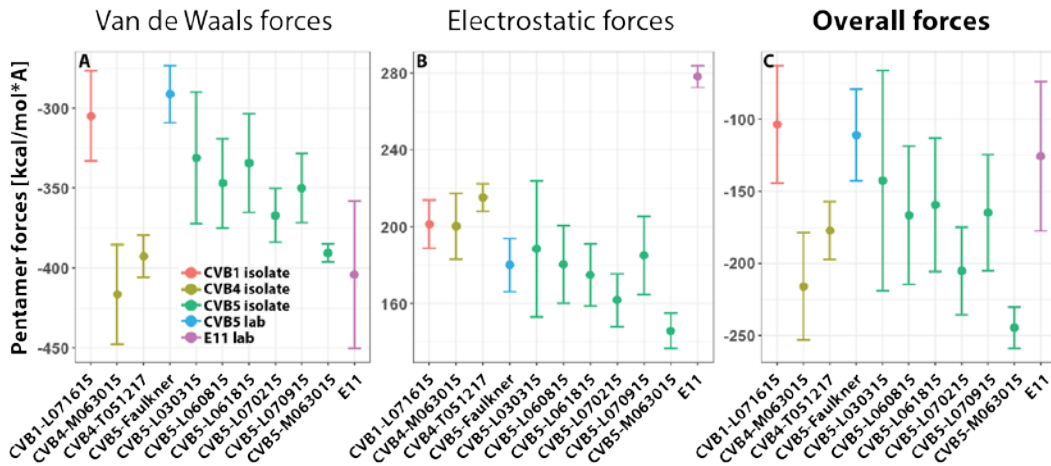


Figure 3.10 Interaction forces at the pentamer interface.

Vand der Waals forces and electrostatic forces in the y axis component of the capsid pentamer interface. The y-axis corresponds to the forces in [kcal/mol*Å]. Negative values indicate an attraction, positive values indicate a repulsion. The overall forces correspond to the sum of both Van de Waals and electrostatics. The error bars correspond to the 95% confidence intervals.

Pocket factor interactions

The pocket factor of coxsackievirus B3 was previously modelled as palmitate and specific hydrophobic residues were described to potentially interact with it¹⁵⁵. These residues were compared to those of the CVB5 Faulkner and environmental strains by protein sequence alignment. Several mutations on these residues or residues located in their vicinity were found (Figure 3.11A), with different hydropathy indexes. Interestingly, the total hydrophobicity of the whole pocket factor-interacting zones exhibited a correlation with the respective breakpoint temperatures of the viruses (Pearson's $r = 0.84$), with a lower hydrophobicity for the most thermolabile viruses (CVB4 isolates and E11) (Figure 3.11B).

A

Virus	Total Hydrophobicity	VP1 Amino acids																																					
		93	98	116	119	145	180	186	192	212	219	234																											
CVB5-Faulkner	0.199	V	N	T	R	Q	D	E	L	T	M	Y	V	R	M	S	I	S	I	A	Y	S	G	I	N	T	L	N	N	M	G	T	L	Y	Y	F	K		
CVB5-L061815	0.218	V	N	T	R	Q	D	E	L	T	M	Y	V	R	I	S	I	S	I	A	Y	S	G	I	N	T	L	N	N	M	G	T	L	Y	Y	F	K		
CVB5-L030315	0.218	V	N	T	R	Q	D	E	L	T	M	Y	V	R	I	S	I	S	I	A	Y	S	G	I	N	T	L	N	N	M	G	T	L	Y	Y	F	K		
CVB5-L070915	0.218	V	N	T	R	Q	D	E	L	T	M	Y	V	R	I	S	I	S	I	A	Y	S	G	I	N	T	L	N	N	M	G	T	L	Y	Y	F	K		
CVB5-M063015	0.218	V	N	T	R	Q	D	E	L	T	M	Y	V	R	I	S	I	S	I	A	Y	S	G	I	N	T	L	N	N	M	G	T	L	Y	Y	F	K		
CVB5-L070215	0.218	V	N	T	R	Q	D	E	L	T	M	Y	V	R	I	S	I	S	I	A	Y	S	G	I	N	T	L	N	N	M	G	T	L	Y	Y	F	K		
CVB5-L060815	0.199	V	N	T	R	Q	D	E	L	T	M	Y	V	R	M	S	I	S	I	A	Y	S	G	I	N	T	L	N	N	M	G	T	L	Y	Y	F	K		
CVB1-L071615	0.186	V	N	T	R	Q	D	E	L	T	M	Y	V	R	M	S	I	S	I	A	Y	S	G	I	N	T	L	N	N	M	G	T	L	Y	Y	F	K		
CVB4-T051217	0.124	V	N	T	R	Q	D	M	E	L	T	M	Y	V	R	M	S	I	A	Y	T	G	V	N	S	L	N	N	M	G	T	L	Y	Y	F	K			
CVB4-M063015	0.124	V	N	T	R	Q	D	M	E	L	T	M	Y	V	R	M	S	I	A	Y	T	G	V	N	S	L	N	N	M	G	T	L	Y	Y	F	K			
E11	0.111	T	I	S	A	R	R	D	V	E	V	T	M	Y	I	R	M	S	I	S	I	A	Y	S	G	V	N	T	L	N	H	M	G	Q	I	Y	Y	F	K

B

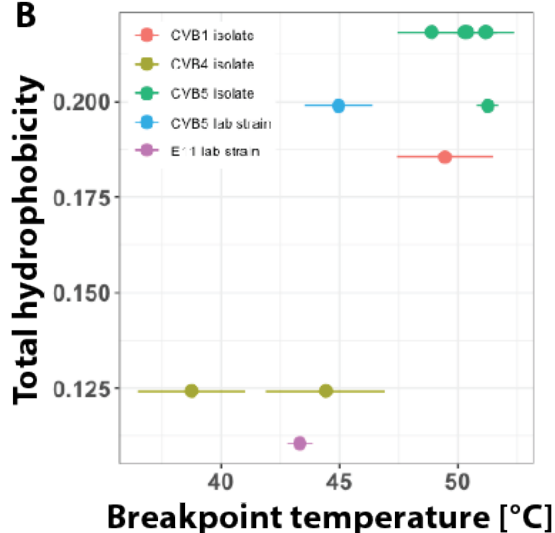


Figure 3.11 Pocket factor

(A) VP1 region potentially responsible of the interaction with the pocket factor. In red: amino acids binding to the pocket factor for CVB3. In blue: highlighted mutations from the Faulkner strain. In the Left: table displaying the total hydrophobicity with the corresponding viruses. (B) Plot of the total hydrophobicity versus the corresponding breakpoint temperatures of all viruses tested. The units of hydrophobicity are based on the HPLC retention time differences with Glycine as amino acid reference¹⁵⁷. The error bars correspond to the 95% confidence intervals

DISCUSSION

Proposed mechanisms of inactivation

Thermal inactivation at 30°C is either not affected by salt (pH 7.4), or inactivation is enhanced (pH 3 and 9). In contrast, at 55 °C, salt protected all viruses studied from inactivation. This finding indicates that thermal inactivation must proceed by two

fundamentally different mechanisms at the two temperatures studied, consistent with previous reports^{152,158}.

Proposed mechanisms at 30°C

An inactivation-enhancing effect of acidic and alkaline pH, as well as of salt, is consistent with a mechanism involving genome cleavage via RNA transesterification and hydrolysis. Specifically, this RNA degradation mechanism is catalysed by both acidic and basic solution constituents¹⁵⁹. Furthermore, at alkaline pH, increasing concentrations of monovalent ions were found to lower the pK_a of the 2'-hydroxyl group, which in turn favoured its deprotonation and enhanced the rate of nucleophilic attack of the 2'-oxyanion at the phosphodiester (transesterification)¹⁶⁰. For an encapsidated RNA molecule, the effect of pH may additionally be linked to the capsid conformational state. Specifically, at pH3, well below the lower isoelectric point coxsackievirus B5¹⁶¹, the virus adopts a conformation that exposes the RNA to degradation, while at a higher pH (>6.75) the capsid conformation allows efficient protection. Finally, an inactivation mechanism involving genome degradation is also supported by our finding of extensive genome degradation at 30 °C under inactivating conditions of pH and salt (Figure 3.3).

Proposed mechanisms at 55°C

The correlation of the inactivation rate constants at 55°C with the breakpoint temperature (Figure 3.7) suggests that protein degradation is the main inactivating mechanism at higher temperatures. The protective effect of salt then stems from its shielding effect of the electrostatic repulsion forces at the capsid pentamer interfaces (Figure 3.6).

Two different hypotheses may explain the dependence of the breakpoint temperatures on pH. First, and as explained above, a pH change may shift the capsid into a more thermosensitive conformation. Alternatively, pH may modify the protonation state of amino acids residues located at the pentamer interfaces, thus changing overall attraction forces, which result in a different temperature breakpoint.

Structural features leading to enhanced thermostability

Antigenic divergence

As described by Presloid and colleagues¹⁶², a shift in antigenicity can be accompanied by an increase in thermostability. Here we observed a shift of antigenicity from the CVB5 laboratory strain to the CVB5 environmental isolates. This shift may be linked with the

differences in breakpoint temperatures observed between the laboratory strain and the environmental isolates (Figure 3.5). Yet, this observation can only be meaningful for viruses within the same serotype, since the serum required a minimum of specificity.

Pentamer interface or pocket factor ?

At the outset of this study, we expected that stronger overall attraction forces at the pentamer interface would increase the breakpoint temperature, as more energy would be required to disrupt the capsid. Interestingly, however, the interaction forces at the pentamer interface of the studied viruses were different but did not correlate with the respective capsid breakpoint temperatures, indicating that the variability of thermoresistance between the different strains stems from a different mechanism.

A potential alternative to pentamer interaction forces for capsid stability is the role of the VP1 hydrophobic pocket region. It was described that this region can contain a pocket-factor ligand, which is modelled in various ways, but mostly as a fatty acid-like structure^{155,163}. Its function is related to the injection of the viral RNA following the binding of the virus capsid to a cell-receptor. Briefly, the current model of its function is the following: upon cell-receptor binding, the pocket factor is released, which destabilizes the capsid, allowing it to complete conformational rearrangements in order to inject the viral RNA into the host (J. Hogle 2002 and references therein¹⁶³), and suggest that it has a role in the capsid thermal stability¹⁶⁴. Specific antiviral compounds were described to block the virus cell infection by binding this specific pocket region, making the capsid unable to undergo conformational rearrangement and inject its RNA¹⁶⁵. WIN 51711 antiviral compound, known to bind in the VP1 pocket region, appeared to prevent the thermal inactivation of poliovirus infectivity, thus indicating a direct stabilizing effect of the virion¹⁶⁶. Muckelbauer and colleagues¹⁵⁵, described the WIN 66393 compound to inhibit the CVB3 uncoating but not the cell attachment, demonstrating that the central role of this pocket region in virus capsid uncoating. Later, the antiviral drug Pleconaril was described to inhibit enterovirus D68 infectivity, by binding to this pocket region and displacing the fatty acid-like structure present therein¹⁶⁷. All these findings indicate that the role of the VP1 pocket in capsid stabilization, and its interaction with the pocket factor may take place within the whole *Picornaviridae* family.

Herein, we observed a correlation of the hydrophobicity index of residues located in the VP1 pocket factor with the breakpoint temperatures. The mechanism would be that a lower hydrophobicity index may induce weaker interactions with the fatty acid-like pocket factor,

and reducing the energy required for its release from the capsid, thus decreasing the breakpoint temperature.

CONCLUSION

Overall, this study demonstrates a major impact of simple matrix variation on virus thermostability. We demonstrate that even simple matrix modifications, such as changing the pH or the salinity, can have a strong capsid stabilizing effects. Different inactivation mechanisms were determined, depending on the temperature applied. Salt appears to enhance genome degradation at acidic and alkaline pH conditions. Yet, the exact mechanisms involved in genome degradation are still an open question, but could be linked to a combination of the capsid conformational state and RNA cleavage. Finally, and in contrary to expectations, the variation in thermostability between different viruses was not linked to the protein interaction forces, but potentially due to a variation in the interaction with the pocket factor.

CHAPTER 4 Structural mechanisms causing heat resistance mediated by thermal adaptation or salt.

Experimental design and data analysis were performed by Meister S.; structural modeling was performed by Prunotto A. (Laboratory for Biomolecular Modeling, EPFL); inactivation experiments were performed by Bachmann V. and Meister S.

INTRODUCTION

Temperature is an important parameter controlling virus persistence in the environment. For example, temperature was found to modulate virus persistence in groundwater¹⁴⁷, soil¹⁴⁸, and on non-porous surfaces¹⁴⁹. Temperature can affect viruses in the environment either indirectly, e.g., by increasing the grazing rate of bacteria and protozoa^{168–170}, or directly by inducing structural changes on the virus capsid that result in inactivation. The selection of thermotolerant viruses would naturally improve the chances of environmentally transmissible viruses to find a new host, by extending their environmental persistence¹⁵⁰.

In this study, we assess the mechanisms that control and promote thermotolerance in coxsackievirus B5 (CVB5), an enteric human pathogen that is frequently detected in the aqueous environment¹⁷¹, and that it is notoriously resistant to disinfection⁶⁹. CVB5 is a member of the Enterovirus genus of the *Picornaviridae* family. These viruses have a single-stranded RNA genome, surrounded by an icosahedral capsid composed of 60 protomer repeats composed of four structural proteins (VP1 to VP4), and organized in pentameric subunits. Single-stranded RNA viruses have high mutation rates, because they lack proofreading during viral replication. This allows enteroviruses to rapidly adapt to a specific host (i.e., cell receptor), or increase their resistance to specific antivirals or physical-chemical stressors^{75,77,172,173}. Adaptation of an enterovirus (poliovirus) to heat was described by Shiomi and colleagues¹⁵², who subjected the virus to three successive cycles of thermal inactivation at 50°C followed by plaque selection. This resulted in the emergence of thermo-resistant strain, which could be attributed to a single valine to alanine mutation in VP1.

The mechanism of thermal inactivation of enteroviruses has been linked to disintegration of the viral capsid. Specifically, the dissociation of the capsid into pentameric subunits with increasing temperature was observed for foot-and-mouth disease virus (FMDV)¹²⁸. This indicates that interaction forces between the capsid pentamers determine the virus's thermostability. Therefore, one option for the virus to improve its thermoresistance is to increase the interaction forces between the pentameric subunits, by selective mutation of the amino acids at the interface. For example, engineering a disulfide bond into the

pentameric interface via the mutation of a single amino acid in VP2 efficiently increased the thermostability of FMDV by shifting the capsid breakpoint (melting temperature) by few degrees^{128,146}. Rincón and colleagues¹²⁶ demonstrated that a similar effect can be achieved by reduction of electrostatic repulsion forces at this interface. Here, they engineered mutations that reduced carboxylate-mediated repulsion forces at the pentameric interface, leading to a more thermostable virus capsid.

The goal of this study was to determine the thermoresistance of CVB5 prior to and after adaptation to temperature, and to determine the associated molecular mechanisms. To this end, we conducted four investigative stages. First, we produced thermoresistant strains by adaptation of CVB5 Faulkner strain to two temperatures (50 and 55 °C), and analysed the mutations selected through this process. Second, we applied structural modelling tools to quantify the protein interaction forces in the viral capsids, and analysed their variation between the thermo-adapted and non-adapted CVB5-Faulkner viruses. Third, we artificially disturbed these electrostatic interactions by increasing the ionic strength of the solution and analysed these effect on the capsid breakpoints. Finally, we investigated possible appearance of fitness trade-offs in the thermoresistant mutants.

MATERIAL AND METHODS

Cells and viruses

Human coxsackievirus B5 Faulkner strain (ATCC VR-185) was purchased from LGC Standards (Molsheim, France). Buffalo Green Monkey Kidney (BGMK) cells were kindly provided by the Spiez Laboratoy (Switzerland). Virus stock solutions were prepared by amplification in BGMK cells as described previously¹⁵¹, and were stored in phosphate-buffered saline (PBS; 5 mM Na₂HPO₄, 10 mM NaCl, pH7.4). Virus infectivity was determined by endpoint dilution with Most Probable Number (MPN) statistics method⁹², using confluent BGMK cells on 96-well plates, with five replicates and eight dilutions for each experimental sample. The cytopathic effect (CPE) was determined through microscopy after five days post-infection and incubation at 37°C with 5% CO₂. The infectivity was then reported as most probable number of cytopathic units per mL (MPNCU mL⁻¹).

Thermal inactivation and determination of breakpoint temperatures.

Two thermal inactivation assays were performed: a time-shift assay, where the virus infectivity is measured at different time points at fixed temperature (55°C) to determine first-order inactivation rate constants (see Chapter 3); and a thermal-shift assay, where different temperatures were applied over a fixed incubation time of one minute, to determine breakpoint temperatures (i.e., the temperature at which viral capsids break down, causing viruses to become inactivated, see Chapter 3). Both inactivation experiments were performed with a PCR thermocycler (Applied Biosystems, GeneAmp PCR system 9700). PCR tubes containing 90 µl of PBS were heated at the desired temperature, then 10 µl of the virus stock solution was spiked in the tube. The tubes were removed from the PCR machine at the designated time points and quickly placed into an aluminium PCR cooling block on ice. The initial virus concentration was measured by spiking 10 µl of virus into 90 µl of room-temperature PBS.

Thermal adaptation

Virus adaptation to high temperature was performed in two specific steps: a founder population (CVB5-Faulkner) was first exposed to 10 passages of cell culture adaptation, followed by 10 passages of thermal adaptation (Figure 4.1A). The cell culture adaptation consisted in infecting confluent T25 flasks of BGMK cells (at a concentration around 10⁵ MPNCU ml⁻¹) until reaching full CPE. The cell lysate was harvested, clarified by

centrifugation, and diluted by 2-log_{10} for the following infection passage. The 10th cell culture adaptation passage was used for the thermal adaptation.

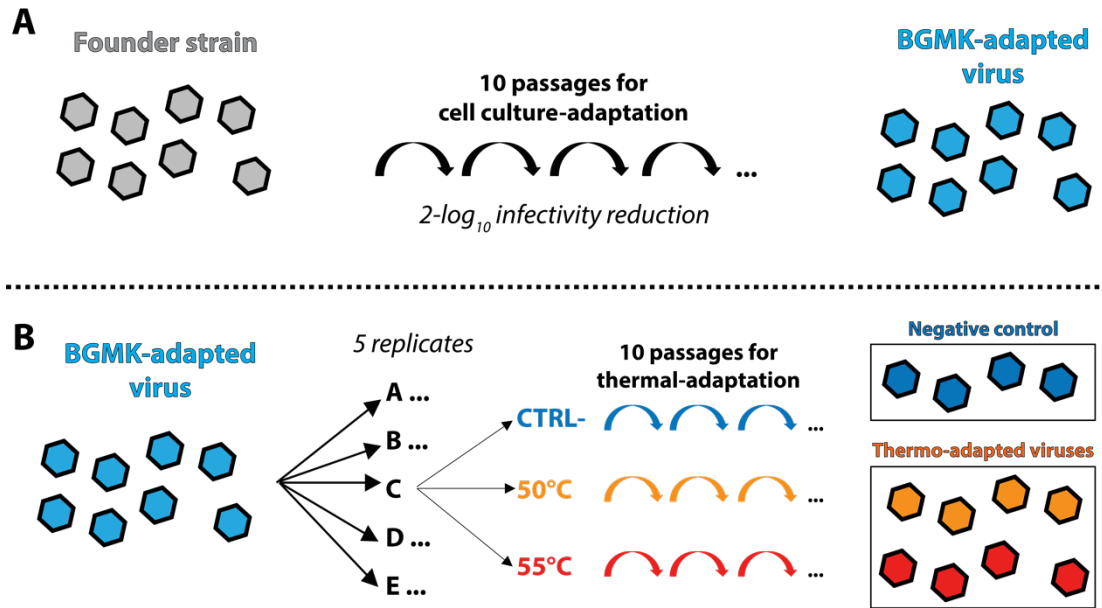


Figure 4.1 Scheme of the thermal adaptation assay.

This assay was performed in two steps, (A) cell-culture adaptation assay, where the Founder strain was passed 10 times in BGMK cell lines, and (B) where the adaptation occurred, with 5 different replicates and three conditions. The negative control (CTRL-) consisted in 2-log_{10} dilution titre by dilution of the virus at each passage, and the 50 and 55°C a 2-log_{10} reduction titre by thermal inactivation.

Temperature adaptation was performed under three separate passaging conditions: negative control (dilution in PBS), inactivation at 50°C, and inactivation at 55°C. Each condition was replicated five times in order to identify the appearance of temperature-unrelated mutations (Figure 4.1B). For the negative control, a simple 2-log_{10} dilution was applied between each passage, whereas for 50 and 55°C inactivation conditions, the cell lysates were concentrated to 100 μl with an Amicon 100 kDa molecular weight cut-off column (Sigma-Aldrich, Germany) and inactivated by approximately 2-log_{10} by thermal selective pressure. The entire concentrate was then used for the next infection passage. After reaching full CPE, all cell lysates were harvested and clarified by centrifugation. Thermal inactivation was performed with a PCR thermocycler, with an incubation time of 2 minutes for 50°C and 25 seconds for 55°C to reach 2-log_{10} reduction.

Genome sequencing

Whole genome sequencing was performed as described in Chapter 2, after the 10th adaptation passage. Mutations were identified by alignment with the original CVB5-Faulkner sequence (GenBank accession number: AF114383).

Competition assay to determine viral fitness

The fitness of the different adapted viruses was compared in a competition assay (Figure 4.2). This assay consisted in co-infecting (at the same titer, to a total of 10⁶ MPNCU ml⁻¹) the negative control and one of the thermo-adapted viruses. The combined virus sample was then either diluted by 2-log₁₀, or was subjected to a 2-log₁₀ inactivation by heat at 55°C. Subsequently, the sample was inoculated onto BGMK cells and was regrown. This process was repeated over four passages. At the end of the fourth passage, the VP1 region was sequenced to identify the dominant strain in the virus sample.

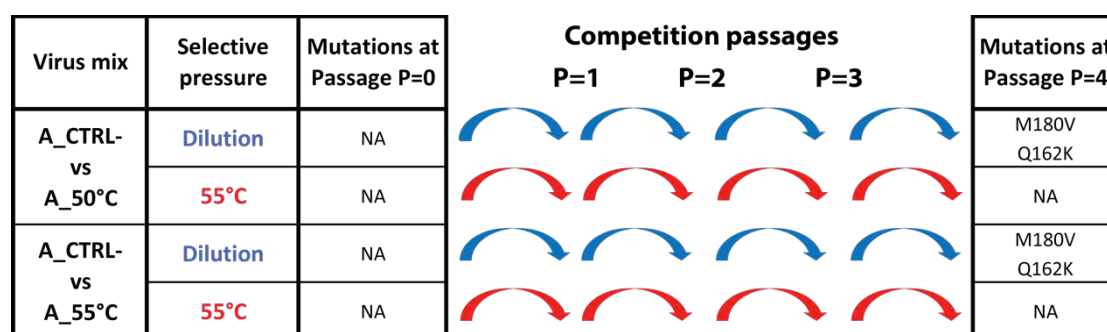


Figure 4.2 Schematic representation of the competition assay.

The competition assay consisted in mixing at the same titer the negative control (CTRL-) and one of the thermo-adapted virus. Two different selective pressure were used, a 2-log₁₀ dilution and a 2-log₁₀ inactivation by heat at 55°C. After reduction in the infective titer, the virus sample was regrown on BGMK cells. After four passages, the VP1 region was sequenced

Structural modelling.

3D capsid models were built using the known crystal structure of coxsackievirus B3 as a scaffold (PDB accession code: 1cov)¹⁵⁵. All models for the different strains were aligned through the Visual Molecular Dynamics (VMD) software¹⁷⁴ in order to recreate the basic unit of the capsid. In particular, for each strain we generated one single pentamer, together with

a portion of the neighboring pentamers. The same procedure was applied for the protomer interface (Figure 4.3). The protonation states of the aminoacids that compose the proteins were assigned with Propka¹⁷⁵. All the models were solvated using a TIP3P water model¹⁷⁶, and ionized. In order to assess the influence of salt concentration on the structural properties of each strain, we tested different levels of NaCl concentration (10 mM, 500 mM, 1 M, 2 M, 3 M). The large size of the systems (~900'000 atoms) did not allow performing long molecular dynamics studies. However, the structures were minimized with 1500 steps of conjugate gradient algorithm, in order to remove eventual clashes encountered during the homology modeling and aligning procedures. The presence of hydrogen bonds within the different models was detected with the HBonds plugin of VMD. The SaltBridges plugin was employed for the analysis of the salt bridges. In both cases, we examined both the total number of bonds within a pentamer, and within two specific interfaces, i.e. the pentamer interface and the protomer interface. Hydrogen bonds and salt bridges are considered to be part of an interface when the two residues that compose the bond are not part of the same domain (pentamer or protomer), but belong to two separate domains.

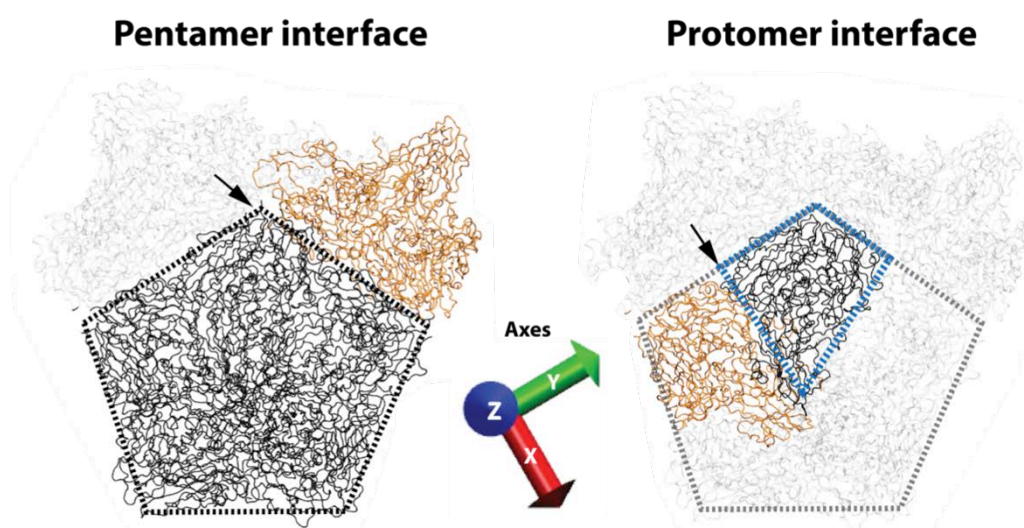


Figure 4.3 Schematic representation of the pentamer and protomer interfaces.

Left: capsid pentamer representation delimited by a black dotted line. Right: capsid protomer representation delimited by a blue dotted line. The black arrows show the direction of each interface. The axes are represented by 3 vector forces, x, y and z. X and z represent the interface shearing forces, and y the opposing forces of interest.

The NAMD molecular dynamics software engine¹⁷⁷ was used to calculate the Van der Waals (VdW) and electrostatic forces (ELEC) acting at these interfaces, with the unit of kilocalories per mole*Ångström (kcal/mol*Å). Those forces were divided in three axes: x and z for

shearing forces, parallel to the interface, and our vector of interest, y for the perpendicular forces. The overall interface force was calculated by calculating the sum of VdWy and ELEC y force vectors. These forces were determined separately for the pentamer and protomer interfaces. The modelling of the interaction forces were performed seven times, and the aberrant outlier values were removed ($< \pm 1000$ kcal/mol*Å).

Data analysis.

Data handling, MPN calculation and statistical analysis were performed using R software¹⁰⁰. The following CRAN packages were used: ggplot2¹⁰², gridExtra¹⁰³ and segmented¹⁰⁵. The breakpoint temperature was calculated using the segmented function from the segmented package using the linear model function (lm) as object. The 55°C inactivation was considered as first order and were calculated based on the log-linear portion of the decay curve, as described in Chapter 2.

RESULTS AND DISCUSSION

Thermal adaptation and its effects on virus inactivation, composition and fitness

Breakpoint temperatures and thermal inactivation rate constants of founder and evolved strains

The breakpoints of thermo-adapted viruses and the negative controls, together with the breakpoint of the founder virus, are shown in Figure 4.4. As is evident from the breakpoints of the negative controls, cell culture adaptation led to a reduction in the thermotolerance of CVB5, resulting in a $> 6^{\circ}\text{C}$ reduction in breakpoint temperature compared to the founder population. In contrast, thermo-adapted viruses were more resistant than the founder population ($> 2^{\circ}\text{C}$ higher breakpoints).

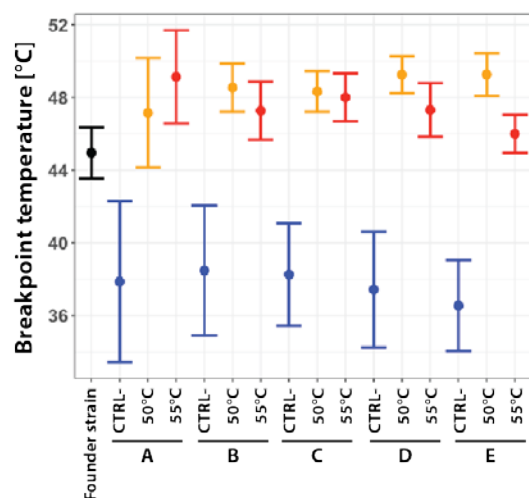


Figure 4.4 Temperature breakpoints after thermal adaptation.

Breakpoints of the five experimental replicates (A to E) of the negative controls (CTRL-), the 50 °C adapted populations and the 55 °C adapted populations. A thermo-adaptation in the condition 50 and 55°C is found, reflected by higher temperature breakpoints. The adapted strains were also more heat resistant than the founder strain (in black). The error bars correspond to the 95% confidence intervals.

After 10 passages of thermal adaptation, the 50 and 55°C adapted viruses exhibited a breakpoint shift of about 10°C compared to the negative controls. The breakpoint temperatures for the 55°C adapted viruses range from 45.9 to 49.1°C, from 47.1 to 49.2 °C for 50°C and from 36.5 to 38.4°C for the negative controls (Figure 4.4).

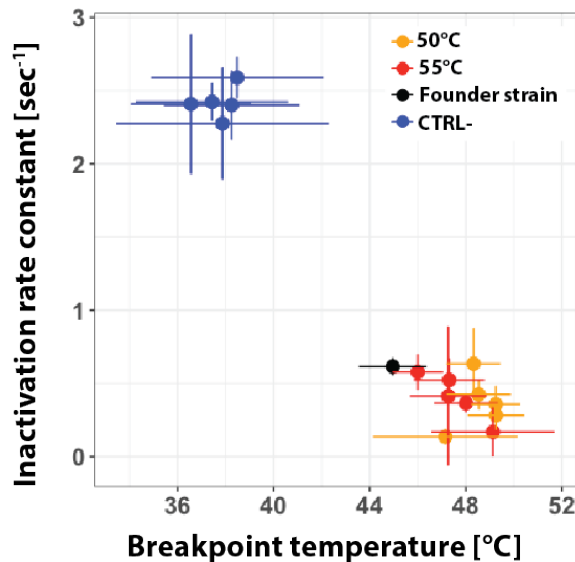


Figure 4.5 Correlation of the capsid breakpoint temperatures and inactivation rate constants at 55°C.

The measured breakpoint temperatures of the founder strain and the three evolved populations (five replicates each) are shown versus their corresponding inactivation rate constant measured at 55 °C. A clustering can be observed which divides the negative controls (CTRL-) from the thermo-adapted viruses, together with the founder strain. The error bars correspond to the 95% confidence intervals.

The breakpoint temperature of all evolved virus populations as well as the founder population were correlated against their inactivation rate constants determined at 55°C (Figure 4.5). A strong correlation was observed between the two variables (Figure 4.5) (Pearson's $r=-0.97$), though this is largely driven by the clustering of the negative controls and the thermo-adapted viruses. Taken separately, the negative control displayed no correlation, whereas within the thermo-resistant virus cluster, the correlation was still robust (Pearson's $r=-0.93$). This correlation is consistent with the notion that virus inactivation at 55 °C may be driven by melting of the viral capsid.

Mutations linked to thermoresistance

Sequencing the structural region of all adapted virus populations revealed no change in the consensus sequence between the founder strain and the negative control (Table 4.1). The observed loss in thermostability of the negative control (Figure 4.4) is thus likely associated with different minority mutations, which are not captured by the sequencing technique (Sanger) used here. The relevant minority mutations can only be identified by next-generation sequencing techniques, though this was out of the scope of this project.

Table 4.1 Mutation after thermal-adaptation

Table showing the occurrence of the mutation in each experimental replicate and condition. In grey: no mutation. Orange or red, occurrence of the mutation at 50 and 55°C, respectively.

		Replicate A			Replicate B			Replicate C			Replicate D			Replicate E		
		CTRL-	50°C	55°C	CTRL-	50°C	55°C	CTRL-	50°C	55°C	CTRL-	50°C	55°C	CTRL-	50°C	55°C
VP1	E26V			■			■			■			■			■
	M180V										■					
	I209F		■			■			■					■		
	N213D			■			■			■			■			■

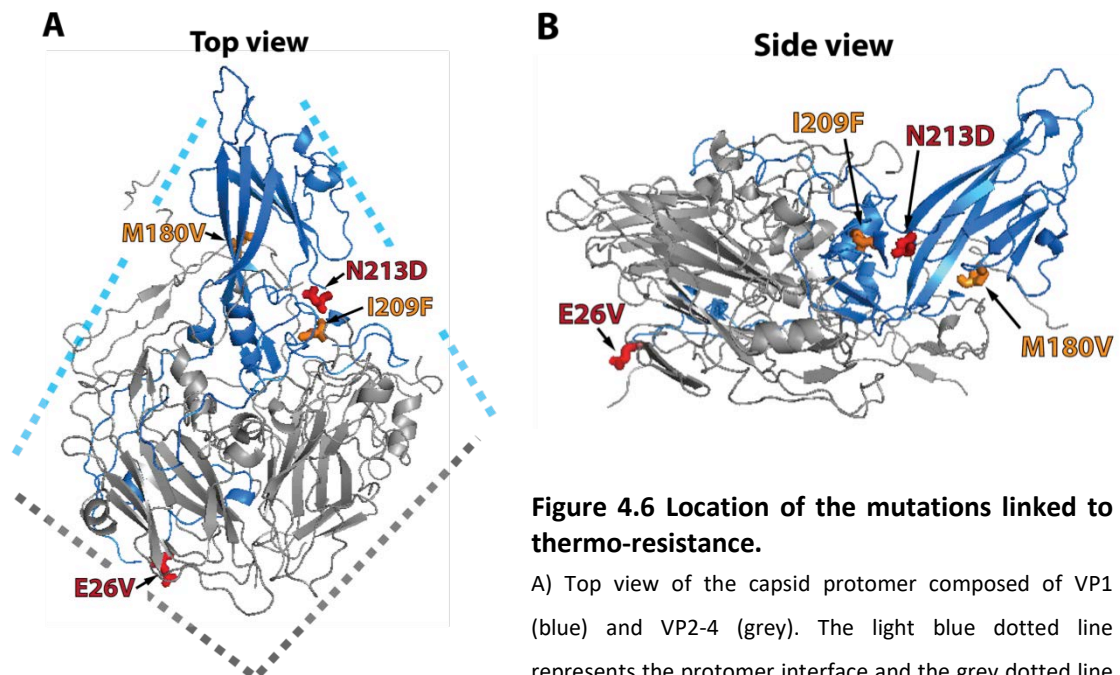


Figure 4.6 Location of the mutations linked to thermo-resistance.

A) Top view of the capsid protomer composed of VP1 (blue) and VP2-4 (grey). The light blue dotted line represents the protomer interface and the grey dotted line the pentamer interface. E26V is located near the pentamer interface, while I209F and N213D near the protomer interface. (B) Side view of the capsid protomer. M180V is located near the VP1 pocket of VP1.

In the heat-adapted strains, four non-synonymous mutations were found, exclusively located in VP1 (Figure 4.6). Two mutations were specific to 50°C-adapted viruses, either I209F or M180V, and two were specific to 55°C adapted strains E26V and N213D. Except for M180V, which only appeared in a single replicate, mutations were repeatedly found in at least four of the five biological replicates per condition. Mutations N213D and I209F

appeared close to the interfaces between capsid protomers, whereas E26V is located close to the pentamer interface. Mutation M180V is located near the binding pocket of VP1, at the center of the pentameric subunit (Figure 4.6A and B).

Comparative fitness of adapted viruses

If heat-adapted viruses were co-infected with the negative control during four passages (Figure 4.2), no mutations associated with the thermoresistant population was found in the final population, indicating that the thermoresistant strain is less efficient than the negative control at replicating on BGMK cells. However, if a mixed population was first inactivated by heat and then co-infected, a thermo-adaptive mutation (M180V) was conserved in the final population (Figure 4.2). Unexpectedly, however, the conserved mutation observed (M180V) was not originally detected in the thermo-adapted strain used (replicate A, containing the mutation I209F), but only observed in the thermo-adapted replicate D (Table 4.1). The appearance of the M180V mutation in at the end of the competition assay suggests that this mutation was present in replicate A, but only as a minority mutation. In addition, a second mutation, Q162K, was also present after the competition through heat-selective pressure.

Based on the results of this competition assay, we conclude that a higher breakpoint temperature is detrimental to viral fitness, if the only selective pressure between passages is dilution. A higher breakpoint temperature, however, gives a selective advantage under thermal pressure.

Influence of protein interaction forces on the thermostability of CVB5

Effect of salt on thermostability of CVB5

To investigate the role of protein interaction forces on virus stability, we determined the breakpoint temperature in buffer solutions with varying salt concentrations. Salt influences the magnitude of protein interaction forces, which in turn may influence thermal stability. The effect of salt on thermal stability was highly significant. Increasing the NaCl concentration from 10 mM to 1 M completely suppressed the virus inactivation of the founder strain at 55 C (Figure 4.7A), which was accompanied by a dramatic increase of temperature breakpoint from 44.9°C to 59.5°C. A strong correlation could be observed between the breakpoints temperatures and the salt concentration, until reaching a plateau around 2 M NaCl (Figure 4.7B).

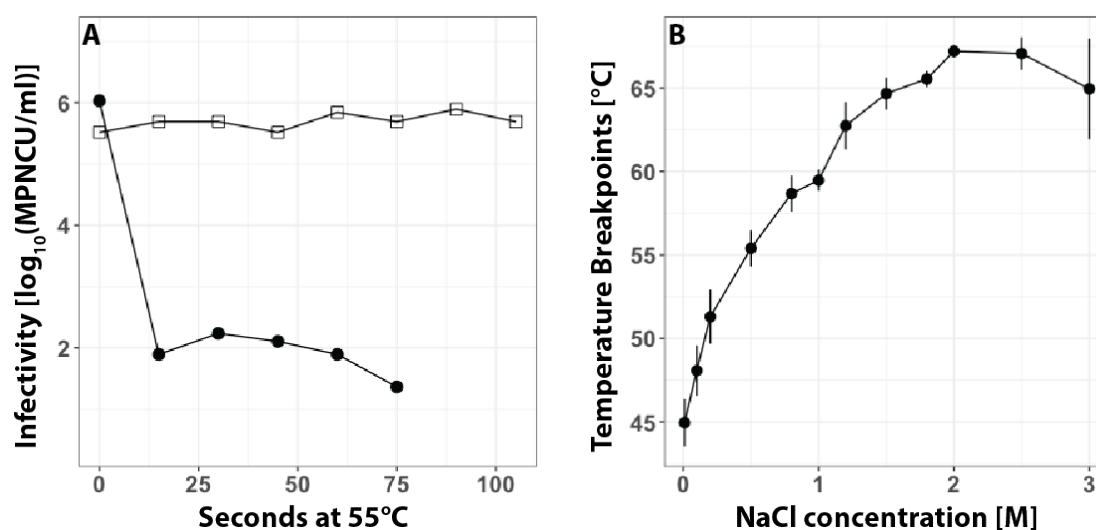


Figure 4.7 Effect of salt on the thermal stability on the founder virus.

(A) Inactivation curve measured at 55°C. Black dots correspond to 10 mM NaCl and white squares correspond to 1M NaCl. (B) Capsid breakpoints at different salt concentrations. The error bars correspond to the 95% confidence intervals.

Increasing the salt concentration affected the adapted strains to a similar extent. From 10 mM to 1 M NaCl, from 12 to 15°C difference in the breakpoints occurred for the founder population, the negative control, the I209F mutant, and the E26V_N213D double mutant (Table 4.2).

Table 4.2 Structural parameters of thermo-adapted and founder strains.

This table summarizes the results obtained for the structural parameter of the capsid for the thermo-adapted strains as well as the founder strain. SE: standard error. The unit the overall forces and its standard error is [kcal/mol*Å], and for the breakpoints and its standard error is [°C]. For the viruses: Orange and red corresponds to respectively 50 and 55°C adapted strains.

virus	NaCl [M]	Pentamer Interface				Protomer Interface				Breakpoints	
		Overall forces Value	SE	Number of H Bonds	Number of Salt Bridges	Overall forces Value	SE	Number of H Bonds	Number of Salt Bridges	Value	SE
Founder	0.01	-111.2	16.2	140	4	-97.8	63.2	148	6	44.96	0.72
E26V_N213D	0.01	-95.2	10.2	143	2	-129.8	70.9	143	6	49.13	1.31
I209F	0.01	-83.3	6.6	142	4	-25.6	58.2	145	6	47.15	1.53
M180V	0.01	-93.8	15.0	142	4	-60.6	94.7	147	6	49.25	0.52
Founder	1	-184.4	24.5	130	4	-186.5	45.8	142	6	59.47	0.32
E26V_N213D	1	-205.8	23.0	129	2	-359.3	124.5	141	6	61.51	0.41
I209F	1	-187.4	14.7	133	4	76.2	164.8	141	6	59.02	0.73
M180V	1	-229.1	24.8	123	4	-392.6	54.2	138	6	NA	NA
Founder	3	-352.5	14.7	96	4	-297.5	63.7	128	6	64.95	1.54
E26V_N213D	3	-359.1	20.0	100	2	-236.8	157.5	127	6	NA	NA
I209F	3	-362.5	23.3	97	4	-384.6	31.2	130	6	NA	NA
M180V	3	-336.8	23.9	101	4	-227.6	87.7	130	6	NA	NA

Effect of salt on protein interaction forces of the founder strain

In a next step, we determined how different protein interactions are influenced by salt, using the founder strain as the example. To this end, we determined the total electrostatic and van der Waals forces at the interface of viral proteins, and we analyzed the number of hydrogen bonds and salt bridges. Hereby, we focused on two interfaces: the pentamer interface, which previous reports have described as the location of capsid disintegration during thermal inactivation¹²⁸, and the protomer interface, which is the interface in closest vicinity to the mutations found herein (Figure 4.6A).

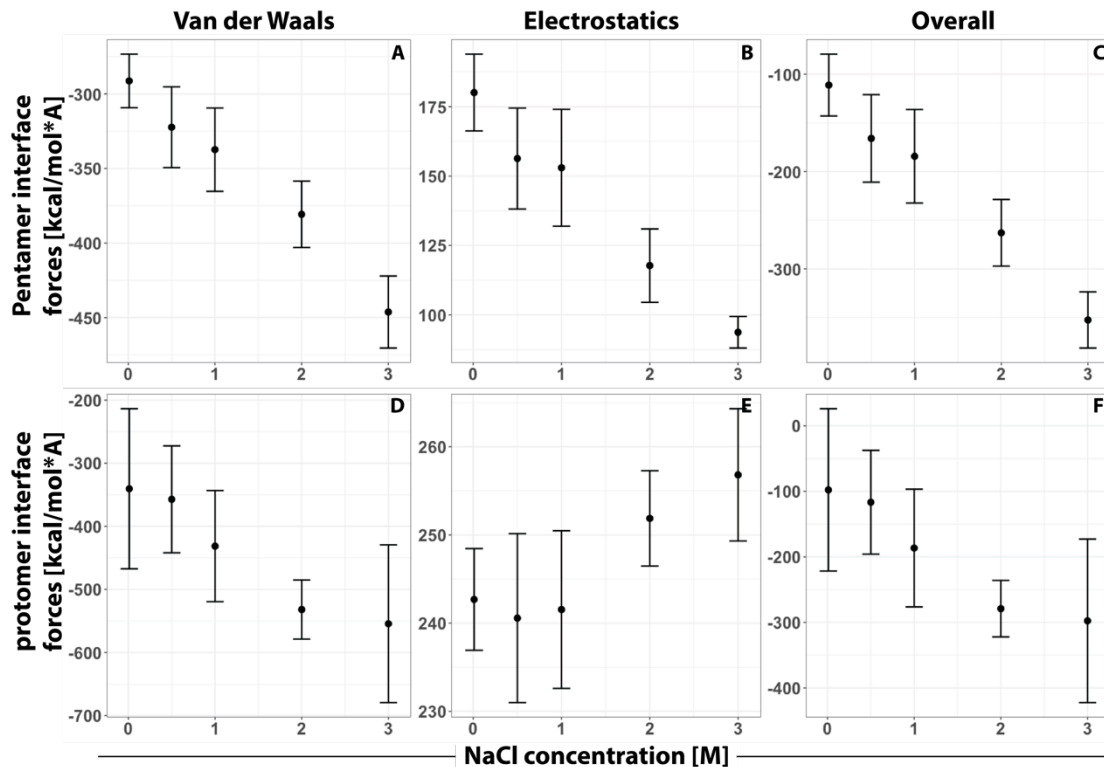


Figure 4.8 Effect of salt on the pentamer and protomer interaction forces

(A-C) Effect of salt on the pentamer interface interaction forces. (D-E) effect of salt on the protomer interface interaction forces. The error bars correspond to the 95% confidence intervals, based on 7 computational replicates. The data displayed here is based on the founder strain (CVB5-Faulkner).

Increasing salt concentrations at the pentamer resulted in a decrease in electrostatic repulsion and a strong increase in van de Waals attraction forces (Figure 4.8A and B). Hence, the presence of salt resulted in an increased of overall attractive forces (Figure 4.8C), which correlated with the capsid breakpoints measured under the corresponding solution conditions (Figure 4.9). Surprisingly, an opposite effect in electrostatic interactions was observed at the protomer interface, with an increase in electrostatic repulsion with increasing salt concentrations (Figure 4.8D and E). Nevertheless the strong concurrent increase in Van de Waals forces still resulted in of an overall increase of attractive forces (Figure 4.8F). The overall attractive forces at both interfaces are in accordance with the rational fact that the virus needs a stable capsid, requiring a significant amount of energy to be disrupted (i.e. by heating).

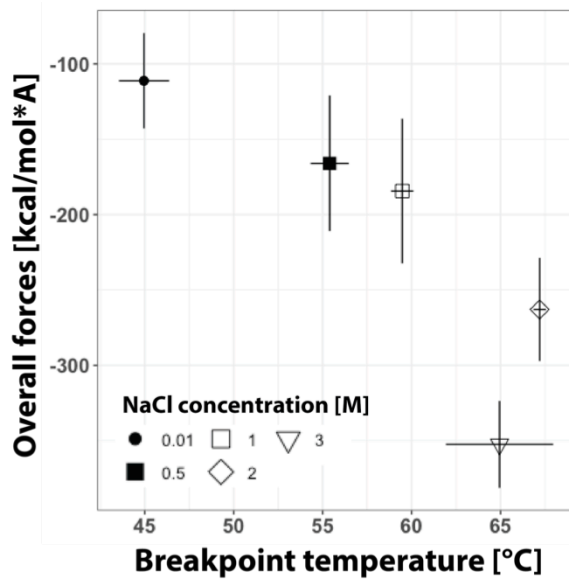


Figure 4.9 Effect of salt concentration on the interaction forces at the pentamer interface of the founder population.

A high correlation was observed between the overall interaction forces at the pentamer interface and the corresponding breakpoint temperature (Pearson's $r=-0.86$). The error bars correspond to the 95% confidence interval. The data displayed here is based on the founder strain (CVB5-Faulkner).

The salt concentration did not affect the number of salt bridges at either interfaces, but had a strong effect on H bonds (Figure 4.10). From 10 mM to 3M, their number reduced by ~40 for the pentamer interface, and by ~15 for the protomer interface (Table 4.2). Interestingly, this major reduction of the number of bonds within all interfaces appears to have a minimal effect compared to the combined thermo-stabilizing effect of reduced repulsions and enhanced Van de Waals forces.

Effect of mutations on protein interaction forces

Given that salt increases thermostability by altering protein interaction forces, it is thus reasonable to assume that mutations associated with thermoresistance may have a similar effect. To test this assumption, we compared the different force components between the evolved viruses and the founder stain. However, very few differences were found. Specifically, the number of salt bridges and hydrogen bonds was slightly lower in the pentamer interface than in the protomer interface. For the pentamer interface, the number of H bonds ranged from 140 to 143. All viruses had four salt bridges in the pentamer, except for the E26V_N213D mutant, which only displayed two salt bridges. At the protomer interface, the number of H bonds ranged from 143 to 147, and all viruses contained six salt bridges (Table 4.2). The capsid mutations that appeared during thermal adaptation did not significantly changed the interaction forces at either the pentamer nor the protomer (Figure 4.11). Changes in protein interaction forces thus cannot explain the role of mutations in thermostability.

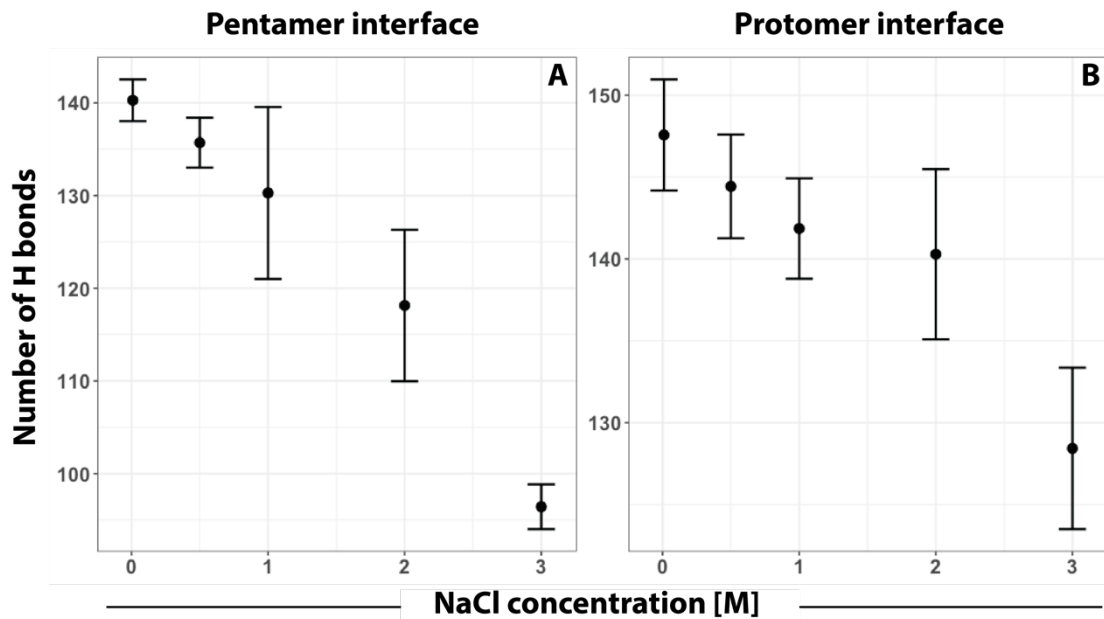


Figure 4.10 Effect of salt on the number of H bonds.

(A) Pentamer interface, and (B) Protomer interface. The error bars correspond to the 95% confidence intervals associated with 7 computational replicates. The data displayed here is based on the founder strain (CVB5-Faulkner).

An alternative explanation for the role of mutations is that they alter thermostability via changing the structure of the VP1 pocket. Specifically, Adeyemi et al. (2016)¹⁵³ described a thermo-stabilizing effect of mutations in the VP1 pocket of poliovirus 1 (I194V). Here, we also observed a mutation situated in the VP1 pocket (M180V), which appeared to be located at the exact position of I194V, by performing a VP1 structural overlay (data not shown). A similar mutation, M180I, was also present in CVB5 environmental isolates (see Chapter 3), changing the methionine to an amino acid with a higher hydrophathy index. Conversely, mutations in this region, acquired during the adaptation to capsid-binding compounds, were found to decrease the thermostability of enterovirus 71 and coxsackievirus A16¹⁷⁸. Combined, these findings indicate that mutation in this region may have a role in the interaction of the VP1 pocket with its pocket factor, and that this interaction is involved in thermostability of a virus.

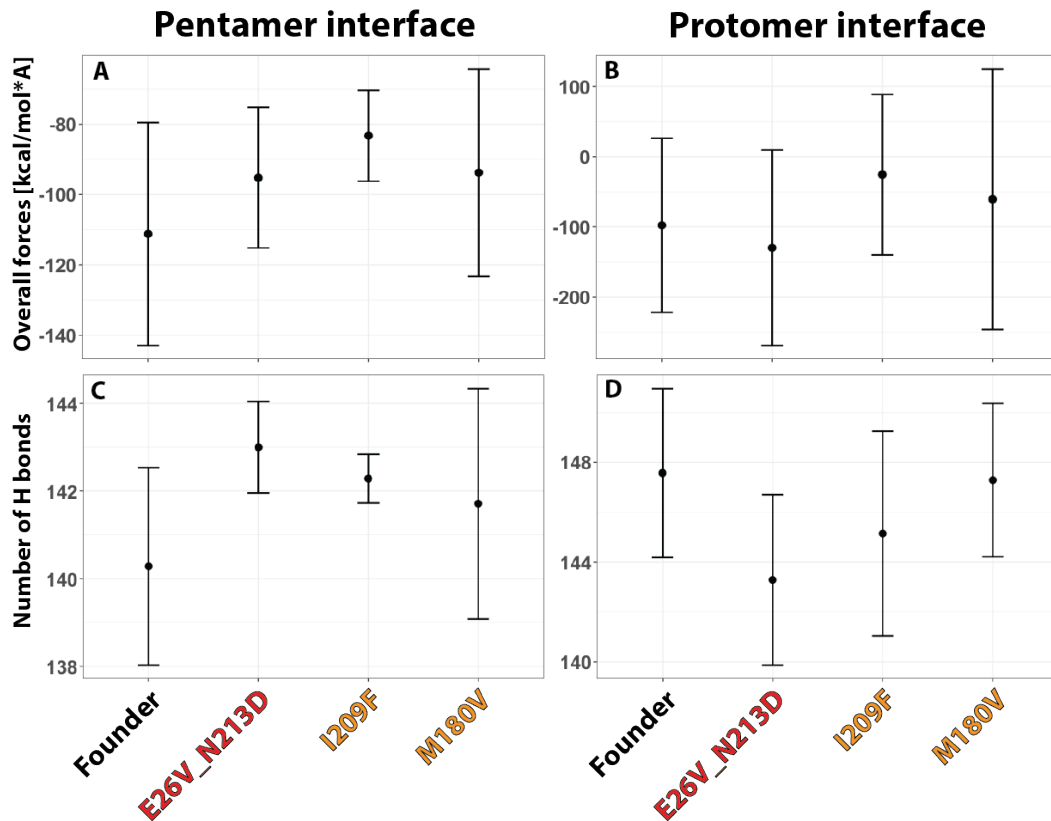


Figure 4.11 Effect of mutation on pentamer and protomer components.

(A and B) Effect on the overall interaction forces, and (C and D) effect on the H bond number. The error bars correspond to the 95% confidence intervals associated with 7 computational replicates. The data displayed here is based on the founder strain (CVB5-Faulkner).

CONCLUSION

We identified two modes of increasing a virus's tolerance to temperature: thermostability driven by the matrix (salt concentration), and thermostability driven by adaptive mutations. Salinity has a strong effect on the interaction forces at the capsid pentamer interfaces, by reducing the repulsion forces and increasing attraction forces, leading to a stronger overall attraction force. In contrast, mutations associated with thermoresistance do not significantly affect protein interaction forces. Instead, a mutation located near the VP1 pocket region may be involved in the interaction and release of the pocket factor, thus changing the thermal stability, but along with a fitness cost. Finally, another study found a mutation responsible for thermostability overlaying exactly with M180V in poliovirus 1, indicating that this specific way of structural thermostabilisation may be exclusive to coxsackievirus serotypes but to the whole *Picornaviridae* family.

CHAPTER 5 CONCLUSION AND PERSPECTIVES

In this study, we described that the laboratory strains are not representative of their respective environmental isolates in terms of disinfection. This may lead to an inaccurate estimation of the disinfection guidelines, and therefore to underestimation of water treatments. Also, a strong variability in inactivation kinetics was observed in the environmental isolates. As raised in Chapter 1, the actual problem of the Ct value database is that it contains predominantly laboratory strains, and should be completed by including a range of environmental isolates for each problematic serotype. Also, periodical isolation of environmental viruses may provide information about the current state of disinfection sensitivity of circulating viruses, and about changes that could occur over time, caused by numerous factors in constant evolution (i.e. climate change and demographics). The two main challenges of periodical virus isolation can be described. First, the volume of the specific matrix required to catch a “living” virus could be problematic. Here, a single litre wastewater influent was used as source, but other environmental matrices may require much larger volumes, with a more intricate isolation method. Second, isolation methods required to be specific enough to target the wanted serotype. Also, we emphasize that the maintenance of the virus laboratory strains stocks should be carefully performed. We observed that few cell culture-adaptation passages can induce a strong decrease of virus thermoresistance, with non-observable mutations through standard Sanger sequencing technique. The number of passages should be limited, and infections for virus stocks should be performed only at a high multiplicity of infection (MOI) to reduce the number of infection cycles.

We also demonstrated that even simple matrices can have a strong stabilizing effect on the virus. This effect was observed with the addition of NaCl at 55°C, and may be relevant for high temperature treatments for food processing. Interestingly, this protective effect appeared to be inverse at 30°C, with the contribution of an acidic or alkaline pH (3 or 9) on the degradation of the virus genome. Nevertheless, additional experiments are required to assess the effect of salt on the genome at high temperature, as well as protein damage at low temperature. High and low temperature assays have highly different incubation time-range (seconds versus days), and the inactivation mechanisms implied could have different kinetic speeds.

Finally, two thermostabilizing mechanisms were found, one matrix-related, and the other virus-related. The first one, implying the ionic strength, induced an increase of attraction

forces between the capsid pentamers, and the other, implying specific mutations, potentially inducing an increase of hydrophobicity in the VP1 binding region of the pocket factor. This indicates, in an adaptive point of view, that significantly increasing the interaction forces at the capsid interfaces may be too deleterious for the virus infectivity. The method of increasing these interaction forces by molecular engineering was proven to be efficient, although only for keeping the integrity of the virus capsid in vaccine design, without any regard in virus infectivity. Nevertheless, the thermostabilizing effect related to the pocket-region was accompanied by a competitive fitness trade-off as a cost, which could imply a slower host-receptor binding and RNA-injection kinetics. The implications of this pocket region in the virus environmental persistence are unknown, as other factors have to be taken in account (i.e. soil adsorption). Still, the interaction of the pocket region with the pocket factor appeared to be present in various viruses present in the *Picornaviridae* family, and higher interaction affinity may be also found in other virus serotypes originating from an environmental source.

Overall, this study highlighted major experimental gaps for an efficient implementation of wastewater treatment guideline for viruses; described the impact of simple matrices on virus thermostability; and targeted the virus structural characteristics responsible of this thermostability. These findings have a great impact on several topics, such as processing and consumption of raw or light-cooked food (i.e. shellfish), where the matrix content may significantly increase the virus thermostability. Furthermore, the fast heat-adaptation observed in this study could also be an interesting alternative to molecular engineering for producing thermostable vaccines at reduced cost, or using the pocket region as an alternative molecular engineering target. Finally, these findings may have an impact on the study of environmental persistence of viruses, by screening the rate of thermostabilizing mutations appearance in various virus serotype populations shed into the environment.

A. Appendix – CHAPTER 2

EXPERIMENTAL INFORMATION

Chemicals

Sodium thiosulfate (98.0%), polyethylene glycol (PEG)-8000, N,N-diethyl-p-phenylenediamine (97%) and NaClO₂ (puriss.) were obtained from Sigma-Aldrich (Germany); NaCl (99.5%), K₂S₂O₈ (99%), HCl (1N) and KCl (99%) from Acros Organics (Geel, Belgium); EDTA (99%) from Roth (Karlsruhe, Germany); Na₂HPO₄ (99.0%) from Fluka (Honeywell International Inc.); Glycine (puriss.) from BioRad (Hercules, USA); Chloroform (for analysis) from Millipore (Billerica, USA); HOCl (13-15%) from Reactolab SA (Servion, Switzerland); agarose powder from Invitrogen (Carlsbad, USA), and Neutral red from Biotium (Fremont, USA). Cell culture media consisted of modified Eagle medium supplemented with 1% penicillin-streptomycin per ml and 10% (growth medium) or 2% (maintenance medium) heat-inactivated fetal bovine serum (all purchased from Gibco, Frederick, MD).

Virus laboratory strains and cells

Human coxsackievirus B5 Faulkner strain (ATCC VR-185) and echovirus 11 Gregory strain (ATCC VR-41) were purchased from LGC Standards (Molsheim, France). Bacteriophage MS2 (DSMZ 13767) and its Escherichia coli host (DSMZ 5695) were obtained from the German Collection of Microorganisms and Cell Cultures (DSMZ, Braunschweig, Germany). Buffalo Green Monkey Kidney (BGMK) cells were provided by Rosina Girones, University of Barcelona.

Plaque assay

Twelve dilutions of the amplified viruses were prepared, and 6-well plates of confluent BGMK cells were infected for 1 hour at 37°C with a volume of 1 mL of the virus stock. An agarose overlay was prepared by mixing 50% v/v of a preheated agarose solution (PBS, 1.5% agarose) and 50% v/v of cell culture media. After the incubation, the virus inoculum was removed, then the cells were covered with the agarose overlay, and the agarose was let to solidify prior to returning it to the cell incubator. After 4-5 days post-infection, the cells were covered with a similar agarose overlay, but additionally containing 0.01% Neutral Red to visualize the plaques. Individual plaques were cut out and were placed in tubes containing 0.5 mL of cell culture media, and an equal volume of chloroform was added. This solution was mixed and centrifuged, and the chloroform-free fraction was harvested and used for downstream experimentation.

Bayesian model

The Bayesian model was based on the following likelihood function, similar to the approach presented originally by Haas⁹⁹:

$$S1 \quad L(\boldsymbol{\theta}|y_{ij}) = \prod_j \prod_i \binom{n_{ij}}{y_{ij}} (1 - \exp(-g(t_j) \cdot v_{ij}))^{y_{ij}} (1 - \exp(-g(t_j) \cdot v_{ij}))^{n_{ij}-y_{ij}}$$

where $g(t)$ is the log-linear function for the concentration of viruses with respect to time and the dose of disinfectant. By using this approach, the inputs to the model were the raw endpoint dilution data (the number of positive and negative wells in a given dilution series), and the model outputs were posterior probability distributions of the rate constants (k). The following vague prior distributions were used for the inactivation rates of Echovirus 11 and the Faulkner strain of CVB5 (Equations S2 – S4).

$$S2 \quad k \sim Normal(\mu = 0, \sigma^2 = 10^4)$$

$$S3 \quad b \sim Normal(\mu = 0, \sigma^2 = 10^4)$$

$$S4 \quad N_o \sim Gamma(\alpha = 10^{-13}, \beta = 10^{-13})$$

The mean and variance of the posterior distribution of the inactivation rate for the Faulkner strain were used to construct an informative prior distribution for inactivation rate coefficients of environmental CVB5 isolates (Equation S5).

$$S5 \quad k \sim Normal(\mu = \mu_{Faulkner}, \sigma^2 = \sigma_{Faulkner}^2)$$

Gibbs sampling was performed in R¹⁰⁰ with JAGS¹⁰¹ using three chains with 10,000 iterations and a burn-in period of 5,000 iterations. Convergence was verified by ensuring that Gelman and Rubin's potential scale reduction factor (PSRF) was <1.05.

ANCOVA analysis

To control the possibility of a batch effect between the replicates and assess the significance of the effect of the viruses and disinfectant on the dose, we implemented an ANCOVA analysis with the following parameters: the disinfectant, the virus type, and the amplification replicate stock. By taking the global results, the disinfectant displayed a significant level with a p-value < 0.05. Then, by analysing each disinfectant separately, the virus factor displayed a significant factor with a p-values well below 0.05, except for ClO₂ (p-value = 0.07). Finally, by taking in account the virus variance, the "replicate" factor for each disinfectant did not displayed any significant level (p-value > 0.05), which indicates that its effect can be neglected from the analysis.

TABLES AND FIGURES

Table A.1. Primer list.

Name	Sequence	Name	Sequence	Name	Sequence
CVB4-1F	AACAGCCTGTGGGTTGTACC	CVB4_M30_F7	ATGAGTCAATCAGGTGGACAA	CVB1_L16_F2	TATAGCACGGTGCCAATGTA
CVB4-1R	GGAAAGTGCATGCGAAACA	CVB4_M30_F8	AATGAAGTGCATGCGAAACA	CVB1_L16_F3	TTACAATGCTTGGAACTCTATGACA
CVB4-2F	ACTTCCCCCGTGTAGTTCAG	CVB4_M30_R1	TCACCTGAACCCCTGTAAGCTT	CVB1_L16_F4	ACACAACCTGATGTCCGCAA
CVB4-2R	TGTCACCATAAAGCAGCCAGTA	CVB4_M30_R2	AGACATTTCCCTGATGGCTGGT	CVB1_L16_F5	TTAGTTCAAGACCTACCAACTCA
CVB4-3F	CCGGTGTGCAATAGAGCAAT	CVB4_M30_R3	ACTGATCTTGTATCTCCCTGTA	CVB1_L16_F6	ATTGGCTGAAGAAAGTTTACAGAA
CVB4-3R	AAGTCCCGGTAGCGACTTTA	CVB4_M30_R5	TAGTTCGGTGAGCGTGGTA	CVB1_L16_F7	TCATCAACACCCCTAGCAA
CVB4-4F	TGTGGGTATAGTGACAGGGTTAGA	CVB4_M30_R6	ACTTCAACAAGTCGGCGATA	CVB1_L16_F8	TCGCCTTTCCGCTTGTCTT
CVB4-4R	TTGCATATTTTGCCTCAAGAG	CVB4_M30_R7	GAGAATTTACCCCTACCACA	CVB1_L16_F9	AAGAGGCCATCTTCTCCAAGTA
CVB4-5F	ACGATCCACGTACAATGCAA	CVB4_M30_R8	TTTACCCCTACCACACCGTT	CVB1_L16_R1	TGCATTGCCGTAATTTTCAGTA
CVB4-5R	TCCACTGGTGTGGGTATATGG	CVB5_F1	TACTTCGAGAAGCCAGTA	CVB1_L16_R2	ATAGAAGGTCCGCGACAT
CVB4-6F	CCACACCAGTGGATTAACCTG	CVB5_F2	TTAAAACAGCCTGTGGGTTGT	CVB1_L16_R3	TGGGTTCTGTAATGATGCCA
CVB4-6R	TGGGTGATGGTATGAAAA	CVB5_F3	TCCGATGCCTGCTCAACT	CVB1_L16_R4	TTTGACATCAGCAGGAACATA
CVB4-7F	TGATGTGACCCCTGAGATGA	CVB5_F4	ACATAAATAGTGTGCCCATGGA	CVB1_L16_R5	ACAGTCTCTGGCTGTGAA
CVB4-7R	CCACAAAACACAAATGTCCAGC	CVB5_F5	CCATGGATTAGCCAAACGCA	CVB1_L16_R6	TCAAATTTGAGCTAGAGCTGTA
CVB4-8F	CGGAAAATTTCTGGCTTGCAT	CVB5_F6	TCAAATAATGTATGTGCCCCCA	CVB1_L16_R7	TGTCATCTGCATCTCATTGA
CVB4-8R	GTCCTCAACATCGCTACTG	CVB5_F7	GAGAGTGAGTACTACCCCTAA	CVB1_L16_R8	AGTCACGAGCATGTCTAGTGAA
CVB4-9F	TTATCAAGGGCCAAACAGAGG	CVB5_F8	AGGTGAAGGAGAGCATGAATT	CVB1_L16_R9	AACCATACCCCTTCCCTGCTT
CVB4-9R	CATTTCTGCATAGCGCTTCAA	CVB5_F9	AAGATCAACATGCCCATGT	CVB5_L18_F1	AGTGTGCCAATGTGGTAGTA
CVB4-10F	TACAAGACAAGTGGCGCAGT	CVB5_F10	ATGATGAAGAGAACTCCAGCA	CVB5_L18_F2	AATCAGCTCGCTGTGTG
CVB4-10R	CGACCAACCCTGCATGAAACA	CVB5_F11	TCAAGGCCAACTTTGAGGA	CVB5_L18_F3	AGCCAGCAGTGTAGGAAAT
CVB4-11F	CGGCATATATGGCTACAATTCA	CVB5_F12	TACAGAGACAACACTACTTTGT	CVB5_L18_F4	ACTACACTGAAGGAAAAGTGT
CVB4-11R	CCACTCTGTAGTTGCCACA	CVB5_F13	TGCTATTTGGCTTGGCACA	CVB5_L18_R1	ACCAACAGGTGTCAACTTGT
CVB4-12F	GTCAGCACAACACTACCGCTCA	CVB5_F14	AGTGTAGATCAGGCGATGA	CVB5_L18_R2	AACCTTTGAAATTCATGGCACAA
CVB4-12R	AGCAAAGCCAAACACCTT	CVB5_F_F1	ATCCGGTATCCACAGAGCAA	CVB5_L18_R3	TGTTGGTACCATGCGATGA
CVB4-13F	GACCTTCTGTGGTTGGAGGA	CVB5_F_F2	AGGTCAATCACATTAGGAACT	CVB5_L18_R4	TTTACAGAGCCGGTAAAGGATA
CVB4-13R	GGGACACTTTCCGCTTGTAG	CVB5_F_F3	ATATACACTACACGTGCAATGCA	CVB5_M30_F1	TTTACAGAGCCGGTAAAGGATA
CVB4-14F	GGCAAAATAACAACCTGGCTCA	CVB5_F_R1	ATTGGTGGCACTGTCACTGT	CVB5_M30_F2	TTAACAAGTTACAGCTGGCAGA
CVB4-14R	TTTGTCTCAGCAGCGTACAG	CVB5_F_R2	TTGCACCTGTGCTGTAACCT	CVB5_M30_F3	TTCTCAGAAACGGTGATCCA
CVB4-15F	TGCTGAAGCAAAAAGGGTCT	CVB5_L2_F1	TTTTCAGTCACTTTGCGT	CVB5_M30_F4	TCAACACCCCAAGCAAAAACA
CVB4-15R	TTGGTGGGACAAAATCAACA	CVB5_L2_F2	TCAACACCCCAAGCAAAAACA	CVB5_M30_F5	AAGTTGGAGGACGCGATTTA
CVB4-16F	TGTTGATTTTGTCCCAACAA	CVB5_L2_R1	AAACTCAACAATCACCACACA	CVB5_M30_F6	AATGAGGACGACATTTGGCA
CVB4-16R	TGGATAGCCTTCCCAACAA	CVB5_L2_R2	TTGGAGAGAATATCCCTTCTTT	CVB5_M30_F7	AATGATTTGCCTATGAGACGA
CVB4-17F	CTGGACATGCTTGTGACTGAA	CVB5_L3_F1	TACAGTGACAGGGTGTGATCT	CVB5_M30_F8	TGGATTGCAATCAAGATACAGAA
CVB4-17R	CCTGCTACGGAGACCAAAAGT	CVB5_L3_F2	ACATCCACGAGTCCATTAGGT	CVB5_M30_F9	TAATAACAGTGACTCTACACTT
CVB4-18F	GTCCTCCGTAGCAGGGATCAAT	CVB5_L3_F3	AGCAGTCTTAAGAAACGGA	CVB5_M30_F10	AACTGTCTGTCTACTGCT
CVB4-18R	TCTACTACGCCCACTTCTGTA	CVB5_L3_R1	ATGATACITTTGCCCTCGGT	CVB5_M30_R1	TTCTGACCAGTGTGTGTAATA
CVB4-19F	GGAGCTGACGCTCTTGAAC	CVB5_L3_R3	TAGCCTGCATCGTTGTGA	CVB5_M30_R2	ACCTTAAGATGCCACCAACA
CVB4-19R	TCCTTGGTGTCCATTTCCA	CVB5_L8_F1	AGTGTGCTAATGTGGTGGT	CVB5_M30_R3	ATCGCTCCATAGGCAATCATT
CVB4-20F	TGGAAATGGACACCAAGGAT	CVB5_L8_F2	TGAGGCTGGTGTGATGCTAAA	CVB5_M30_R4	TCTGTGCTGATGCCAATGT
CVB4-20R	GTGGTCAACAGCTTCCATCA	CVB5_L8_F3	AGGATGATAGCGTATGGGGA	CVB5_M30_R5	TGCTACTTCTCAGCTGACCT
CVB4-21F	TGATGGAAGCTGTTGACCAC	CVB5_L8_F4	ACACGTCATCTGGGATGTT	CVB5_M30_R6	ACGCACAAGTAGTGTITGCT
CVB4-21R	CTTTGGCCACTTTCTCTGCT	CVB5_L8_F5	AGTGACCAGGAGCAATATTTT	CVB5_M30_R7	AGCTAGCCACTTCTACTGT
CVB4-22F	AGCAGAGAAAGTGGCCAAAG	CVB5_L8_R1	TGCCCTCAGTGTGTTAACT	CVB5_M30_R8	ATCTTAATTTCCCTGTACACTGGT
CVB4-22R	ATGGGAATACCCCAAGTTTT	CVB5_L8_R2	AGCTTCATGGGTTCCGTACT	CVB5_M30_R9	TTGGCTATACATCGAGATAACTT
CVB4-23F	AAAAGCTGGGATATCCCATATA	CVB5_L8_R5	AGCAACGCTGATTTTGATCTCT	CVB5_M30_R10	AAGCCAGCAAAACAGCTTATA
CVB4-23R	CAAGCCATAGCCTTTTCCAG	CVB5_L9_F1	AGCGGAACCGACTACTTT	CVB5_R1	TAGACTTTCGCACCATGT
CVB4-24F	CCAGTGTGCAATCAAAGA	CVB5_L9_F2	TGGCAACATCAACTAACCCAA	CVB5_R2	TAGGTAGGCCACACTCCATA
CVB4-24R	GTGAATTTACCCCGACCACA	CVB5_L9_F3	AATGCACCAACAGTGTGAGA	CVB5_R3	TGACAGTGGCGCAATGT
CVB4_F12_F1	TAGCAAGTTTACAGAACCAAGT	CVB5_L9_F5	ACCCGTAGGACGCTTCAATA	CVB5_R4	ACGAAGCACAAAGTCTTGCA
CVB4_F12_F2	AGGGTAATGCACCACCAA	CVB5_L9_F6	AGTTCACAGAACCAGTAAAGGA	CVB5_R5	TAGCCCAACCATCATAGAACAT
CVB4_F12_F3	ACTCAAGGTCAACTTTGAAGAA	CVB5_L9_F7	ACATCCTCTCCAAGAGGACT	CVB5_R6	TTCAACCCCATGGTGACGA
CVB4_F12_R1	ATCGCGCAGAAAATCGTT	CVB5_L9_F8	AGGGTATACTCATAAGGAAACCA	CVB5_R7	CTTTTTGCTCAGCAGCATA
CVB4_F12_R2	TAGTGGGCGAAAATTTGGACATT	CVB5_L9_R1	ATTGTCAACATAAGCAGCCA	CVB5_R8	TGCTGTGGTGTGACTCCCT
CVB4_F12_R3	TTAGTATGAGGGCTCTGATT	CVB5_L9_R2	ACACCTCAAAAATACCCACAAT	CVB5_R9	TCTGATGCTCTGAACTTCTCATT
CVB4_M30_F1	AAGTTCACAGATGCACTATCA	CVB5_L9_R3	ACATCTCAGTAACCCAGTGT	CVB5_R10	TCTCCAGTTTCAATTTGGTT
CVB4_M30_F2	ATCACAGTTGATCCAAGTGA	CVB5_L9_R4	TTTTCAGTCACTTTGTGTATCA	CVB5_R11	TCACCATATGCAATCATCTCT
CVB4_M30_F3	TCACTCAAGGCCCTTAGTCAA	CVB5_L9_R5	TGAGGGCTGGCATTGACT	CVB5_R12	GCACCGAATGCGGAAATTTACCCCT
CVB4_M30_F4	AGTGACAGACTATGGCTTTCTT	CVB5_L9_R6	TGCAGACCCGCAAAAACATAA	CVB5_R14	TGYCTGGTTTGCATRTGT
CVB4_M30_F5	AAGCCGAGGGTATCCCTAT	CVB5_L9_R7	AAGGGTATGCTCATCTGATCT		
CVB4_M30_F6	AATGGCAGCACTGGAGGA	CVB1_L16_F1	TAACCTGGCAACAGGCAA		

Table A.2. Percentage of nucleotide identity.

This table is base on the VP1 coding sequence.

Virus											
	Echovirus 11	CVB4 M063015	CVB4 T051217	CVB1 L071615	CVB5 L030315	CVB5 L070915	CVB5 L061815	CVB5 L070215	CVB5 M063015	CVB5 Faulkner	CVB5 L060815
Echovirus 11	100										
CVB4-M063015	58.64	100									
CVB4-T051217	59.55	88.14	100								
CVB1-L071615	60.34	64.07	64.77	100							
CVB5-L030315	59.66	65.15	64.57	66.27	100						
CVB5-L070915	59.77	65.27	64.45	66.16	99.41	100					
CVB5-L061815	60.00	64.22	63.75	67.22	90.81	91.17	100				
CVB5-L070215	59.32	64.22	64.57	65.69	90.46	90.34	91.40	100			
CVB5-M063015	59.66	64.45	64.45	65.57	90.34	90.46	91.52	98.94	100		
CVB5-Faulkner	60.90	65.27	65.38	67.69	77.03	76.80	77.50	77.39	77.15	100	
CVB5-L060815	61.81	64.57	65.15	67.22	79.15	79.15	79.15	80.21	80.33	81.74	100

Table A.3. Percentage of protein identity.

This table is based on the translated region of the virus structural proteins (VP1 to VP4).

Virus											
	Echovirus 11	CVB4 M063015	CVB4 T051217	CVB1 L071615	CVB5 Faulkner	CVB5 L061815	CVB5 L060815	CVB5 L030315	CVB5 L070915	CVB5 L070215	CVB5 M063015
Echovirus 11	100										
CVB4-M063015	89.44	100									
CVB4-T051217	89.63	99.76	100								
CVB1-L071615	90.22	93.52	93.62	100							
CVB5-Faulkner	90.83	92.13	92.45	92.82	100						
CVB5-L061815	90.72	91.77	92.10	92.82	99.06	100					
CVB5-L060815	91.07	92.13	92.69	92.58	98.94	98.94	100				
CVB5-L030315	90.72	91.89	92.45	92.58	98.71	99.18	99.53	100			
CVB5-L070915	90.72	91.89	92.45	92.58	98.59	99.06	99.41	99.88	100		
CVB5-L070215	90.83	91.77	92.33	92.46	98.59	99.06	99.65	99.76	99.65	100	
CVB5-M063015	90.95	91.89	92.22	92.58	98.71	99.18	99.53	99.65	99.53	99.88	100

Table A.4. Kinetic inactivation parameters for individual virus strains.

Summary of *k* values and their 95% confidence intervals (CI95) for all viruses and all inactivation methods. The last three columns represent the *Ct* values for 1, 2 and 4- \log_{10} virus inactivation, calculated based on the corresponding *k* values. The corresponding units for *Ct* values is $\text{mJ}\cdot\text{cm}^{-2}$ for UV_{254} and sunlight, $\text{mg}\cdot\text{min}\cdot\text{L}^{-1}$ for free chlorine and chlorine dioxide, and seconds for heat. For ClO_2 , the *k* values are based on a disinfectant doses up to the segmental linear regression breakpoint, thus *Ct* greater required values are not shown (asterisk).

Virus	Disinf.	k value	95CI		Ct value		
			Lower	Upper	1- \log_{10}	2- \log_{10}	4- \log_{10}
MS2	UV ₂₅₄	0.15	0.14	0.15	15.85	31.69	63.38
Echovirus 11	UV ₂₅₄	0.35	0.32	0.37	6.66	13.32	26.65
CVB1-L071615	UV ₂₅₄	0.28	0.26	0.31	8.12	16.24	32.47
CVB4-M063015	UV ₂₅₄	0.35	0.33	0.37	6.51	13.03	26.05
CVB4-T051217	UV ₂₅₄	0.38	0.35	0.41	6.12	12.24	24.48
CVB5-Faulkner	UV ₂₅₄	0.37	0.35	0.39	6.21	12.42	24.83
CVB5-L070215	UV ₂₅₄	0.33	0.31	0.36	6.88	13.76	27.51
CVB5-L030315	UV ₂₅₄	0.34	0.31	0.36	6.86	13.71	27.43
CVB5-L060815	UV ₂₅₄	0.36	0.34	0.39	6.33	12.66	25.32
CVB5-L070915	UV ₂₅₄	0.37	0.34	0.39	6.30	12.60	25.20
CVB5-L061815	UV ₂₅₄	0.32	0.30	0.35	7.11	14.23	28.45
CVB5-M063015	UV ₂₅₄	0.37	0.35	0.39	6.18	12.36	24.72
MS2	Sunlight	0.0013	0.0012	0.0013	1809.60	3619.21	7238.41
Echovirus 11	Sunlight	0.0017	0.0014	0.0020	1357.55	2715.10	5430.20
CVB1-L071615	Sunlight	0.0059	0.0053	0.0064	393.06	786.12	1572.23
CVB4-M063015	Sunlight	0.0057	0.0052	0.0062	404.33	808.67	1617.34
CVB4-T051217	Sunlight	0.0059	0.0051	0.0067	388.47	776.94	1553.89
CVB5-Faulkner	Sunlight	0.0032	0.0029	0.0036	712.13	1424.25	2848.50
CVB5-L070215	Sunlight	0.0081	0.0076	0.0085	285.70	571.41	1142.82
CVB5-L030315	Sunlight	0.0077	0.0073	0.0082	297.73	595.46	1190.92
CVB5-L060815	Sunlight	0.0089	0.0083	0.0094	259.57	519.15	1038.30
CVB5-L070915	Sunlight	0.0078	0.0072	0.0083	296.87	593.74	1187.48
CVB5-L061815	Sunlight	0.0080	0.0073	0.0086	288.58	577.16	1154.33
CVB5-M063015	Sunlight	0.0090	0.0084	0.0097	255.43	510.87	1021.73
MS2	Free Chlorine	5.88	5.76	5.99	0.39	0.78	1.57
Echovirus 11	Free Chlorine	8.04	6.75	9.41	0.29	0.57	1.15
CVB1-L071615	Free Chlorine	1.44	1.31	1.57	1.60	3.20	6.41
CVB4-M063015	Free Chlorine	6.56	5.97	7.15	0.35	0.70	1.40
CVB4-T051217	Free Chlorine	5.71	4.99	6.48	0.40	0.81	1.61
CVB5-Faulkner	Free Chlorine	4.12	3.83	4.42	0.56	1.12	2.23
CVB5-L070215	Free Chlorine	0.83	0.71	0.93	2.79	5.58	11.16
CVB5-L030315	Free Chlorine	3.36	3.12	3.62	0.69	1.37	2.74
CVB5-L060815	Free Chlorine	4.87	4.55	5.22	0.47	0.94	1.89
CVB5-L070915	Free Chlorine	2.83	2.67	2.99	0.81	1.63	3.26
CVB5-L061815	Free Chlorine	3.06	2.82	3.31	0.75	1.50	3.01
CVB5-M063015	Free Chlorine	3.17	2.96	3.39	0.73	1.45	2.90
MS2	Chlorine dioxide	37.94	36.20	39.75	0.06	0.12	*
Echovirus 11	Chlorine dioxide	43.95	27.40	60.64	0.05	*	*
CVB1-L071615	Chlorine dioxide	46.06	40.25	51.82	0.05	0.10	*
CVB4-M063015	Chlorine dioxide	17.11	15.00	19.28	0.13	0.27	0.54
CVB4-T051217	Chlorine dioxide	24.90	22.31	27.62	0.09	0.18	0.37
CVB5-Faulkner	Chlorine dioxide	33.55	26.87	40.02	0.07	0.14	*
CVB5-L070215	Chlorine dioxide	35.07	29.10	41.23	0.07	0.13	*
CVB5-L030315	Chlorine dioxide	20.83	13.39	28.28	0.11	*	*
CVB5-L060815	Chlorine dioxide	24.33	22.43	26.22	0.09	0.19	0.38
CVB5-L070915	Chlorine dioxide	28.54	25.38	31.72	0.08	0.16	*
CVB5-L061815	Chlorine dioxide	36.32	28.71	43.82	0.06	0.13	*
CVB5-M063015	Chlorine dioxide	16.44	13.91	19.00	0.14	0.28	0.56
MS2	Heat (55°C)	0.0083	0.0081	0.0085	277.41	554.82	1109.64
Echovirus 11	Heat (55°C)	1.15	0.95	1.37	2.00	3.99	*
CVB1-L071615	Heat (55°C)	0.25	0.19	0.32	9.04	18.09	*
CVB4-M063015	Heat (55°C)	0.72	0.67	0.76	3.21	6.41	12.83
CVB4-T051217	Heat (55°C)	2.11	1.90	2.32	1.09	2.19	4.37
CVB5-Faulkner	Heat (55°C)	0.62	0.57	0.68	3.68	7.37	14.74
CVB5-L070215	Heat (55°C)	0.23	0.21	0.26	9.83	19.66	39.32
CVB5-L030315	Heat (55°C)	0.18	0.14	0.21	13.11	26.22	*
CVB5-L060815	Heat (55°C)	0.20	0.18	0.23	11.35	22.70	*
CVB5-L070915	Heat (55°C)	0.22	0.21	0.24	10.24	20.48	40.97
CVB5-L061815	Heat (55°C)	0.16	0.15	0.18	13.99	27.98	*
CVB5-M063015	Heat (55°C)	0.19	0.18	0.21	11.99	23.98	47.96

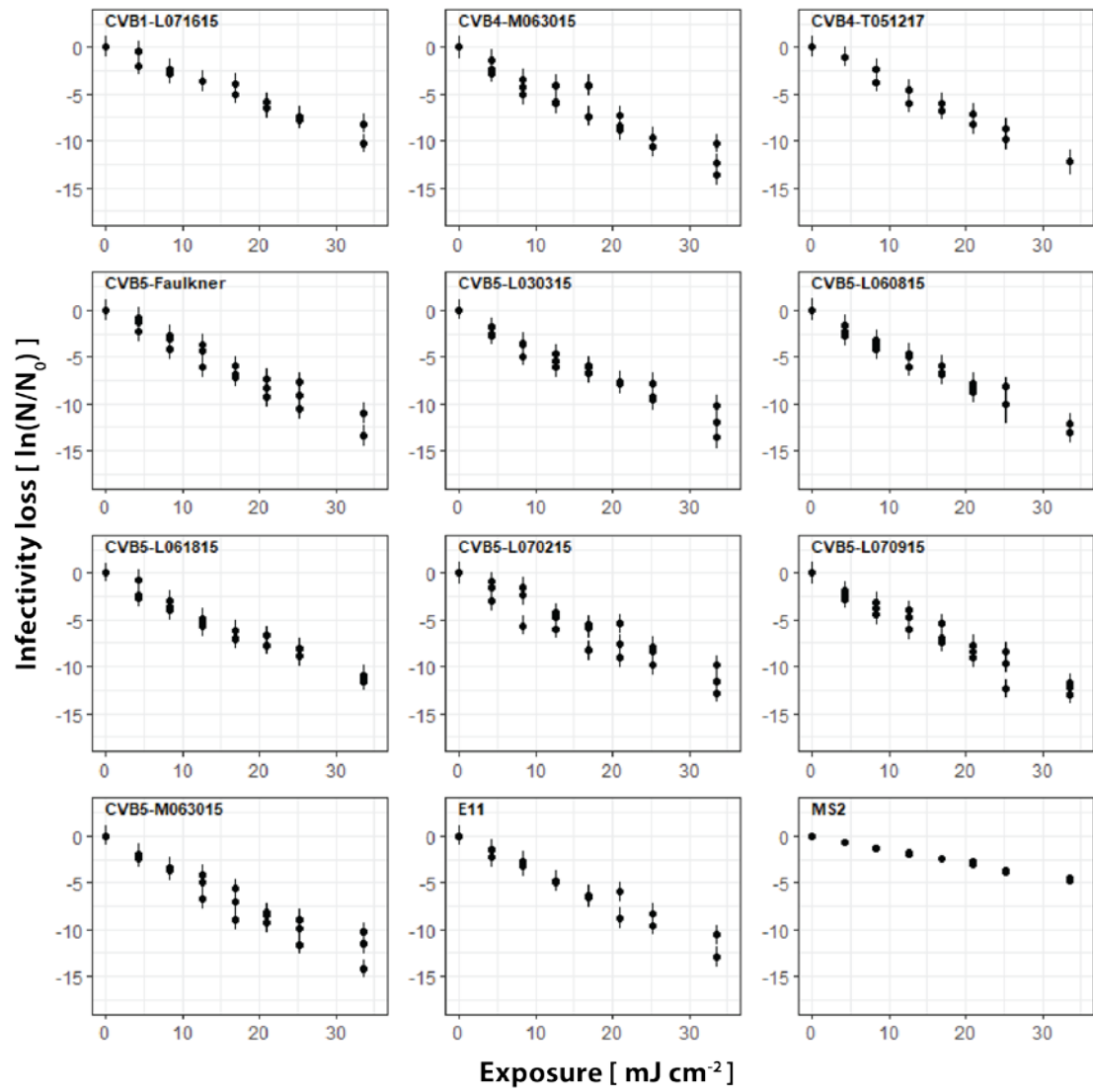


Figure A.1. UV₂₅₄ inactivation curves for all viruses.

The error bars represent the 95% confidence intervals associated with the measured infectivity loss.

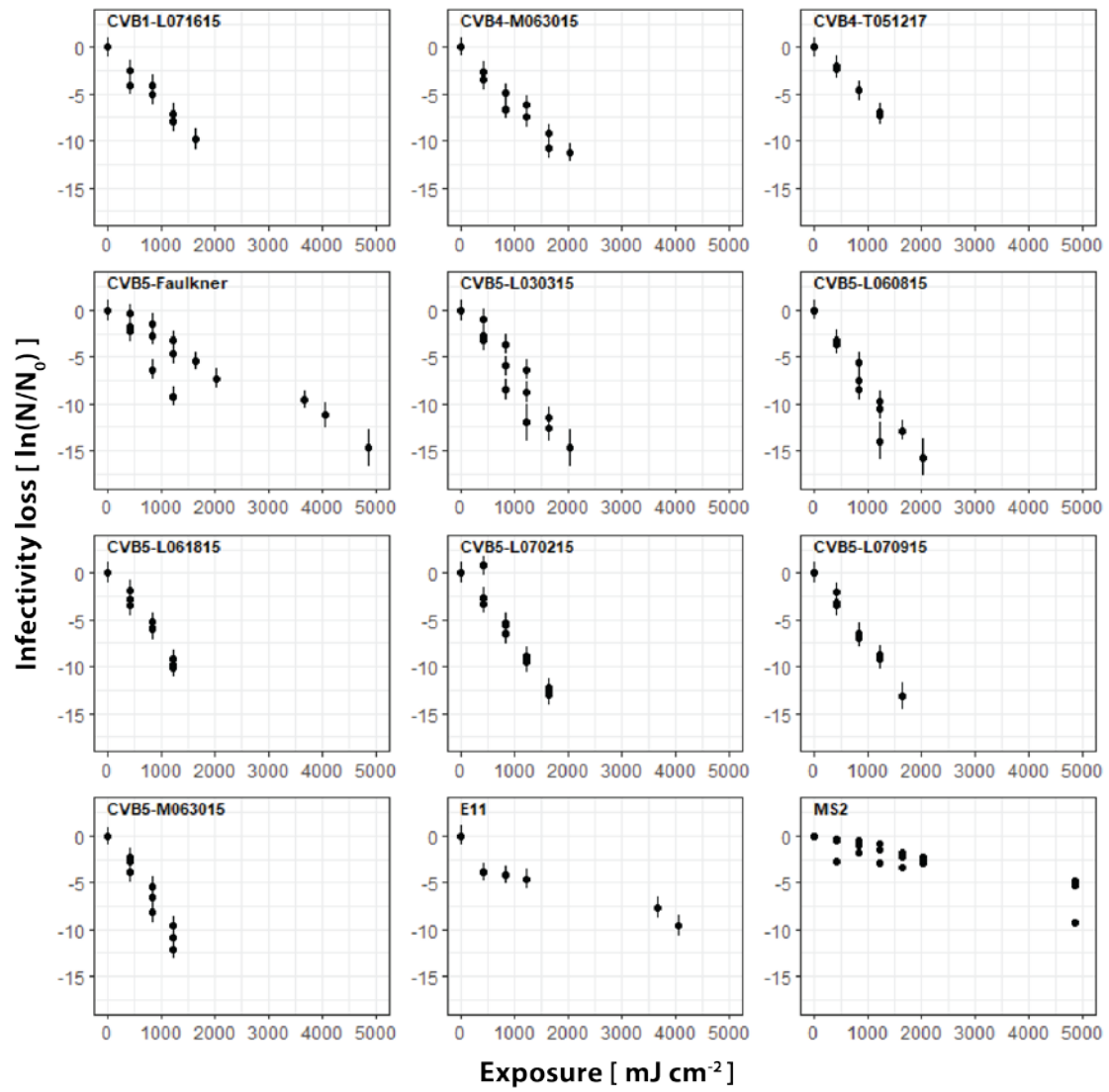


Figure A.2. Sunlight inactivation curves for all viruses.

The error bars represent the 95% confidence intervals associated with the measured infectivity loss.

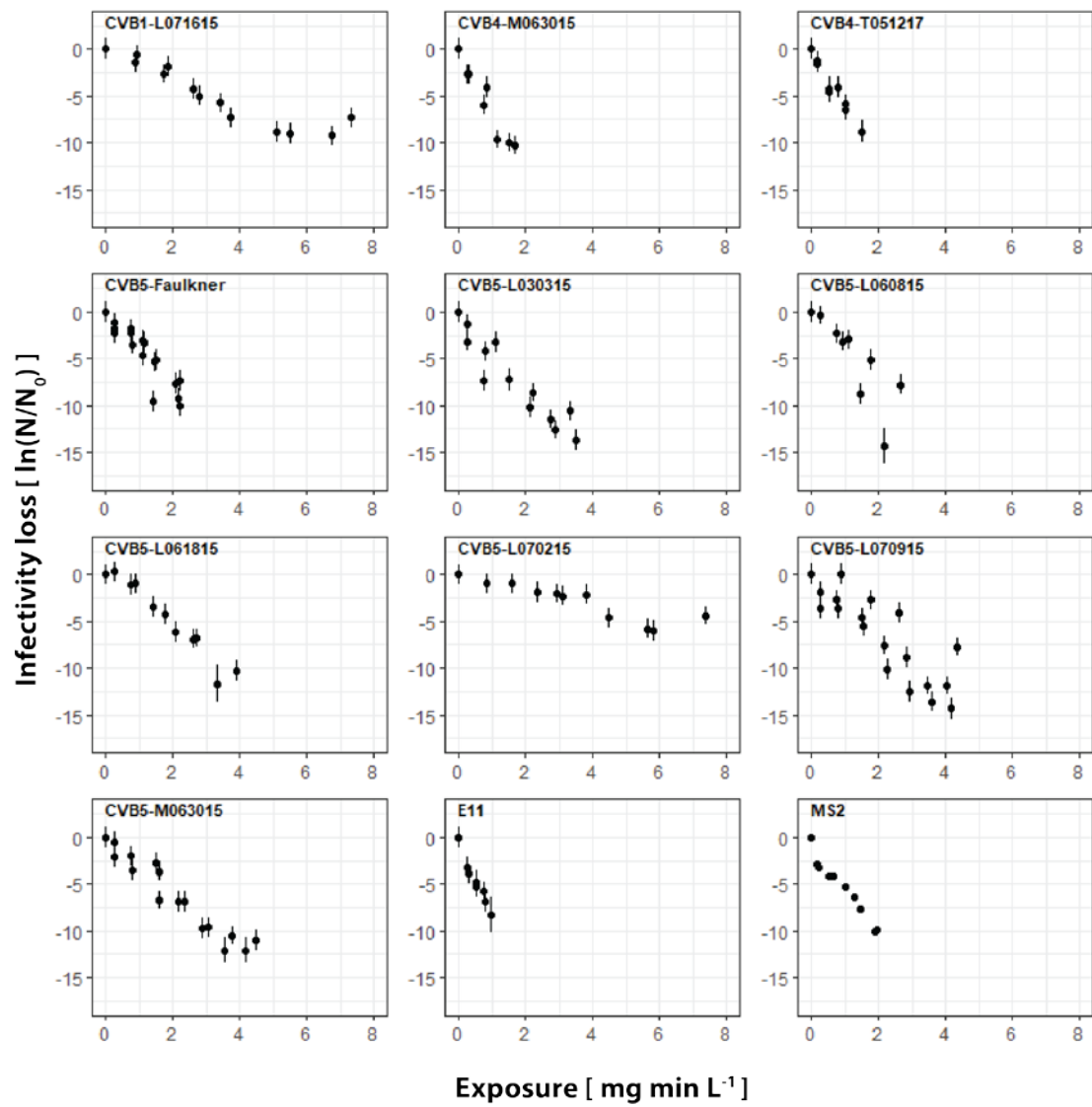


Figure A.3. Free chlorine (FC) inactivation curves for all viruses.

The error bars represent the 95% confidence intervals associated with the measured infectivity loss.

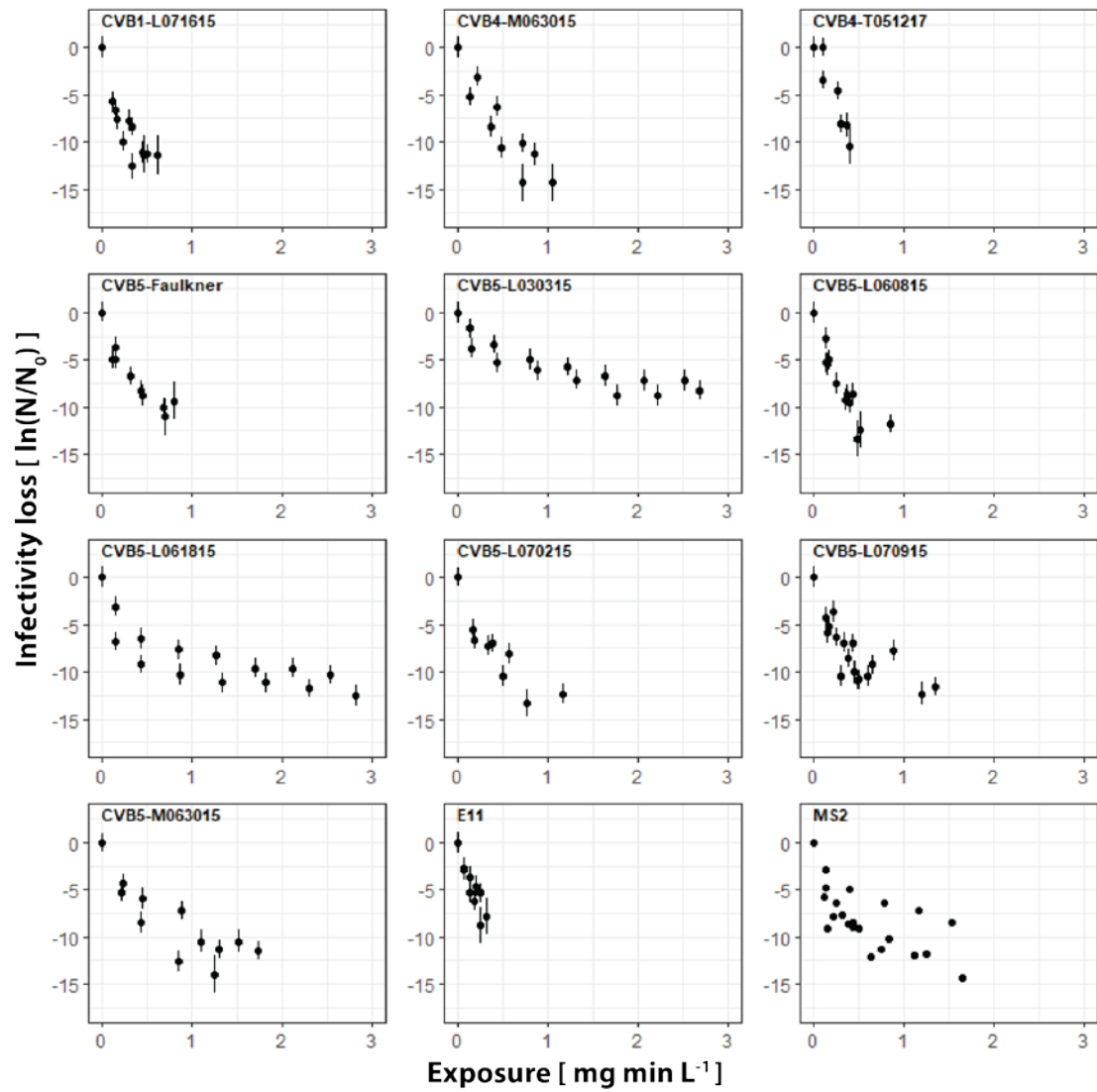


Figure A.4. Chlorine dioxide (ClO₂) inactivation curves for all viruses.

The error bars represent the 95% confidence intervals associated with the measured infectivity loss.

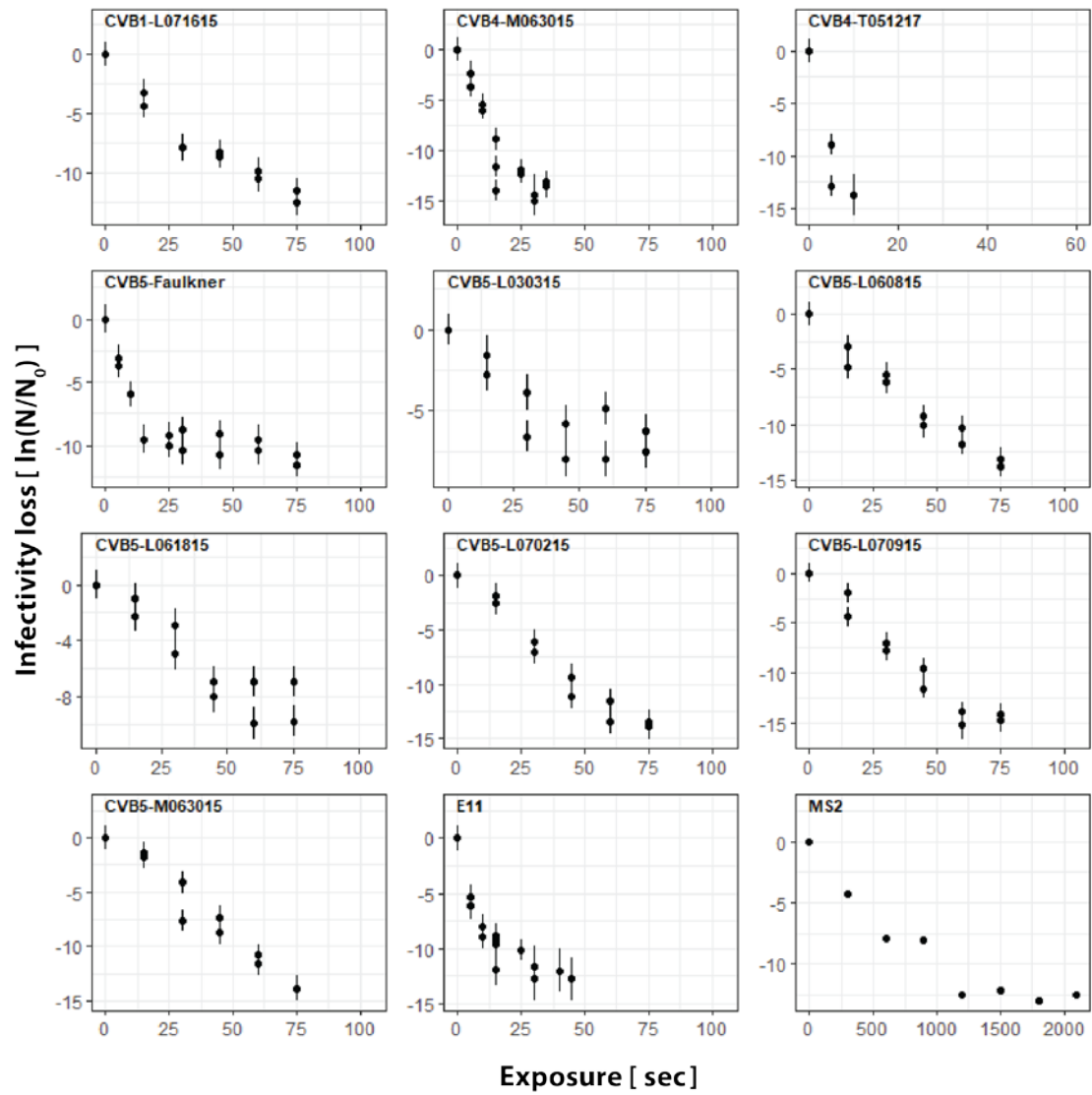


Figure A.5. Heat inactivation curves for all viruses.

The error bars represent the 95% confidence intervals associated with the measured infectivity loss.

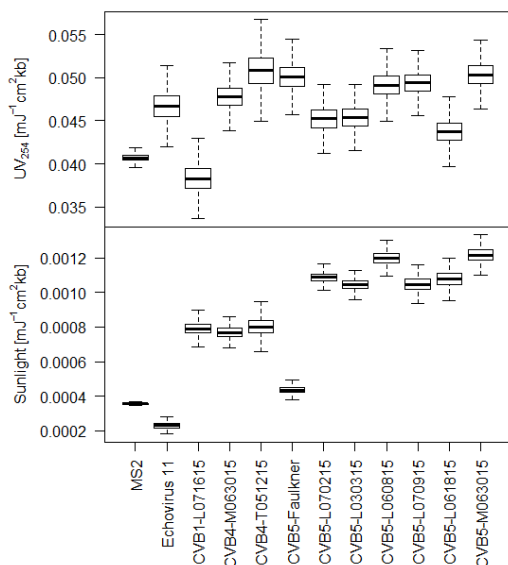


Figure A.6. Genome length normalization of k_{UV} and k_{SUN} .

Boxplots displaying the k_{UV} and k_{SUN} values normalized for genome length in kilobases (kb). For MS2 and enteroviruses, a genome length of 3.569 and 7.400 kb, respectively, was assumed.

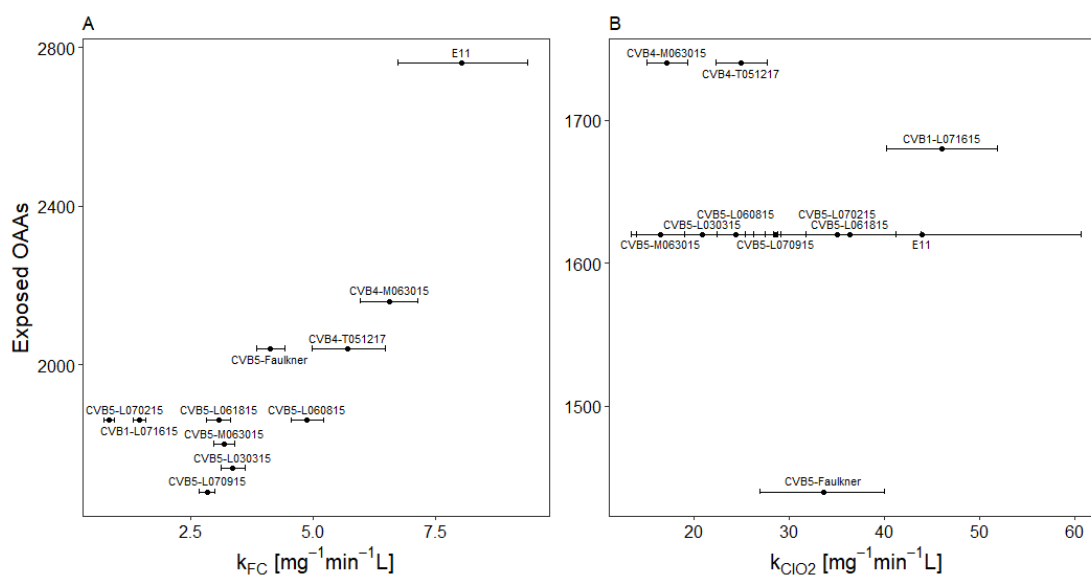


Figure A.7. Correlation of k_{FC} and k_{ClO_2} with exposed oxidizable amino acids.

Correlation of the number of total surface-exposed, oxidizable amino acids (OAAs) on the virus capsid versus (A) k_{FC} and (B) k_{ClO_2} . OAAs include all amino acids with a reactivity greater than $10^4 \text{ M}^{-1}\text{s}^{-1}$ toward FC or ClO_2 . For FC, this included Methionine, Cysteine, Cystine, Histidine and Tryptophan, and for ClO_2 Cysteine, Tyrosine and Tryptophan^{179,180}. To identify surface-exposed OAAs, the 3D capsid structure of all viruses was modelled using the Swiss-MODEL¹⁸¹. The crystal structure of Coxsackievirus B3 (1COV, PDB) was used as template for homology modeling¹⁸², and the surface-exposed residues were identified using PyMOL¹⁸³.

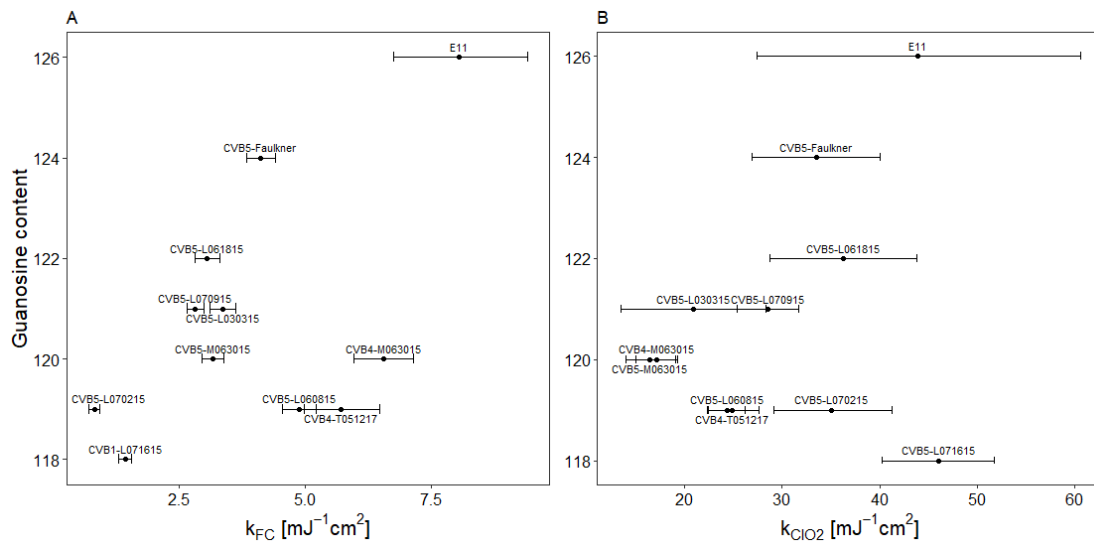


Figure A.8. Correlation of k_{FC} and k_{ClO_2} with guanosine content.

Total guanosine content present in the genomic 5'NCR correlated to (A) k_{FC} and (B) k_{ClO_2} . The chosen 5'NCR portion corresponds to residues 257-742 (based on Faulkner strain, accession number: AF114383¹⁸⁴), which were identified for all viruses tested.

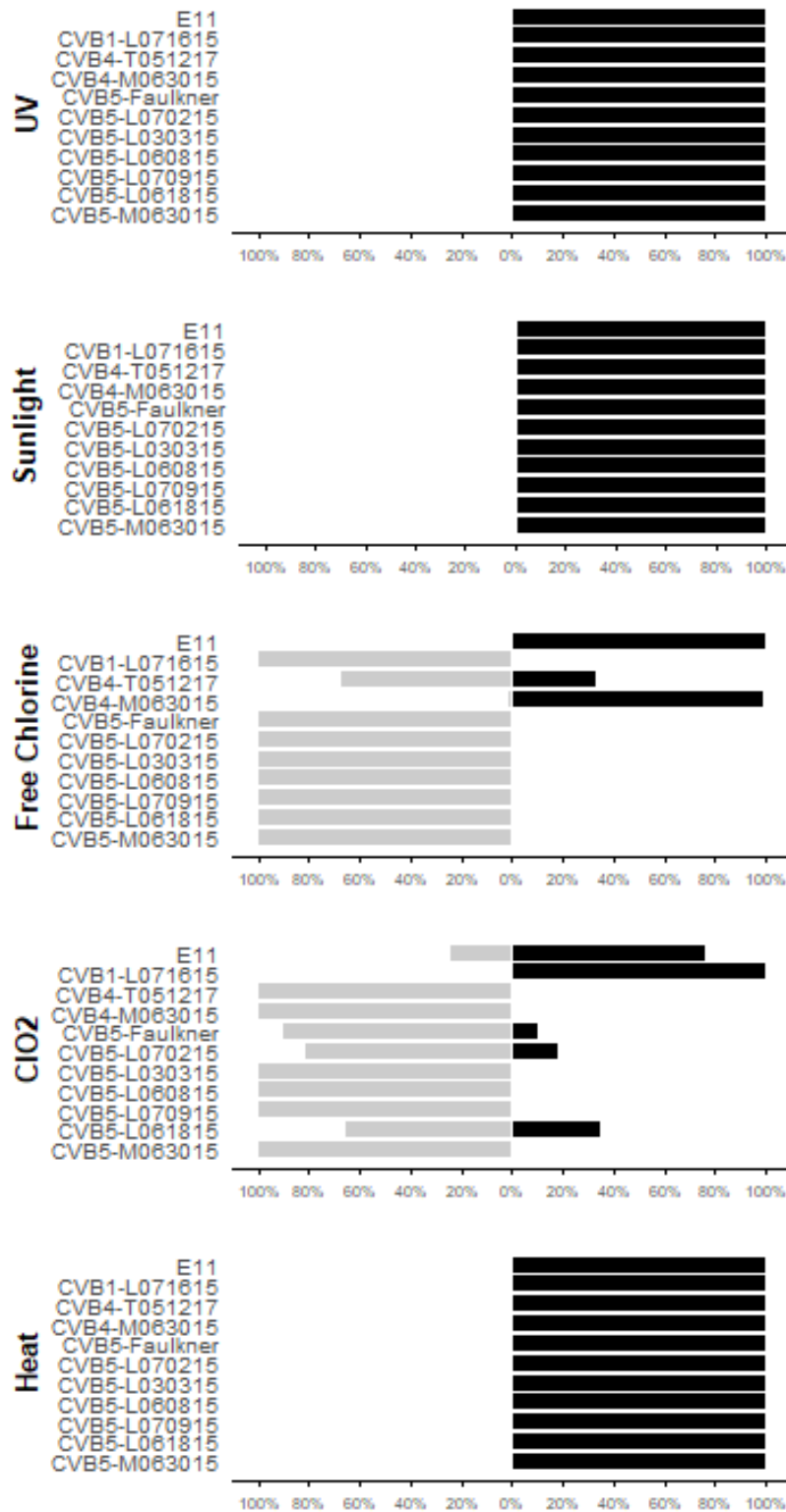


Figure A.9. Bayesian comparison of enteroviruses and MS2.

Bar plot showing a comparison of the probabilities of inactivation rate constants (k values) for all viruses with MS2 bacteriophage. Grey bars indicate the probability that k of a given virus is smaller than the k associated with MS2 (the virus is more resistant than MS2); black bars indicates the probability that k of a given virus is greater than k of MS2 (the virus is less resistant than MS2).

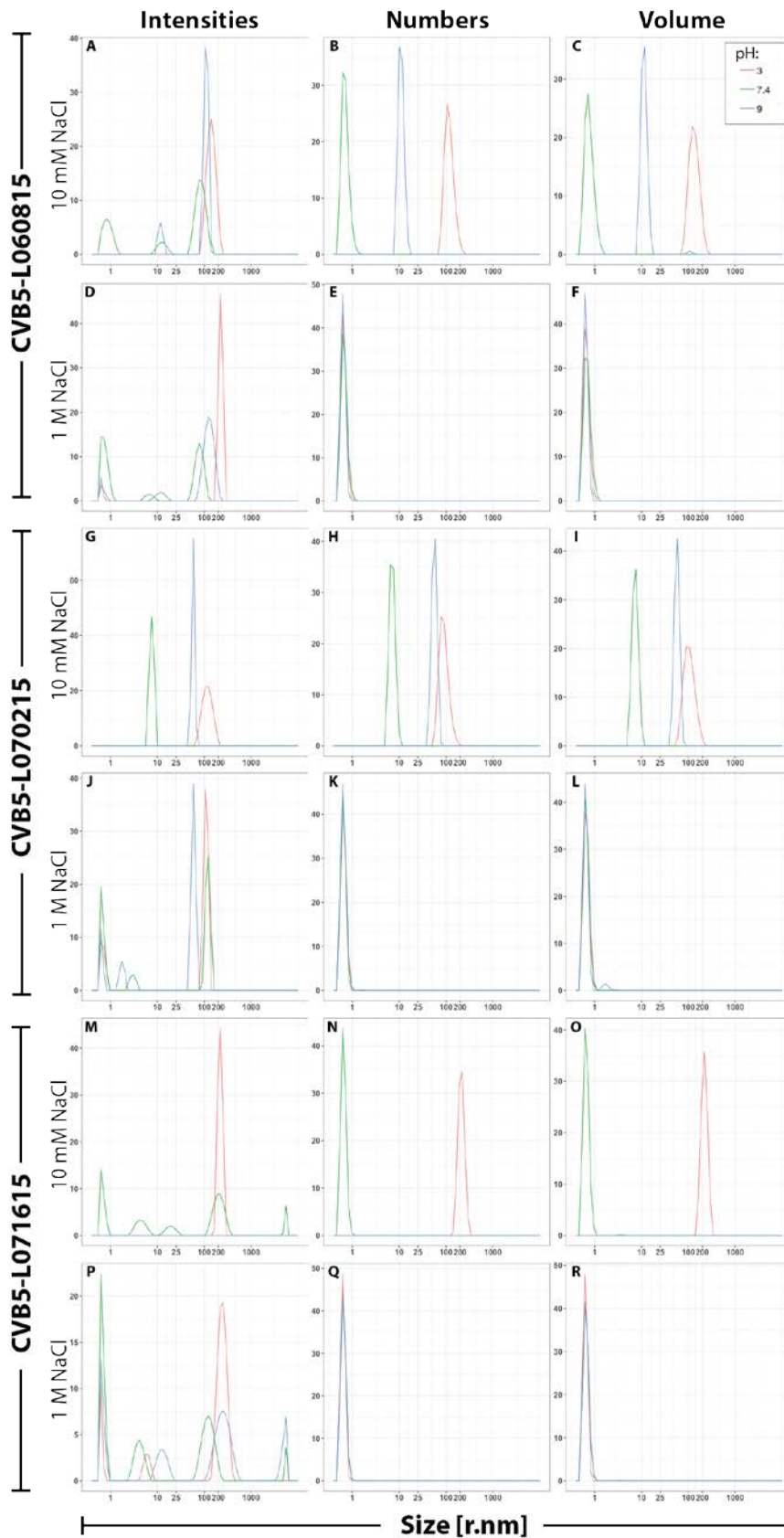


Figure A.10. Dynamic light scattering analysis on virus particles.

Dynamic light scattering (DLS) analysis on three viruses, under low salt (10 mM NaCl) and high salt conditions (1M NaCl), and under acid (pH 3), near neutral (pH7.4), and alkaline conditions (pH9). Intensities, volume and number units are in percentage (y axis), and the size in nanometers radius (x axis).

B. Appendix – CHAPTER 3

Table B.1. Primers couples for genome damage assay

Couple	Name	Sequence
1	5 UTR 2 fwd	ATGGAAATGCGGAGTGT
	VP4 rev	TCTTGCCTATTTGCGGAAT
2	VP2 2 fwd	CTACTTGAGGGACGATGAA
	VP2 rev	TGTCACGTGTGATCGGTACAT
3	VP3 1C 2 fwd	AGATTGCGGAGTGGAT
	VP3 C1 rev	TGACACAAAGCACAAAATCT
4	VP1 1D fwd	AGATCCGCATGTGTTACTACA
	VP1 1D 2 rev	TCAAATCTAGCCCATCCATCAT
5	2A fwd	ACTACCGGAGTGTATTTCTGT
	2B rev	TGATTTCTTACCACAATAACCAGT
6	2C 2 fwd	AGAAAGGCATCTTGTTCACTT
	3A rev	AGTTGACCTCAGGAACCAA
7	3B fwd	TCAAGGTGCATACACAGGAA
	3C 2 rev	TTGATGACCATTCCCACCAA

Table B.2. Inactivation rate constants at 55°C

Table showing the inactivation rate constants k at 55°C in [sec⁻¹]. SE: standard error.

Virus	pH	NaCl [M]	Inactivation rate k	
			Value	SE
CVB1-1071615	7.4	0.01	0.254	0.035
CVB4-M063015	7.4	0.01	0.710	0.065
CVB4-T051217	7.4	0.01	1.481	0.356
CVB5-Faulkner	3	0.01	0.071	0.033
CVB5-Faulkner	7.4	0.01	0.615	0.031
CVB5-Faulkner	9	0.01	0.595	0.012
CVB5-I030315	7.4	0.01	0.174	0.042
CVB5-I060815	7.4	0.01	0.203	0.027
CVB5-I061815	7.4	0.01	0.164	0.028
CVB5-I070215	7.4	0.01	0.234	0.018
CVB5-I070915	7.4	0.01	0.208	0.016
CVB5-M063015	7.4	0.01	0.191	0.013
E11	7.4	0.01	1.146	0.156
CVB1-1071615	7.4	1	0.011	0.005
CVB4-T051217	7.4	1	0.008	0.007
CVB5-Faulkner	3	1	0.013	0.004
CVB5-Faulkner	7.4	1	0.005	0.003
CVB5-Faulkner	9	1	0.006	0.004
CVB5-I060815	7.4	1	0.014	0.005
CVB5-I070215	7.4	1	0.012	0.005
CVB5-M063015	7.4	1	-0.022	0.017

Table B.3. Inactivation rate constants at 30°CTable showing the inactivation rate constants k at 30°C in [day^{-1}]. SE: standard error.

Virus	pH	NaCl [M]	Inactivation rate k	
			Value	SE
CVB1-L071615	3	1	2.79	NA
CVB1-L071615	7.4	1	0.47	0.12
CVB1-L071615	9	1	0.97	0.16
CVB4-M063015	3	1	12.97	NA
CVB4-M063015	7.4	1	0.42	0.13
CVB4-M063015	9	1	1.90	0.43
CVB5-Faulkner	3	1	3.96	0.72
CVB5-Faulkner	7.4	1	0.32	0.08
CVB5-Faulkner	9	1	1.57	0.32
CVB5-L060815	3	1	6.54	1.45
CVB5-L060815	7.4	1	0.24	0.03
CVB5-L060815	9	1	0.98	0.18
CVB5-L070215	3	1	5.54	1.68
CVB5-L070215	7.4	1	0.23	0.09
CVB5-L070215	9	1	1.27	0.16
CVB5-L070915	3	1	6.51	NA
CVB5-L070915	7.4	1	0.50	0.10
CVB5-L070915	9	1	1.28	0.23
E11	3	1	NA	NA
E11	7.4	1	0.24	0.09
E11	9	1	1.36	NA
CVB1-L071615	3	0.01	0.71	0.08
CVB1-L071615	7.4	0.01	0.35	0.11
CVB1-L071615	9	0.01	0.33	0.04
CVB4-M063015	3	0.01	1.36	0.19
CVB4-M063015	7.4	0.01	0.29	0.10
CVB4-M063015	9	0.01	0.25	0.13
CVB5-Faulkner	3	0.01	0.72	0.05
CVB5-Faulkner	7.4	0.01	0.22	0.07
CVB5-Faulkner	9	0.01	0.27	0.11
CVB5-L060815	3	0.01	0.92	0.18
CVB5-L060815	7.4	0.01	0.54	0.06
CVB5-L060815	9	0.01	0.18	0.06
CVB5-L070215	3	0.01	0.88	0.06
CVB5-L070215	7.4	0.01	0.28	0.08
CVB5-L070215	9	0.01	0.12	0.10
CVB5-L070915	3	0.01	0.91	0.05
CVB5-L070915	7.4	0.01	0.27	0.07
CVB5-L070915	9	0.01	0.23	0.11
E11	3	0.01	1.17	0.05
E11	7.4	0.01	0.13	0.05
E11	9	0.01	0.30	0.11

Table B.4. Breakpoint temperature

Table showing the breakpoint temperature in [°C]. SE: standard error.

Virus	pH	NaCl [M]	Breakpoint [°C]	
			Value	SE
CVB1-L071615	7.4	1	57.22	1.21
CVB5-Faulkner	3	1	59.29	0.59
CVB5-Faulkner	7.4	1	59.47	0.32
CVB5-Faulkner	9	1	59.11	0.37
CVB5-L061815	7.4	1	61.44	0.57
E11	7.4	1	58.97	1.08
CVB1-L071615	7.4	0.01	49.44	1.03
CVB4-M063015	7.4	0.01	44.42	1.28
CVB4-T051217	7.4	0.01	38.77	1.16
CVB5-Faulkner	7.4	0.01	44.96	0.72
CVB5-I030315	7.4	0.01	51.19	0.61
CVB5-L060815	7.4	0.01	51.25	0.23
CVB5-L061815	7.4	0.01	50.37	0.63
CVB5-L070215	7.4	0.01	48.89	0.73
CVB5-L070915	7.4	0.01	51.13	0.27
CVB5-M063015	7.4	0.01	50.26	0.25
E11	7.4	0.01	43.33	0.26
CVB5-Faulkner	3	0.01	47.19	0.92
CVB5-Faulkner	9	0.01	40.86	0.84

C. Appendix – CHAPTER 4

Table C.1. Breakpoint temperature

Table with the breakpoint temperature of the heat adapted and non-adapted viruses. SE: standard error.

Replicate	Treatment	Virus	pH	NaCl [M]	Breakpoint [°C]	
					Value	SE
A	50°C	A50-V232A-I209F	7.4	1	59.02	0.73
A	55°C	A55-V232A-E26V-N213D	7.4	1	61.51	0.41
A	Dilution	Aneg-V232A	7.4	1	53.62	1.06
A	50°C	A50-V232A-I209F	7.4	0.01	47.15	1.53
A	55°C	A55-V232A-E26V-N213D	7.4	0.01	49.13	1.31
A	Dilution	Aneg-V232A	7.4	0.01	37.87	2.26
B	50°C	B50-V232A-I209F	7.4	0.01	48.54	0.68
B	55°C	B55-V232A-E26V-N213D	7.4	0.01	47.27	0.81
B	Dilution	Bneg-V232A	7.4	0.01	38.48	1.83
C	50°C	C50-V232A-I209F	7.4	0.01	48.32	0.57
C	55°C	C55-V232A-E26V-N213D	7.4	0.01	48.00	0.68
C	Dilution	Cneg-V232A	7.4	0.01	38.26	1.44
D	50°C	D50-V232A-M180V	7.4	0.01	49.25	0.52
D	55°C	D55-V232A-E26V-N213D	7.4	0.01	47.31	0.75
D	Dilution	Dneg-V232A	7.4	0.01	37.43	1.62
E	50°C	E50-V232A-I209F	7.4	0.01	49.26	0.60
E	55°C	E55-V232A-E26V-N213D	7.4	0.01	46.00	0.53
E	Dilution	Eneg-V232A	7.4	0.01	36.55	1.27

Table C.2 Inactivation rate constant at 55°C

Table with the rate constants k at 55°C of the heat adapted and non-adapted viruses. SE: standard error.

Replicate	Treatment	Virus	pH	NaCl [M]	Inactivation rate k [sec ⁻¹]	
					Value	SE
A	50°C	A50-V232A-I209F	7.4	0.01	0.14	0.03
A	55°C	A55-V232A-E26V-N213D	7.4	0.01	0.17	0.09
A	Dilution	Aneg-V232A	7.4	0.01	2.28	0.19
B	50°C	B50-V232A-I209F	7.4	0.01	0.42	0.05
B	55°C	B55-V232A-E26V-N213D	7.4	0.01	0.41	0.24
B	Dilution	Bneg-V232A	7.4	0.01	2.59	0.07
C	50°C	C50-V232A-I209F	7.4	0.01	0.63	0.12
C	55°C	C55-V232A-E26V-N213D	7.4	0.01	0.36	0.03
C	Dilution	Cneg-V232A	7.4	0.01	2.40	0.12
D	50°C	D50-V232A-M180V	7.4	0.01	0.36	0.06
D	55°C	D55-V232A-E26V-N213D	7.4	0.01	0.52	0.08
D	Dilution	Dneg-V232A	7.4	0.01	2.42	0.07
E	50°C	E50-V232A-I209F	7.4	0.01	0.28	0.05
E	55°C	E55-V232A-E26V-N213D	7.4	0.01	0.58	0.06
E	Dilution	Eneg-V232A	7.4	0.01	2.41	0.24

REFERENCES

1. Gilbert, C. & Feschotte, C. Genomic fossils calibrate the long-term evolution of hepadnaviruses. *PLoS Biol.* (2010). doi:10.1371/journal.pbio.1000495
2. Bannert, N. & Kurth, R. The Evolutionary Dynamics of Human Endogenous Retroviral Families. *Annu. Rev. Genomics Hum. Genet.* (2006). doi:10.1146/annurev.genom.7.080505.115700
3. Emerman, M. & Malik, H. S. Paleovirology - Modern consequences of ancient viruses. *PLoS Biology* (2010). doi:10.1371/journal.pbio.1000301
4. Koelle, D. M. & Wald, a. Herpes simplex virus: the importance of asymptomatic shedding. *J. Antimicrob. Chemother.* (2000). doi:10.1093/jac/45.suppl_4.1
5. Chonmaitree, T. *et al.* Symptomatic and asymptomatic respiratory viral infections in the first year of life: Association with acute otitis media development. *Clin. Infect. Dis.* (2015). doi:10.1093/cid/ciu714
6. Flint, S.J., Enquist, L.W., Krug, R.M., Racaniello, V.R., Skalka, A. M. Principles of virology, molecular biology, pathogenesis, and control. *The Lancet Infectious Diseases* (2000). doi:10.1016/S1473-3099(09)70195-1
7. Legendre, M. *et al.* In-depth study of *Mollivirus sibericum*, a new 30,000-y-old giant virus infecting *Acanthamoeba*. *Proc. Natl. Acad. Sci.* (2015). doi:10.1073/pnas.1510795112
8. Hulo, C. *et al.* ViralZone: A knowledge resource to understand virus diversity. *Nucleic Acids Res.* (2011). doi:10.1093/nar/gkq901
9. Malik, Y. S. & Matthijssens, J. Enteric viral infection in human and animal. *VirusDisease* **25**, 145–146 (2014).
10. Khetsuriani, N., Lamonte-Fowlkes, A., Oberst, S. & Pallansch, M. A. Enterovirus surveillance - United States, 1970-2005. *Morb. Mortal. Wkly. Rep. Surveill. Summ.* **55**, 1–20 (2006).
11. Le Guyader, F., Haugarreau, L., Miossec, L., Dubois, E. & Pommepuy, M. Three-year study to assess human enteric viruses in shellfish. *Appl. Environ. Microbiol.* **66**, 3241–3248 (2000).
12. Sinclair, R. G., Jones, E. L. & Gerba, C. P. Viruses in recreational water-borne disease outbreaks: A review. *Journal of Applied Microbiology* **107**, 1769–1780 (2009).
13. Keswick, B. H., Secor, S. L., Gerba, C. P. & Cech, I. Survival of enteric viruses and indicator bacteria in groundwater. *J. Environ. Sci. Heal. Part A Environ. Sci. Eng.* **17**, 903–912 (1982).
14. Lo, S., Gilbert, J. & Hetrick, F. Stability of human enteroviruses in estuarine and marine waters. *Appl. Environ. Microbiol.* **32**, 245–249 (1976).
15. Liew, P. F. & Gerba, C. P. Thermostabilization of enteroviruses by estuarine sediment. *Appl. Environ. Microbiol.* **40**, 305–308 (1980).
16. Rusinol, M. and Girones, R. Summary of Excreted and Waterborne Viruses. *J.B. Rose and B. Jiménez-Cisneros, (eds) Global Water Pathogen Project* (2017). at <<http://www.waterpathogens.org/book/summary-of-excreted-and-waterborne-viruses>>
17. Zell, R. Picornaviridae—the ever-growing virus family. *Archives of Virology* (2018).

doi:10.1007/s00705-017-3614-8

18. Sanjuan, R., Nebot, M. R., Chirico, N., Mansky, L. M. & Belshaw, R. Viral Mutation Rates. *J. Virol.* (2010). doi:10.1128/JVI.00694-10
19. Luring, A. S., Frydman, J. & Andino, R. The role of mutational robustness in RNA virus evolution. *Nat Rev Microbiol* **11**, 327–336 (2013).
20. Oberste, M. S., Maher, K., Kilpatrick, D. R. & Pallansch, M. A. Molecular evolution of the human enteroviruses: correlation of serotype with VP1 sequence and application to picornavirus classification. *J. Virol.* **73**, 1941–1948 (1999).
21. Wang, M. *et al.* A novel enterovirus species identified from severe diarrheal goats. *PLoS One* (2017). doi:10.1371/journal.pone.0174600
22. Racaniello, V. R. & Baltimore, D. Molecular cloning of poliovirus cDNA and determination of the complete nucleotide sequence of the viral genome. *Proc. Natl. Acad. Sci. U. S. A.* (1981). doi:10.1016/S0009-2614(89)87028-9
23. Baggen, J., Thibaut, H. J., Strating, J. R. P. M. & Van Kuppeveld, F. J. M. The life cycle of non-polio enteroviruses and how to target it. *Nature Reviews Microbiology* (2018). doi:10.1038/s41579-018-0005-4
24. Dhole, T. N. *et al.* Non-polio enteroviruses in acute flaccid paralysis children of India: Vital assessment before polio eradication. *J. Paediatr. Child Health* (2009). doi:10.1111/j.1440-1754.2009.01529.x
25. Laxmivandana, R., Yergolkar, P., Gopalkrishna, V. & Chitambar, S. D. Characterization of the Non-Polio Enterovirus Infections Associated with Acute Flaccid Paralysis in South-Western India. *PLoS One* (2013). doi:10.1371/journal.pone.0061650
26. Suresh, S., Forgie, S. & Robinson, J. Non-polio Enterovirus detection with acute flaccid paralysis: A systematic review. *J. Med. Virol.* (2018). doi:10.1002/jmv.24933
27. Kennedy, J. L., Turner, R. B., Braciale, T., Heymann, P. W. & Borish, L. Pathogenesis of rhinovirus infection. *Current Opinion in Virology* (2012). doi:10.1016/j.coviro.2012.03.008
28. Rhoades, R. E., Tabor-Godwin, J. M., Tsueng, G. & Feuer, R. Enterovirus infections of the central nervous system. *Virology* (2011). doi:10.1016/j.virol.2010.12.014
29. Pons-Salort, M., Parker, E. P. K. & Grassly, N. C. The epidemiology of non-polio enteroviruses: Recent advances and outstanding questions. *Current Opinion in Infectious Diseases* (2015). doi:10.1097/QCO.0000000000000187
30. Oxford John, Kellam Paul, C. L. *Human virology.* (2011).
31. Bosch, a & Bosch, a. Human enteric viruses in the water environment: a minireview. *Int. Microbiol.* **1**, 191–6 (1998).
32. Bosshard, F., Armand, F., Hamelin, R. & Kohn, T. Mechanisms of Human Adenovirus Inactivation by Sunlight and UVC Light as Examined by Quantitative PCR and Quantitative Proteomics. *Appl. Environ. Microbiol.* **79**, 1325–1332 (2013).
33. Sigstam, T. *et al.* Subtle differences in virus composition affect disinfection kinetics and mechanisms. *Appl. Environ. Microbiol.* **79**, 3455–3467 (2013).
34. Wigginton, K. R., Pecson, B. M., Sigstam, T., Bosshard, F. & Kohn, T. Virus inactivation mechanisms: Impact of disinfectants on virus function and structural integrity. *Environ. Sci. Technol.* **46**, 12069–12078 (2012).

35. Davies-Colley, R. J., Donnison, A. M., Speed, D. J., Ross, C. M. & Nagels, J. W. Inactivation of faecal indicator micro-organisms in waste stabilisation ponds: Interactions of environmental factors with sunlight. *Water Res.* (1999). doi:10.1016/S0043-1354(98)00321-2
36. Silverman, A. I., Nguyen, M. T., Schilling, I. E., Wenk, J. & Nelson, K. L. Sunlight Inactivation of Viruses in Open-Water Unit Process Treatment Wetlands: Modeling Endogenous and Exogenous Inactivation Rates. *Environ. Sci. Technol.* **49**, 2757–2766 (2015).
37. Sommer, B. *et al.* SODIS - An emerging water treatment process. *J. Water Supply Res. Technol. - AQUA* (1997). doi:10.1038/NMAT2982
38. USEPA. *USEPA - Wastewater Technology Fact Sheet: Ultraviolet Disinfection.* (1999).
39. USEPA. *Primer for Municipal Wastewater Treatment Systems.* (2004).
40. Kirmeyer, G. J. & Foundation, A. R. *Optimizing Chloramine Treatment.* (American Water Works Association, 2004). at <<https://books.google.ch/books?id=UERSAAAAMAAJ>>
41. World Health Organization. Chapter 2 - Chemistry of Disinfectants and Disinfectant By-Products. *EHC 216 Disinfect. Disinfect. By-Prod.* (2000).
42. Wolf, C., Von Gunten, U. & Kohn, T. Kinetics of Inactivation of Waterborne Enteric Viruses by Ozone. *Environ. Sci. Technol.* (2018). doi:10.1021/acs.est.7b05111
43. Bull, R. J. Health effects of drinking water disinfectants and disinfectant by-products. *Environ. Sci. Technol.* (1982). doi:10.1021/es00104a719
44. Eaton, J. W., Kolpin, C. F., Swofford, H. S., Kjellstrand, C. M. & Jacob, H. S. Chlorinated urban water: a cause of dialysis induced hemolytic anemia. *Science* (80-.). (1973). doi:10.1126/science.181.4098.463
45. Kasparek, T. & Rodriguez, O. E. What medical directors need to know about dialysis facility water management. *Clin. J. Am. Soc. Nephrol.* (2015). doi:10.2215/CJN.11851214
46. Abarnou, A. & Miossec, L. Chlorinated waters discharged to the marine environment chemistry and environmental impact. An overview. *Sci. Total Environ.* (1992). doi:10.1016/0048-9697(92)90490-J
47. Richardson, S. D. Disinfection by-products and other emerging contaminants in drinking water. *TrAC - Trends in Analytical Chemistry* (2003). doi:10.1016/S0165-9936(03)01003-3
48. Richardson, S. D., Plewa, M. J., Wagner, E. D., Schoeny, R. & DeMarini, D. M. Occurrence, genotoxicity, and carcinogenicity of regulated and emerging disinfection by-products in drinking water: A review and roadmap for research. *Mutation Research - Reviews in Mutation Research* (2007). doi:10.1016/j.mrrev.2007.09.001
49. U.S. EPA. Disinfection Profiling and Benchmarking Guidance Manual. *Environ. Prot. Agency Off. Water* 1–192 (1999).
50. Deborde, M. & von Gunten, U. Reactions of chlorine with inorganic and organic compounds during water treatment-Kinetics and mechanisms: A critical review. *Water Research* (2008). doi:10.1016/j.watres.2007.07.025
51. Keswick, B. H., Gerba, C. P., DuPont, H. L. & Rose, J. B. Detection of enteric viruses in treated drinking water. *Appl. Environ. Microbiol.* (1984).

52. Andreottola, G., Foladori, P. & Ziglio, G. Biological treatment of winery wastewater: An overview. *Water Science and Technology* (2009). doi:10.2166/wst.2009.551
53. Guillot, E. & Loret, J.-F. *Waterborne Pathogens: Comprehensive Review for the Drinking Water Industry*. (IWA Publishing, 2009). doi:10.2166/9781780401744
54. Qiao, Z., Ye, Y., Chang, P. H., Thirunarayanan, D. & Wigginton, K. R. Nucleic Acid Photolysis by UV254 and the Impact of Virus Encapsidation. *Environ. Sci. Technol.* (2018). doi:10.1021/acs.est.8b02308
55. Templeton, M. R., Andrews, R. C. & Hofmann, R. Particle-associated viruses in water: Impacts on disinfection processes. *Critical Reviews in Environmental Science and Technology* (2008). doi:10.1080/10643380601174764
56. Hirneisen, K. A. *et al.* Viral Inactivation in Foods: A Review of Traditional and Novel Food-Processing Technologies. *Comprehensive Reviews in Food Science and Food Safety* **9**, 3–20 (2010).
57. Gerba, C. P., Goyal, S. M., Hurst, C. J. & Labelle, R. L. Type and strain dependence of enterovirus adsorption to activated sludge, soils and estuarine sediments. *Water Res.* (1980). doi:10.1016/0043-1354(80)90176-1
58. Mattle, M. J. *et al.* Impact of virus aggregation on inactivation by peracetic acid and implications for other disinfectants. *Environ. Sci. Technol.* (2011). doi:10.1021/es201633s
59. Mattle, M. J. & Kohn, T. Inactivation and tailing during UV254 disinfection of viruses: Contributions of viral aggregation, light shielding within viral aggregates, and recombination. *Environ. Sci. Technol.* **46**, 10022–10030 (2012).
60. Zhong, Q., Carratalà, A., Ossola, R., Bachmann, V. & Kohn, T. Cross-Resistance of UV- or Chlorine Dioxide-Resistant Echovirus 11 to Other Disinfectants. *Front. Microbiol.* **8**, 1928 (2017).
61. Graci, J. D. *et al.* Mutational Robustness of an RNA Virus Influences Sensitivity to Lethal Mutagenesis. *J. Virol.* (2012). doi:10.1128/JVI.05712-11
62. Hurst, C. J., Benton, W. H. & McClellan, K. A. Thermal and water source effects upon the stability of enteroviruses in surface freshwaters. *Can. J. Microbiol.* **35**, 474–480 (1989).
63. Pepper, I., Gerba, C. P. & Gentry, T. J. *Environmental Microbiology. Environmental Microbiology* (2015). doi:10.1016/B978-0-12-394626-3.00020-X
64. Khetsuriani, N., Lamonte-Fowlkes, A., Oberst, S. & Pallansch, M. A. Enterovirus surveillance--United States, 1970-2005. *MMWR. Surveill. Summ. Morb. Mortal. Wkly. report. Surveill. Summ. / CDC* **55**, 1–20 (2006).
65. USEPA CCL4. United States Environmental Protection Agency. <https://www.epa.gov/ccl/microbial-contaminants-ccl-4> (2016).
66. Caro, V., Guillot, S., Delpeyroux, F. & Crainic, R. Molecular strategy for 'serotyping' of human enteroviruses. *J. Gen. Virol.* **82**, 79–91 (2001).
67. Petterson, S. R. & Stenström, T. A. Quantification of pathogen inactivation efficacy by free chlorine disinfection of drinking water for QMRA. *J. Water Health* **13**, 625–644 (2015).
68. Cromeans, T. L., Kahler, A. M. & Hill, V. R. Inactivation of adenoviruses, enteroviruses, and murine norovirus in water by free chlorine and monochloramine.

- Appl. Environ. Microbiol.* **76**, 1028–1033 (2010).
69. Payment, P., Tremblay, M. & Trudel, M. Relative resistance to chlorine of poliovirus and coxsackievirus isolates from environmental sources and drinking water. *Appl. Environ. Microbiol.* **49**, 981–983 (1985).
 70. Harakeh, S. The behavior of viruses on disinfection by chlorine dioxide and other disinfectants in effluent. *FEMS Microbiol. Lett.* **44**, 335–341 (1987).
 71. Floyd, R. & Sharp, D. G. Inactivation by Chlorine of Single poliovirus in water. *Environ. Sci. Technol.* **13**, 438–442 (1979).
 72. Sharp, D. G. & Leong, J. Inactivation of poliovirus I (Brunhilde) single particles by chlorine in water. *Appl. Environ. Microbiol.* **40**, 381–385 (1980).
 73. Gerba, C. P., Gramos, D. M. & Nwachuku, N. Comparative Inactivation of Enteroviruses and Adenovirus 2 by UV Light. *Appl. Environ. Microbiol.* **68**, 5167–5169 (2002).
 74. Heaselgrave, W. & Kilvington, S. The efficacy of simulate solar disinfection (SODIS) against coxsackievirus, poliovirus and hepatitis A virus. *J. Water Health* **10**, 531–538 (2012).
 75. Bates, R. C., Shaffer, P. T. B. & Sutherland, S. M. Development of Poliovirus Having Increased Resistance to Chlorine Inactivation. *Appl. Environ. Microbiol.* **34**, 849–853 (1977).
 76. Shaffer, P. T. B., Metcalf, T. G. & Sproul, O. J. Chlorine resistance of poliovirus isolants recovered from drinking water. *Appl. Environ. Microbiol.* **40**, 1115–1121 (1980).
 77. Carratalà, A. *et al.* Experimental adaptation of human echovirus 11 to ultraviolet radiation leads to tolerance to disinfection and resistance to ribavirin. *Virus Evol.* **Accepted**, (2017).
 78. Tree, J. A., Adams, M. R. & Lees, D. N. Chlorination of Indicator Bacteria and Viruses in Primary Sewage Effluent. *Appl. Environ. Microbiol.* **69**, 2038–2043 (2003).
 79. WHO. Evaluating Household Water Treatment Options : Health-Based Targets and Microbiological Performance Specifications. *NML Classif. WA 675* 1–68 (2011).
 80. Aw, T. G., Howe, A. & Rose, J. B. Metagenomic approaches for direct and cell culture evaluation of the virological quality of wastewater. *J. Virol. Methods* **210**, 15–21 (2014).
 81. Lewis, G. D. & Metcalf, T. G. Polyethylene glycol precipitation for recovery of pathogenic viruses, including hepatitis A virus and human rotavirus, from oyster, water, and sediment samples. *Appl. Environ. Microbiol.* **54**, 1983–1988 (1988).
 82. Shieh, Y. S., Wait, D., Tai, L. & Sobsey, M. D. Methods to remove inhibitors in sewage and other fecal wastes for enterovirus detection by the polymerase chain reaction. *J. Virol. Methods* **54**, 51–66 (1995).
 83. Calgua, B. *et al.* New methods for the concentration of viruses from urban sewage using quantitative PCR. *J. Virol. Methods* **187**, 215–221 (2013).
 84. Carratalà, A. *et al.* Solar disinfection of viruses in polyethylene terephthalate bottles. *Appl. Environ. Microbiol.* **82**, 279–288 (2016).
 85. Oberste, M. S., Nix, W. A., Maher, K. & Pallansch, M. A. Improved molecular identification of enteroviruses by RT-PCR and amplicon sequencing. *J. Clin. Virol.* **26**, 375–377 (2003).

86. Pickett, B. E. *et al.* ViPR: An open bioinformatics database and analysis resource for virology research. *Nucleic Acids Res.* **40**, 593–598 (2012).
87. Kang, Y., Chatterjee, N. K., Nodwell, M. J. & Yoon, J.-W. Complete nucleotide sequence of a strain of coxsackie B4 virus of human origin that induces diabetes in mice and its comparison with nondiabetogenic coxsackie B4 JBV strain. *J. Med. Virol.* **44**, 353–361 (1994).
88. Kearse, M. *et al.* Geneious Basic: An integrated and extendable desktop software platform for the organization and analysis of sequence data. *Bioinformatics* **28**, 1647–1649 (2012).
89. Edgar, R. C. MUSCLE: Multiple sequence alignment with high accuracy and high throughput. *Nucleic Acids Res.* **32**, 1792–1797 (2004).
90. Saitou, N. & Nei, M. The neighbour-joining method: a new method for reconstructing phylogenetic trees. *Mol Biol Evo* **4**, 406–425 (1987).
91. Pecson, B. M., Martin, L. V. & Kohn, T. Quantitative PCR for determining the infectivity of bacteriophage MS2 upon inactivation by heat, UV-B radiation, and singlet oxygen: Advantages and limitations of an enzymatic treatment to reduce false-positive results. *Appl. Environ. Microbiol.* **75**, 5544–5554 (2009).
92. Kott, Y. Estimation of low numbers of Escherichia coli bacteriophage by use of the most probable number method. *Appl. Microbiol.* **14**, 141–144 (1966).
93. Rahn, R. Potassium Iodide as a Chemical Actinometer for 254 nm Radiation : Use of Iodate as an Electron Scavenger. *Photochem. Photobiol.* **66**, 450–455 (1997).
94. Rahn, R. O., Bolton, J. & Stefan, M. I. The iodide/iodate actinometer in UV disinfection: determination of the fluence rate distribution in UV reactors. *Photochem. Photobiol.* **82**, 611–615 (2006).
95. Beckmann, M. *et al.* glUV: A global UV-B radiation data set for macroecological studies. *Methods Ecol. Evol.* **5**, 372–383 (2014).
96. Clesceri, L. S. *et al.* *Standard methods for the examination of water and wastewater.* (American Public Health Association, 1989).
97. Chick, H. & Martin, C. J. The Principles involved in the Standardisation of Disinfectants and the Influence of Organic Matter upon Germicidal value. *Epidemiol. Infect.* **8**, 654–697 (1908).
98. Watson, H. E. A Note on the Variation of the Rate of Disinfection with Change in the Concentration of the Disinfectant. *J. Hyg. (Lond).* **8**, 536–542 (1908).
99. Haas, C. N. Estimation of microbial densities from dilution count experiments. *Appl. Environ. Microbiol.* **55**, 1934–1942 (1989).
100. R Development Core Team. R Software. *R: A Language and Environment for Statistical Computing* (2013).
101. Plummer, M. JAGS: just another Gibbs sampler. in *Proceedings of the 3rd International Workshop on Distributed Statistical Computing (DSC 2003)* (2005).
102. Wickham, H. ggplot2 Elegant Graphics for Data Analysis. *Media* **35**, 211 (2009).
103. Auguie, B. gridExtra: Miscellaneous Functions for ‘Grid’ Graphics. (2016). at <<https://cran.r-project.org/package=gridExtra>>
104. Plummer, M. rjags: Bayesian graphical models using MCMC. *R package* 19 (2016).

doi:<http://cran.r-project.org/package=rjags>

105. Muggeo, V. M. R. segmented: An R package to Fit Regression Models with Broken-Line Relationships. *R News* **8**, 20–25 (2008).
106. Charif, D. *et al.* Package seqinr. *R Packag.* 218 (2015). at <<http://seqinr.r-forge.r-project.org/>>
107. Lüdecke, D. sjPlot: Data Visualization for Statistics in Social Science. *R Packag.* (2017). at <<https://cran.r-project.org/package=sjPlot>>
108. Bolker, B. & Team, R. D. C. bbmle: Tools for general maximum likelihood estimation. *R package* 0–28 (2013).
109. Best, N. G., Cowles, K., Vines, K. & Plummer, M. Package ‘coda’. *Citeseer* (2010). doi=10.1.1.168.669
110. Bodenhofer, U., Bonatesta, E., Horejš-Kainrath, C. & Hochreiter, S. msa: an R package for multiple sequence alignment. *Bioinformatics* **31**, 3997–9 (2015).
111. Paradis, E., Claude, J. & Strimmer, K. APE: analyses of phylogenetics and evolution in R language. *Bioinformatics* **20**, 289–290 (2004).
112. Yu, G., Smith, D. K., Zhu, H., Guan, Y. & Lam, T. T. Y. ggtree: an r package for visualization and annotation of phylogenetic trees with their covariates and other associated data. *Methods Ecol. Evol.* **8**, 28–36 (2017).
113. Rezig, D., Ben Yahia, A., Ben Abdallah, H., Bahri, O. & Triki, H. Molecular Characterization of Coxsackievirus B5 Isolates. *J. Med. Virol.* **72**, 268–274 (2004).
114. Antona, D. *et al.* Surveillance of enteroviruses in France, 2000-2004. *Eur. J. Clin. Microbiol. Infect. Dis.* **26**, 403–412 (2007).
115. Roth, B., Enders, M., Arents, A., Pfitzner, A. & Terletskaia-Ladwig, E. Epidemiologic aspects and laboratory features of enterovirus infections in Western Germany, 2000–2005. *J. Med. Virol.* **79**, 956–962 (2007).
116. Trallero, G. *et al.* Enteroviruses in Spain over the decade 1998-2007: Virological and epidemiological studies. *J. Clin. Virol.* **47**, 170–176 (2010).
117. Hijnen, W. a M., Beerendonk, E. F. & Medema, G. J. Inactivation credit of UV radiation for viruses, bacteria and protozoan (oo)cysts in water: A review. *Water Res.* **40**, 3–22 (2006).
118. Silverman, A. I., Peterson, B. M., Boehm, A. B., McNeill, K. & Nelson, K. L. Sunlight inactivation of human viruses and bacteriophages in coastal waters containing natural photosensitizers. *Environ. Sci. Technol.* **47**, 1870–1878 (2013).
119. Lytle, C. D. & Sagripanti, J.-L. Predicted Inactivation of Viruses of Relevance to Biodefense by Solar Radiation. *J. Virol.* **79**, 14244–14252 (2005).
120. Canning, A. *et al.* Validation of relationship between free chlorine dose and pathogen inactivation in drinking water. *Water J. Aust. Water Assoc.* **42**, 65–70 (2015).
121. Hornstra, L. M., Smeets, P. & Medema, G. J. Inactivation of bacteriophage MS2 upon exposure to very Low concentrations of chlorine dioxide. *Water Res.* **45**, 1847–1855 (2010).
122. Sigstam, T., Rohatschek, A., Zhong, Q., Brennecke, M. & Kohn, T. On the cause of the tailing phenomenon during virus disinfection by chlorine dioxide. *Water Res.* **48**, 82–89 (2014).

123. Hauchman, F. S., Noss, C. I. & Olivieri, V. P. Chlorine dioxide reactivity with nucleic acids. *Water Res.* **20**, 357–361 (1986).
124. Prütz, W. A. Hypochlorous acid interactions with thiols, nucleotides, DNA, and other biological substrates. *Arch. Biochem. Biophys.* **332**, 110–120 (1996).
125. Jin, M. *et al.* Chlorine dioxide inactivation of enterovirus 71 in water and its impact on genomic targets. *Environ. Sci. Technol.* **47**, 4590–4597 (2013).
126. Rincón, V. *et al.* Identification of the structural basis of thermal lability of a virus provides a rationale for improved vaccines. *Structure* **22**, 1560–1570 (2014).
127. Shiomi, H. *et al.* Isolation and characterisation of poliovirus mutants resistant to heating at 50°C for 30 min. *J. Med. Virol.* **74**, 484–491 (2004).
128. Kotecha, A. *et al.* Structure-based energetics of protein interfaces guides foot-and-mouth disease virus vaccine design. *Nat. Struct. & Mol. Biol.* **22**, 788–794 (2015).
129. Zhong, Q. *et al.* Resistance of Echovirus 11 to ClO₂ Is Associated with Enhanced Host Receptor Use, Altered Entry Routes, and High Fitness. *Environ. Sci. Technol.* 10746–10755 (2017). doi:10.1021/acs.est.7b03288
130. Pfeifer, G. P., You, Y.-H. & Besaratinia, A. Mutations induced by ultraviolet light. *Mutat. Res.* **571**, 19–31 (2005).
131. Eischeid, A. C. & Linden, K. G. Molecular indications of protein damage in adenoviruses after UV disinfection. *Appl. Environ. Microbiol.* **77**, 1145–1147 (2011).
132. Meschke, J. S. & Sobsey, M. D. Comparative adsorption of Norwalk virus, poliovirus 1 and F+ RNA coliphage MS2 to soils suspended in treated wastewater. *Water Sci. Technol.* **38**, 187–189 (1998).
133. Battigelli, D. A., Sobsey, M. D. & Lobe, D. C. The inactivation of hepatitis A virus and other model viruses by UV irradiation. *Water Sci. Technol.* **27**, 339–342 (1993).
134. Black, S., Thurston, J. A. & Gerba, C. P. Determination of Ct values for chlorine of resistant enteroviruses. *J. Environ. Sci. Health. A. Tox. Hazard. Subst. Environ. Eng.* **44**, 336–9 (2009).
135. Kahler, A. M., Cromeans, T. L., Roberts, J. M. & Hill, V. R. Effects of source water quality on chlorine inactivation of adenovirus, coxsackievirus, echovirus, and murine norovirus. *Appl. Environ. Microbiol.* **76**, 5159–5164 (2010).
136. Kahler, A. M., Cromeans, T. L., Roberts, J. M. & Hill, V. R. Source water quality effects on monochloramine inactivation of adenovirus, coxsackievirus, echovirus, and murine norovirus. *Water Res.* **45**, 1745–1751 (2011).
137. Schmelcher, M. & Loessner, M. J. Application of bacteriophages for detection of foodborne pathogens. *Bacteriophage* **4**, e28137: 1-14 (2014).
138. Bertrand, I. *et al.* The impact of temperature on the inactivation of enteric viruses in food and water: A review. *Journal of Applied Microbiology* **112**, 1059–1074 (2012).
139. Butot, S., Putallaz, T. & Sánchez, G. Effects of sanitation, freezing and frozen storage on enteric viruses in berries and herbs. *Int. J. Food Microbiol.* **126**, 30–35 (2008).
140. Pintó, R. M., Costafreda, M. I. & Bosch, A. Risk assessment in shellfish-borne outbreaks of hepatitis A. *Appl. Environ. Microbiol.* **75**, 7350–7355 (2009).
141. Nappier, S. P., Graczyk, T. K. & Schwab, K. J. Bioaccumulation, retention, and

- depuration of enteric viruses by *Crassostrea virginica* and *Crassostrea ariakensis* oysters. *Appl. Environ. Microbiol.* **74**, 6825–6831 (2008).
142. Souza, D. S. M., Dominot, A. F. Á., Moresco, V. & Barardi, C. R. M. Presence of enteric viruses, bioaccumulation and stability in *Anomalocardia brasiliensis* clams (Gmelin, 1791). *Int. J. Food Microbiol.* **266**, 363–371 (2018).
 143. Sokhey, J., Gupta, C. K., Sharma, B. & Singh, H. Stability of oral polio vaccine at different temperatures. *Vaccine* **6**, 12–13 (1988).
 144. Billah, M. M. *et al.* Cold-Chain Adaptability during Introduction of Inactivated Polio Vaccine in Bangladesh, 2015. *J. Infect. Dis.* **216**, S114–S121 (2017).
 145. Samant, Y. *et al.* Evaluation of the Cold-Chain for Oral Polio Vaccine in a Rural District of India. *Public Health Rep.* **122**, 112–121 (2007).
 146. Porta, C. *et al.* Rational Engineering of Recombinant Picornavirus Capsids to Produce Safe, Protective Vaccine Antigen. *PLoS Pathog.* **9**, (2013).
 147. Yates, M. V., Gerba, C. P. & Kelley, L. M. Virus persistence in groundwater. *Appl. Environ. Microbiol.* **49**, 778–781 (1985).
 148. Hurst, C. J., Gerba, C. P. & Cech, I. Effects of environmental variables and soil characteristics on virus survival in soil. *Appl. Environ. Microbiol.* **40**, 1067–1079 (1980).
 149. Mbithi, J. N., Springthorpe, V. S. & Sattar, S. A. Effect of Relative Humidity and Air Temperature on Survival of Hepatitis A Virus on Environmental Surfaces. *Appl. Environ. Microbiol.* **57**, 1394–1399 (1991).
 150. Rzezutka, A. & Cook, N. Survival of human enteric viruses in the environment and food. *FEMS Microbiology Reviews* **28**, 441–453 (2004).
 151. Meister, S., Verbyla, M. E., Klinger, M. & Kohn, T. Variability in Disinfection Resistance between Currently Circulating Enterovirus B Serotypes and Strains. *Environ. Sci. Technol.* **52**, 3696–3705 (2018).
 152. Shiomi, H. *et al.* Isolation and characterisation of poliovirus mutants resistant to heating at 50°C for 30 min. *J. Med. Virol.* **74**, 484–491 (2004).
 153. Adeyemi, O. O., Nicol, C., Stonehouse, N. J. & Rowlands, D. J. Increasing type-1 poliovirus capsid stability by thermal selection. *J. Virol.* **91**, JVI.01586-16 (2016).
 154. Pecson, B. M., Ackermann, M. & Kohn, T. Framework for using quantitative PCR as a nonculture based method to estimate virus infectivity. *Environ. Sci. Technol.* (2011). doi:10.1021/es103488e
 155. Muckelbauer, J. K. *et al.* The structure of coxsackievirus B3 at 3.5 Å resolution. *Structure* (1995). doi:10.1016/S0969-2126(01)00201-5
 156. Osorio, D., Rondón-Villarreal, P., Torres, R., Rondón-Villarreal, P. & Torres, R. Peptides: A Package for Data Mining of Antimicrobial Peptides. *R J.* (2012). doi:10.1080/07294360701658781
 157. Cowan, R. & Whittaker, R. Hydrophobicity indices for amino acid residues as determined by high-performance liquid chromatography. *Pept. Res.* (1990).
 158. Salo, R. J. & Cliver, D. O. Effect of acid pH, salts, and temperature on the infectivity and physical integrity of enteroviruses. *Arch. Virol.* **52**, 269–282 (1976).
 159. Perreault, D. M. & Anslyn, E. V. Unifying the Current Data on the Mechanism of

- Cleavage-Transesterification of RNA. *Angewandte Chemie (International Edition in English)* (1997). doi:10.1002/anie.199704321
160. Li, Y. & Breaker, R. R. Kinetics of RNA degradation by specific base catalysis of transesterification involving the 2 γ -hydroxyl group. *J. Am. Chem. Soc.* (1999). doi:10.1021/ja990592p
 161. Butler, M., Medlen, A. R. & Taylor, G. R. Electrofocusing of viruses and sensitivity to disinfection. *Water Sci. Technol.* (1985).
 162. Preslold, J. B., Mohammad, T. F., Lauring, A. S. & Novella, I. S. Antigenic diversification is correlated with increased thermostability in a mammalian virus. *Virology* **496**, 203–214 (2016).
 163. Hogle, J. M. Poliovirus Cell Entry: Common Structural Themes in Viral Cell Entry Pathways. *Annu. Rev. Microbiol.* (2002). doi:10.1146/annurev.micro.56.012302.160757
 164. Filman, D. *et al.* Structural factors that control conformational transitions and serotype specificity in type 3 poliovirus. *EMBO J.* (1989). doi:10.1007/s10393-010-0362-6
 165. Dove, a W. & Racaniello, V. R. An antiviral compound that blocks structural transitions of poliovirus prevents receptor binding at low temperatures. *J. Virol.* (2000). doi:10.1128/JVI.74.8.3929-3931.2000
 166. Fox, M. P., Otto, M. J. & McKinlay, M. A. Prevention of rhinovirus and poliovirus uncoating by WIN 51711, a new antiviral drug. *Antimicrob. Agents Chemother.* (1986). doi:10.1128/AAC.30.1.110
 167. Liu, Y. *et al.* Structure and inhibition of EV-D68, a virus that causes respiratory illness in children. *Science (80-)*. (2015). doi:10.1126/science.1261962
 168. Deng, L. *et al.* Grazing of heterotrophic flagellates on viruses is driven by feeding behaviour. *Environ. Microbiol. Rep.* (2014). doi:10.1111/1758-2229.12119
 169. Miki, T. & Jacquet, S. Complex interactions in the microbial world: Underexplored key links between viruses, bacteria and protozoan grazers in aquatic environments. *Aquatic Microbial Ecology* (2008). doi:10.3354/ame01190
 170. Akunyili, A. A. *et al.* Ingestion without inactivation of bacteriophages by tetrahymena. in *Journal of Eukaryotic Microbiology* (2008). doi:10.1111/j.1550-7408.2008.00316.x
 171. Mena, K. D., Gerba, C. P., Haas, C. N. & Rose, J. B. Risk assessment of waterborne coxsackievirus. *J. / Am. Water Work. Assoc.* (2003). doi:10.1002/j.1551-8833.2003.tb10413.x
 172. Zhong, Q., Carratalà, A., Ossola, R., Bachmann, V. & Kohn, T. Cross-resistance of UV- or chlorine dioxide-resistant echovirus 11 to other disinfectants. *Front. Microbiol.* (2017). doi:10.3389/fmicb.2017.01928
 173. Sadeghipour, S., Bek, E. J. & McMinn, P. C. Ribavirin-Resistant Mutants of Human Enterovirus 71 Express a High Replication Fidelity Phenotype during Growth in Cell Culture. *J. Virol.* (2013). doi:10.1128/jvi.02139-12
 174. Humphrey, W., Dalke, A. & Schulten, K. VMD: Visual molecular dynamics. *J. Mol. Graph.* **14**, 33–38 (1996).
 175. Rostkowski, M., Olsson, M. H., Søndergaard, C. R. & Jensen, J. H. Graphical analysis of

- pH-dependent properties of proteins predicted using PROPKA. *BMC Struct. Biol.* **11**, (2011).
176. Jorgensen, W. L., Chandrasekhar, J., Madura, J. D., Impey, R. W. & Klein, M. L. Comparison of simple potential functions for simulating liquid water Comparison of simple potential functions for simulating liquid water. *J. Chem. Phys* **79**, 926–935 (1983).
 177. Phillips, J. C. *et al.* Scalable molecular dynamics with NAMD. *Journal of Computational Chemistry* **26**, 1781–1802 (2005).
 178. Kelly, J. T. *et al.* Potent antiviral agents fail to elicit genetically-stable resistance mutations in either enterovirus 71 or Coxsackievirus A16. *Antiviral Res.* (2015). doi:10.1016/j.antiviral.2015.10.006
 179. Pattison, D. I. & Davies, M. J. Absolute rate constants for the reaction of hypochlorous acid with protein side chains and peptide bonds. *Chem. Res. Toxicol.* **14**, 1453–1464 (2001).
 180. Sharma, V. K. & Sohn, M. Reactivity of chlorine dioxide with amino acids, peptides, and proteins. *Environ. Chem. Lett.* **10**, 255–264 (2012).
 181. Bordoli, L. *et al.* Protein structure homology modeling using SWISS-MODEL workspace. *Nat. Protoc.* **4**, 1–13 (2008).
 182. Muckelbauer, J. K. *et al.* Structure determination of coxsackievirus B3 to 3.5 Å resolution. *Acta Crystallogr. Sect. D Biol. Crystallogr.* **51**, 871–887 (1995).
 183. DeLano, W. L. The PyMOL Molecular Graphics System, Version 1.8. *Schrödinger LLC* <http://www.pymol.org> (2014). doi:10.1038/hr.2014.17
 184. Lindberg, a M. & Polacek, C. Molecular analysis of the prototype coxsackievirus B5 genome. *Arch. Virol.* **145**, 205–21 (2000).

Curriculum Vitae

Personal Information :

Name :	Meister	Adress :	Rue d'Italie 7
First name :	Simon		1800 Vevey
Date of birth:	February 19. 1988		Suisse
Nationality :	Swiss and Colombian	Mobile phone:	079.317.98.45
Status :	single		

Email addresses : s.meister.romero@gmail.com

Education and diplomas :

Master in biology : 2011-2013 – University of Lausanne

- MLS section : Molecular Life Sciences
- Master project : *Production of recombinant hepatitis C virus nonstructural protein 4B in mammalian cells.*
Laboratory of Molecular virology and pathogenesis of hepatitis C, Prof. Darius Moradpour.

Bachelor in biology : 2008-2011 – University of Lausanne

Federal maturity : 2004-2007 – Gymnasium of Burier

- Option : biology and chemistry, enhanced mathematics.

Languages :

- French : mother tongue
- German : medium level
- English : good level
- Spanish : good level

Professional experiences :

Adam Luring Laboratory, Ann Arbor (Michigan, US) : August 2016

- Techniques learning in the laboratory of Adam Luring.

Laboratoire de Chimie Environnementale, EPFL : Since Novembre 2015

- Start of a PhD thesis in the laboratory of Tamar Kohn.

Laboratoire de Virologie, HUG : January to August 2014

- Start of a PhD thesis in the laboratory of Caroline Tapparel and Laurent Kaiser.

IBCP, Lyon : April 2013

- Collaboration in the laboratory of François Penin.

IMUL, CHUV : March to November 2013

- Hired as Assistant Researcher in the laboratory of Darius Moradpour.

IMUL, CHUV : September 2011 to February 2013

- Pre-master and Master in the laboratory of Angela Ciuffi and Darius Moradpour.

IMUL, CHUV : August to September 2011

- Internship in the laboratory of Prof. Amalio Telenti.
-

EPFL, Assistant Researcher : 2011-2012

- Processing files, thesis research, CVs ranking.

AGENA, Moudon : 2008, 2009, 2010 and 2011 (total of nine months)

- Installer in solar energy systems.

Publications, presentations and posters of interest :

Publications :

1. Meister, S., Verbyla, M. E., Klinger, M., & Kohn, T. (2018). **Variability in Disinfection Resistance between Currently Circulating Enterovirus B Serotypes and Strains.** *Environmental Science and Technology*, 52(6), 3696–3705. <http://doi.org/10.1021/acs.est.8b00851>
2. Gouttenoire, J., Montserret, R., Paul, D., Castillo, R., Meister, S., Bartenschlager, R., ... Moradpour, D. (2014). **Aminoterminal Amphipathic α -Helix AH1 of Hepatitis C Virus Nonstructural Protein 4B Possesses a Dual Role in RNA Replication and Virus Production.** *PLoS Pathogens*.
<http://doi.org/10.1371/journal.ppat.1004501>

Présentations :

1. Meister, S., Prunotto, A., Dal Peraro, M., Kohn, T. (2018). **Structural characterization of thermoresistant enteroviruses.** *ISFEV, Tempe, Arizona, USA.*
2. Meister, S., Klinger, M., Kohn, T. (2016). **Isolation and characterization of disinfection-resistant enteroviruses.** *ISFEV, Kusatsu, Japan.*

Poster :

1. Meister, S., Verbyla, M. E., Klinger, M., Kohn, T. (2018). **Variability in phenotypic properties within and between currently circulating Enterovirus B serotypes.** *Virus2018, Barcelona, Spain.*
2. Meister, S., Verbyla, M. E., Klinger, M., Kohn, T. (2018). **Variability in phenotypic properties within and between currently circulating Enterovirus B serotypes.** *Swiss Virology Meeting, Fribourg, Switzerland*
3. Meister, S., Klinger, M., Kohn, T. (2016). **Isolation and characterization of disinfection-resistant enteroviruses.** *Swiss Virology Symposium, Bern, Switzerland.*
4. Meister, S., Gouttenoire, G., Moradpour, D. (2013). **Production of Recombinant Hepatitis C virus Nonstructural Protein 4B in Mammalian cells.** *Swiss Gastroenterology meeting, Basel, Switzerland.*

Other activities :

- Certificate of violin with honors, amateur guitar.
- Volleyball at VBC Bussigny.
- Licence PADI Divemaster.
- Paraglider pilot.
- Bouldering

